Environmental controls on marine ecosystem recovery following mass extinctions, with an example from the Early Triassic

Hengye Wei[a,b,*], Jun Shen[a,c], Shane D. Schoepfer[d], Leo Krystyn[e], Sylvain Richoz[f], and Thomas J. Algeo[a,c,g,*]

[a] Department of Geology, University of Cincinnati, Cincinnati, OH 45221, U.S.A.

[b] College of Earth Science, East China Institute of Technology, Nanchang, Jiangxi, 330013, P.R. China

[c] State Key Laboratory of Geological Processes and Mineral Resources, China University of Geosciences, Wuhan, Hubei, 430074, P.R. China

[d] Department of Earth and Space Sciences, University of Washington, Seattle, WA 98195, U.S.A.

[e] Institute for Paleontology, Vienna University, Althanstrasse 14, 1090 Vienna, Austria

[f] Institute of Earth Sciences, Graz University, Heinrichstrasse 26, 8020 Graz, Austria

[g] State Key Laboratory of Biogeology and Environmental Geology, China University of Geosciences, Wuhan, Hubei, 430074, P.R. China

* Corresponding authors: H. Wei: email (weihengye@163.com), Tel (86-18870073972); T.J. Algeo: email (Thomas.Algeo@uc.edu), Tel (513-5564195).

ABSTRACT

The recovery of marine ecosystems following a mass extinction event involves an extended interval of increasing biotic diversity and ecosystem complexity. The pace of recovery may be controlled by intrinsic ecosystem or extrinsic environmental factors. Here, we present an analysis of changes in marine conditions following the end-Permian mass extinction with the objective of evaluating the role of environmental factors in the protracted

(~5-Myr-long) recovery of marine ecosystems during the Early Triassic. Specifically, our study examines changes in weathering, productivity, and redox proxies in three sections in South China (Chaohu, Daxiakou, and Zuodeng) and one in northern India (Mud). Our results reveal: 1) recurrent environmental perturbations during the Early Triassic; 2) a general pattern of high terrestrial weathering rates and more intensely reducing marine redox conditions during the early Griesbachian, late Griesbachian, mid-Smithian, and (more weakly) the mid-Spathian; 3) increases in marine productivity during the aforementioned intervals except for the early Griesbachian; and 4) stronger and more temporally discrete intervals of environmental change in deepwater sections (Chaohu and Daxiakou) relative to shallow and intermediate sections (Zuodeng and Mud). Our analysis reveals a close relationship between episodes of marine environmental deterioration and a slowing or reversal of ecosystem recovery based on metrics of biodiversity, within-community (alpha) diversity, infaunal burrowing, and ecosystem tiering. We infer that the pattern and pace of marine ecosystem recovery was strongly modulated by recurrent environmental perturbations during the Early Triassic. These perturbations were associated with elevated weathering and productivity fluxes, implying that nutrient and energy flows were key influences on recovery. More regular secular variation in deepwater relative to shallow-water environmental conditions implies that perturbations originated at depth (i.e., within the oceanic thermocline) and influenced the ocean-surface layer irregularly. Finally, we compared patterns of environmental disturbance and ecosystem recovery following the other four “Big Five” Phanerozoic mass extinctions to evaluate whether commonalities exist. In general, the pace of ecosystem recovery depends on the degree of stability of the post-crisis marine environment.

Keywords: productivity; redox; anoxia; weathering; South China; India

Contents

---

1. Introduction

Each major mass extinction event in the geologic record has been followed by an interval of restructuring of marine ecosystems, reflected in changes in clade dominance, ecological niche partitioning, and community organization (e.g., Erwin, 1998). Increased productivity among primary producers and consumers can generate ecological niches higher in the marine trophic system (Kirchner and Weil, 2000), allowing a progressive rebuilding of a stable, complex ecosystem structure (Chen and Benton, 2012). Although lacking a specific quantitative definition, "ecosystem recovery" is generally regarded as the reappearance of marine communities with a high biotic diversity and an integrated and complex structure that is stable at multimillion-year timescales (Harries and Kauffman, 1990). The progress of post-extinction recovery commonly has been evaluated using metrics related to overall biodiversity and/or species origination rates (e.g., Jacobsen et al., 2011; Payne et al., 2011). However, "ecosystem recovery" is not simply a return to pre-extinction levels of biodiversity but, rather, the expansion and re-integration of entire marine ecosystems or communities (Erwin et al., 2008; Chen and Benton, 2012) as reflected by metrics such as alpha diversity (i.e., within-community species richness; Bambach, 1977; Clapham et al., 2006) and ecological tiering (Twitchett, 1999; Fraiser, 2011).

In the case of the Permian-Triassic (P-Tr) boundary mass extinction, an initial, aborted recovery occurred soon after the end-Permian crisis, during the Induan stage of the Early Triassic (Baud et al., 2008; Brayard et al., 2009; Stanley, 2009), and a more sustained recovery took place during the late Olenekian stage (Spathian substage) (Chen et al., 2011; Song et al., 2011; Payne et al., 2011), but full ecosystem recovery probably did not occur until the Middle Triassic (Erwin and Pan, 1996; Bottjer et al., 2008; Chen and Benton, 2012). The recovery of marine invertebrate ecosystems following the end-Permian crisis was apparently the most protracted of any major mass extinction (Bottjer et al., 2008), i.e., the "Big Five" Phanerozoic mass extinctions of Sepkoski (1984, 1986). An important unresolved issue is what controlled the long duration of the post-extinction recovery interval during the Early Triassic. At least three hypotheses have been advanced, linking the protracted recovery to: (1)

113 the intensity of the mass extinction (Sepkoski, 1984; Solé et al., 2002), (2) the persistence of
114 harsh environmental conditions (Hallam, 1991; Isozaki, 1997; Payne et al., 2004; Erwin,
115 2007), and (3) episodic occurrence of strong environmental disturbances during the recovery
116 interval (Algeo et al., 2007, 2008; Orchard, 2007; Retallack et al., 2011) (Fig. 1).
117 Examination of long-term records of Early Triassic marine environmental conditions has
118 the potential to provide information relevant to these hypotheses. In this study, we (1) review
119 existing literature on the recovery of marine ecosystems following the end-Permian mass
120 extinction, (2) analyze changes in marine productivity and redox conditions at four locales in
121 China and India from the latest Permian through the Spathian substage of the Early Triassic,
122 (3) evaluate the importance of marine environmental changes during the Early Triassic as
123 controls on the marine ecosystem recovery, and (4) compare the Early Triassic marine
124 ecosystem recovery with those following other Phanerozoic mass extinctions. Our
125 comparative analysis of recoveries following each of the 'Big Five' Phanerozoic mass
126 extinctions is intended to identify general features or patterns of marine ecosystem recovery
127 and their relationships to contemporaneous environmental changes.
128
129 **2. Background**
130
131 *2.1. The end-Permian biotic crisis*
132
133 The end-Permian mass extinction was the most severe biocrisis of the Phanerozoic (Fig.
134 2; Erwin et al., 2002; Irmis and Whiteside, 2011). It killed ~80-96% of marine invertebrate
135 species and ~70% of terrestrial vertebrate species (McKinney, 1995; Benton and Twitchett,
136 2003). There appear to have been two pulses of marine extinction (Yin et al., 2012; Song-HJ
137 et al., 2013) and environmental disturbance (Xie et al., 2005, 2007), rather than a single event
138 during this biocrisis (Rampino and Adler, 1998; Jin et al., 2000; Shen-SZ et al., 2011). As an
139 example, foram species in South China exhibit a ~57% extinction rate during the latest
140 Permian pulse and a ~31% extinction rate during the earliest Triassic pulse (Song-HJ et al.,

2013). According to high-precision U-Pb dating in South China sections, the interval between these extinction pulses was 60±48 kyr (Burgess et al., 2014). The end-Permian mass extinction coincided with eruption of the Siberian Traps Large Igneous Province (Campbell et al., 1992; Renne et al., 1995; Reichow et al., 2009; Sobolev et al., 2011) as well as with major environmental changes including global sea-level rise (Hallam and Wignall, 1999), ocean anoxia (Wignall and Twitchett, 1996; Isozaki, 1997), global warming (Joachimski et al., 2012; Sun et al., 2012; Romano et al., 2013), and, possibly, marine acidification (Payne et al., 2010; Hinojosa et al., 2012; Kershaw et al., 2012).

2.2. The Early Triassic marine ecosystem recovery

The recovery of marine ecosystems during the Early Triassic was a multi-step process. There were several phases of incomplete or aborted recovery during the Induan, and recovery from the P-Tr boundary mass extinction is generally regarded as not having been completed until the Middle Triassic, ~5 Myr after the end-Permian crisis (Mundil et al., 2004; Ovtcharova et al., 2006; Lehrmann et al., 2006; Shen-SZ et al., 2011). Both benthic and planktonic cyanobacteria bloomed immediately after the end-Permian mass extinction (Fig. 2; Lehrmann, 1999; Wang et al., 2005; Xie et al., 2005; Luo et al., 2011). Cyanobacterial microbialites reappeared episodically in different regions throughout the Early Triassic but they largely disappeared by the early Middle Triassic (Baud et al., 2007; Xie et al., 2010). An Early Triassic “chert gap” (Beauchamp and Baud, 2002) was caused by the loss of biosilica deposits from radiolarians and siliceous sponges, although occurrences of thin chert beds in the late Griesbachian and Dienerian (Kakuwa, 1996; Takemura et al., 2007; Sano et al., 2010) document a temporary local early recovery of siliceous faunas.

Some secondary consumers such as conodonts and ammonoids rebounded rapidly from the end-Permian mass extinction (Orchard, 2007; Brayard et al., 2009; Stanley, 2009). Their rapid recovery may have been assisted by a microphagous habit (Fischer and Bottjer, 1995), allowing them to benefit directly from increased biomass among primary producers. These

169 clades subsequently declined during biocrises at the end of Griesbachian, Smithian, and
170 Spathian substages of the Early Triassic, although they tended to rediversify rapidly during
171 the intervening intervals (Fig. 2; Brayard et al., 2009; Stanley, 2009). However, conodonts
172 display a strong Lilliput effect during the Smithian/Spathian boundary crisis (Chen et al.,
173 2013). Compared to conodonts and ammonoids, recovery rates for benthic primary consumers
174 such as foraminifers, gastropods, bivalves, brachiopods and ostracods were more gradual (Fig.
175 2; Payne et al., 2011). Among foraminifers, a sustained diversity increase began in the early
176 Smithian (early Olenekian) (Song et al., 2011) and accelerated during the Anisian (early
177 Middle Triassic) (Payne et al., 2011). Similar recovery patterns are observed also among
178 brachiopods (Chen et al., 2005) and ostracods (Crasquin-Soleau et al., 2007). The sizes of
179 gastropod and bivalve shells were reduced across the P-Tr boundary and during the
180 Griesbachian but returned to pre-extinction dimensions by the Anisian (Fig. 2; Fraiser and
181 Bottjer, 2004; Payne, 2005; Twitchett, 2007). However, the high diversity, low dominance,
182 and ecological complexity of mollusc fauna during the late Griesbachian and early Dienerian
183 at Shanggan, South China (Hautmann et al., 2011) and on the Wasit Block in Oman (Krystyn
184 et al., 2003; Twitchett et al., 2004) may represent an early recovery phase of these faunas.
185 The meso-consumer trace-makers and reef-builders can shed light on the recovery of
186 benthic marine ecosystems. Generally, trace-makers decreased during the end-Permian
187 biocrisis and recovered slowly in the Early Triassic (Fig. 2; Pruss and Bottjer, 2004; Chen et
188 al., 2011). Locally, trace-fossil diversity shows occasional peaks during the Griesbachian to
189 Smithian (Twitchett and Wignall, 1996; Twitchett, 1999; Zonneveld et al., 2010; Chen et al.,
190 2011). However, small trace-fossil burrow size, low tiering levels, and low ichnofabric indices
191 (bioturbation) generally persisted until the end of the Smithian substage, and the early
192 Spathian is marked by a strong increase in trace-fossil diversity and complexity (Pruss and
193 Bottjer, 2004; Chen et al., 2011). Nonetheless, Spathian ichnofaunas are less diverse than
194 those of the Middle Triassic (Knaust, 2007). This pattern may suggest a stepwise recovery of
195 trace-makers during Early to Middle Triassic (Twitchett and Barras, 2004). Furthermore, the
196 recovery of trace-makers may have been diachronous, with a more rapid increase in

197 ichnodiversity at high northern paleolatitudes than in the equatorial region (Twitchett and
198 Barras, 2004; Pruss and Bottjer, 2004). With regard to reef-builders, a new metazoan reef
199 ecosystem formed by various sponges and serpulid worms associated with microbial
200 carbonates and eukaryotic organisms developed in the early Smithian, latest Smithian, and
201 early to middle Spathian on the eastern Panthalassic margin, in Utah and Nevada (Fig. 2;
202 Brayard et al., 2011). These equatorial sponge-microbe reefs are found as early as 1.5 Myr
203 after the P-Tr boundary and represent a temporary recovery at least regionally (Brayard et al.,
204 2011, Chen and Benton, 2012). However, the "reef gap", as represented by the absence of
205 heavily calcified corals, persisted through the Early Triassic (Payne et al., 2006).
206 As for the top trophic level in the marine ecosystem, predatory fish and reptiles
207 displayed different recovery trajectories. Fishes were rare in the Griesbachian-to-Smithian
208 equatorial ocean (Fig. 2; Fraiser et al., 2005; Tong et al., 2006; Zhao and Lu, 2007; Sun et al.,
209 2012) but more common in the middle to late Spathian (Goto, 1994; Wang et al., 2001;
210 Benton et al., 2013). High-latitude regions had a more abundant and diverse fish fauna in the
211 Early Triassic than the equatorial ocean (Scheaffer et al., 1976; Stemmerik et al., 2001; Mutter
212 and Neuman, 2006; Romano and Brinkmann, 2010; Benton et al., 2013). Globally, fish
213 diversity recovered by the Middle Triassic (Jin, 2006; Zhang et al., 2010; Hu et al., 2011).
214 Marine reptiles first reappeared in the Smithian in high-latitude regions (Cox and Smith, 1973;
215 Callaway and Brinkman, 1989) but later, in the Spathian, in equatorial regions (Li et al., 2002;
216 Zhao et al., 2008). A high level of diversity among marine reptiles was achieved by the
217 Middle to Late Triassic (Zhang et al., 2009).
218 To summarize, animals that were low in the marine trophic system tended to recover
219 faster than those at higher trophic levels (Fig. 2; cf. Chen and Benton, 2012). Pelagic and
220 nektonic faunas recovered faster than benthos as shown by rapid increases to multiple
221 biodiversity peaks for ammonoids and conodonts during the Early Triassic, versus a slow
222 return to pre-crisis diversity levels by the Middle Triassic for most bottom-dwellers. In
223 Olenekian time, offshore benthos like calcareous algae and *Tubiphytes* recovered faster than
224 those in nearshore environments in South China (Song et al., 2011). High-latitude biotas

recovered faster than equatorial marine biota (Pruss and Bottjer, 2004). These differentiated responses may suggest that the pattern and intensity of environmental changes during the Early Triassic had an important influence on the pathways and tempo of marine ecosystem recovery.

2.3. Environmental change during the Early Triassic recovery

During the recovery interval following the end-Permian mass extinction, major changes in the environment related to volcanism, sea level, and paleoceanographic conditions took place. The eruption of the Siberian Traps large igneous province (LIP), which had begun at ~252 Ma close to the P-Tr boundary, continued strongly for ~1.5 Myr and more weakly for several million years longer (Fig. 3). The eruption history of this LIP is delineated by U-Pb ages for gabbroic intrusive rocks of 252±4 Ma (Kuzmichev and Pease, 2007) and silicic tuff ages of 251.7±0.4 (Kamo et al., 2003), an Ar-Ar age of 250.3±1.1 Ma for the final stages of extrusive volcanism (Reichow et al., 2009), and younger Ar-Ar ages of 242.2±0.6 Ma for a basalt (Reichow et al., 2009). This range of dates documents activity of the Siberian Traps LIP from 252 Ma to 242 Ma with a main eruptive phase at ~252 to 250 Ma (Reichow et al., 2009). Altogether, the Siberian Traps degassed ~6300 to 7800 Gt sulfur, ~3400 to 8700 Gt chlorine, and ~7100 to 13600 Gt fluorine (Black et al., 2012). The high volatile contents increased the likelihood that volatiles reached the stratosphere and, thus, caused a drastic deterioration of global environments through direct toxicity and acid rainfall (Devine et al., 1984), ozone depletion (Johnston, 1980), and rapid climatic changes that may have included both global cooling (Sigurdsson et al., 1992; Wignall, 2001; Timmreck et al., 2010) and global warming (Ganino and Arndt, 2009). This interval coincided with a long-term eustatic rise from the Late Permian until the middle Late Triassic, with the most rapid rise during the Early Triassic (Fig. 3; Haq et al., 1987; Haq and Schutter, 2008).

Major changes in tropical sea-surface temperatures accompanied the P-Tr boundary crisis. Temperatures increased gradually from ~60 kyr prior to the mass extinction event and

253 then spiked rapidly at the time of this event (Joachimski et al., 2012; Burgess et al., 2014).
254 During the Early Triassic, temperatures reached a maximum in the mid- to late Griesbachian
255 (~36-40°C), cooled slightly during the latest Griesbachian to the early Smithian, and then
256 reached a second peak of extreme warmth in the late Smithian (Fig. 3; Sun et al., 2012,
257 Romano et al., 2013). A pronounced retreat from peak temperatures occurred in the early
258 Spathian, an event resulting in a major turnover and geographic displacement of marine
259 invertebrate faunas (Galfetti et al., 2007a,b; Stanley, 2009). A weak warming episode in the
260 mid-late Spathian was followed by a second large cooling step around the Early-Middle
261 Triassic boundary, yielding distinctly more moderate temperatures during the Anisian
262 although still warmer than in the pre-extinction Late Permian (Sun et al., 2012; Romano et al.,
263 2013).

264 Ocean redox conditions exhibit pronounced geographic and secular variation during the
265 latest Permian and Early Triassic. More reducing conditions developed widely at mid-water
266 depths (i.e., with the oceanic thermocline) during the pre-extinction late Changhsingian
267 (Algeo et al., 2012; Shen et al., 2013; Feng and Algeo, 2014). The end-Permian crisis was
268 marked by a transient expansion of anoxia into shallow-marine settings, especially in the
269 Tethyan Ocean (Fig. 3; Horacek et al., 2007; Grice et al., 2005; Algeo et al., 2007, 2008; Bond
270 and Wignall, 2010; Brennecka et al., 2011; Shen-Y et al., 2011), although some places (e.g.,
271 Oman, Iran) remained oxic (Krystyn et al., 2003; Richoz et al., 2010). Thereafter, the Early
272 Triassic is characterized by a complex pattern of redox variation (Song et al., 2012; Grasby et
273 al., 2013). The intensity of anoxia appears to have declined during the Spathian, and episodes
274 of marine anoxia seem to have terminated around the Early-Middle Triassic boundary
275 (Hermann et al., 2011; Song et al., 2012).

276 Marine productivity can vary greatly during major biocrises (Kump and Arthur, 1999).
277 Several factors during the P-Tr boundary crisis might have led to higher productivity: 1)
278 phosphate liberated from sediments under anoxic conditions can stimulate productivity (Ingall
279 and van Cappellen, 1990), and 2) intensified subaerial weathering can increase the flux of
280 river-borne P to the oceans (Algeo and Twitchett, 2010; Algeo et al., 2011b). Variations in

281 marine productivity can be reconstructed using carbon isotopes or elemental data (Kump and
282 Arthur, 1999; Algeo et al., 2013; Schoepfer et al., 2014). The 'biological pump' removes
283 ^{12}C-enriched carbon from the ocean-surface layer and transfers it to the ocean thermocline,
284 producing a vertical gradient in the $\delta^{13}C$ of dissolved inorganic carbon ($\Delta^{13}C_{DIC}$). Changes in
285 $\Delta^{13}C_{DIC}$ can thus provide information about the intensity of the organic carbon sinking flux
286 and, indirectly, primary productivity (Hilting et al., 2008). A large vertical $\delta^{13}C_{DIC}$ gradient in
287 the Nanpanjiang Basin of South China was interpreted as evidence of elevated marine
288 productivity during the Early Triassic (Fig. 3; Meyer et al., 2011), although this gradient has
289 also been attributed to intensified water-column stratification (Song-HY et al., 2013; Luo et
290 al., 2014). However, an analysis of marine productivity changes based on organic carbon
291 burial fluxes suggested a productivity crash in Early Triassic seas of the South China craton
292 (Algeo et al., 2013). The large carbon-isotope excursions of the Early Triassic (Payne et al.,
293 2004; Tong et al., 2007; Clarkson et al., 2013) were hypothesized to have been due to marine
294 productivity fluctuations (Algeo et al., 2011b), an inference supported by patterns of
295 $\delta^{13}C$-$\delta^{34}S$ covariation (Song et al., 2014). The ultimate control on these fluctuations appears to
296 have been temperature, with warm intervals associated with reduced productivity (Song et al.,
297 2014).

298 Seawater pH values may have fluctuated during the P-Tr boundary crisis, as shown by
299 analysis of calcium isotopes (Payne et al., 2010; Hinojosa et al., 2012). Calcium isotopic
300 fractionation caused by the precipitation of carbonate minerals results in ^{40}Ca-rich marine
301 sediments and ^{44}Ca-rich in seawater (Skulan et al., 1997; De La Rocha and DePaolo, 2000;
302 Fantle and DePaolo, 2005; Tang et al., 2008). Abrupt negative excursions of $\delta^{44/40}Ca$ in both
303 bulk carbonate and conodont apatite, representing a shift in seawater $\delta^{44/40}Ca$, occurred
304 synchronously with the end-Permian biocrisis (Fig. 3; Payne et al., 2010; Hinojosa et al.,
305 2012). The underlying cause of this change may have been eruption of the Siberian Traps,
306 which injected a large amount of CO_2 into the atmosphere-ocean system, causing seawater
307 acidification and increased riverine ^{40}Ca-rich calcium input owing to accelerated terrestrial

weathering of carbonates (Payne et al., 2010; Blätter et al., 2011). Ocean acidification during Permian-Triassic transition may lead to the preferential extinction of heavily calcified marine organisms (Knoll et al., 2007; Kiessling and Simpson, 2011; Clapham and Payne, 2011) and could explain the abrupt transition on carbonate platforms from skeletal to microbial and abiotic carbonate factories described by Kershaw et al. (2011).

To summarize, eruption of the Siberian Traps during the Late Permian to Early Triassic resulted in a major perturbation of the atmosphere-ocean system. Environmental changes linked to early phases of the eruption appear began slowly during an interval of at least ~60 kyr preceding the main mass extinction, but accelerated sharply at the end of the Permian. Major environmental effects related to continuing eruption of Siberian Traps flood basalts persisted for ~1.5 to 2.0 million years during the Early Triassic, with some effects continuing until the Early-Middle Triassic boundary, nearly 5 million years after the end of the Permian. The main phase of the eruption, coinciding with the Induan Stage of the Early Triassic, coincided with highly disturbed marine ecosystems, sea-level rise, seawater acidification, and widespread oceanic anoxia. These relationships show that environmental instability coincided with, and probably caused or contributed to, the delayed recovery of marine ecosystems during the Early Triassic.

3. Study sections

Three of the sections chosen for this study are from the South China craton, which was located in the eastern Paleotethys Ocean during the Permian-Triassic transition. The Chaohu section was deposited in a deep ramp setting on the northeastern (paleo-northwestern) margin of this craton, Daxiakou on the mid-ramp of the same margin, and Zuodeng on a shallow carbonate platform within the Nanpanjiang Basin on the southwestern (paleo-southeastern) margin of this craton (Fig. 4A). These sections were widely separated, with a distance of ~650 km between Chaohu and Daxiakou, and a distance of ~950 km between the latter and Zuodeng. The fourth study section is Mud, from the Spiti Valley of northern India, which was

located in the south-central Neotethys Ocean during the Permian-Triassic transition (Fig. 4B). We collected a total of 794 samples from 167 m of section at Chaohu, 302 samples from 71 m of section at Daxiakou, 351 samples from 109 m of section at Zuodeng, and 135 samples from 26.5 m of section at Mud. Average sample spacing thus ranges from 20 to 31 cm for the four study sections, which equates to an average temporal interval of ~4 to 10 kyr between samples (see Supplementary Table 1 for the geologic timescale used in this study, and the Supplementary Information for age-depth models of the study sections).

3.1. Chaohu, Anhui Province, China

The Chaohu section is located in proximity to Chaohu city in Anhui Province (Fig. 4A). It is a composite section comprising sections at West Majiashan, West Pingdingshan, and South Majiashan, all of which are located within a ~1-km^2 area (Tong et al., 2003). These sections contain, respectively, the narrow P-Tr boundary interval, the Griesbachian to Smithian, and the Spathian (Fig. 5), according to conodont biostratigraphic data (Zhao et al., 2007). The top of the South Majiashan section coincides approximately with the Spathian-Anisian (Early-Middle Triassic) boundary (Zhao et al., 2007). During the Early Triassic, the Chaohu area was on the deep lower margin of a ramp about 300 km to the north (paleo-west) of the Cathaysia Oldland (Fig. 4A; Tong et al., 2003). Estimated depositional water depths in the Chaohu area were ~300-500 m (Song-HY et al., 2013). However, relative sea-level elevations began to decrease during the Spathian (Tong et al., 2001, 2007b; Chen et al., 2011) as a consequence of a collision between the North China and South China blocks that culminated in the late Middle Triassic (Li, 2001).

This section has been subject to detailed analysis of conodont and ammonoid biostratigraphy (Zhao et al., 2007), sequence stratigraphy (Tong, 1997; Li et al., 2007), carbon isotopes (Tong et al., 2007a), and paleomagnetic polarity (Tong et al., 2003), permitting development of a high-resolution geochronological framework for this study. The West Pingdingshan section is a candidate for the Global Stratotype Section and Point (GSSP) of the

Induan-Olenekian boundary (Tong et al., 2003). Conodonts are found in abundance in the upper Griesbachian through Dienerian-Smithian boundary, the middle Smithian, and lower Spathian but are rarer in other stratigraphic intervals (Tong et al., 2003; Zhao et al., 2007). Foraminifers are found in the Induan stage (Song et al., 2011), ammonoids are particularly abundant around the Smithian-Spathian boundary, and some marine vertebrate fossils are found in the Olenekian (Tong et al., 2003).

The carbonate fraction of the sediment shows an increase upsection at Chaohu, from ~30% around the P-Tr boundary to ~40-70% in the Griesbachian and Dienerian, ~75% in the Smithian (except for a local decline to ~20% in the mid-Smithian), and ~87% in the Spathian (Fig. 5, Supplementary Table 2). Chert, which is probably mainly of biogenic origin, decreases upsection, from ~28% around the P-Tr boundary to ~5% in the Spathian. Clay-mineral content shows a similar upsection decrease, from ~50% around the P-Tr boundary to ~8% in the Spathian. These mineralogic changes are reflected in an upsection shift in lithology from cherty mudrock with minor limestone interbeds around the P-Tr boundary to thin-bedded marls with mudrock interbeds in the Griesbachian and Dienerian, dominant mudrock with marlstone interbeds in the Smithian, and thick-bedded limestone with marlstone interbeds in the Spathian (Fig. 5; Tong et al., 2003, 2007a; Guo et al., 2008).

3.2. Daxiakou, Hubei Province, China

The Daxiakou section is located in Xingshan county, Yichang city, in the Yangtze Gorge area of Hubei Province (Fig. 4A). During the Early Triassic, it was located in a deep-ramp setting on the northern margin of the South China Block (Tong and Yin, 2002; Zhao et al., 2005), ~850 km from the Kangdian Oldland (Fig. 4A). Conodont biostratigraphy shows that the section spans the early Changhsingian through mid-Smithian interval (Zhao et al., 2005). Fossils of ammonoids, conodonts, and bivalves, among others are found in particular abundance in upper Dienerian to lowermost Smithian strata (Li et al., 2009), implying relatively high primary productivity at that time (Tong, 1997). Estimated depositional water

depths in the Daxiakou area were ~200-300 m (Song-HY et al., 2013).

The carbonate component is high (>80%) throughout the section except for the P-Tr boundary interval and in Dienerian to lower Smithian strata (Fig. 5, Supplementary Table 3). In the P-Tr transition, average carbonate, chert, and clay-mineral contents are ~30%, ~20%, and 50%, respectively, and strata consist of thin-bedded, dark-gray to black cherty shales (cf. Wu et al., 2012). In the Dienerian to lower Smithian, average carbonate, chert, and clay-mineral contents are ~60%, ~10%, and ~30%, respectively, and strata consist of marlstones with mudrock intercalations.

3.3. Zuodeng, Guangxi Province, China

The Zuodeng section is located in Zuodeng county, Tiandong city, in Guangxi Province. During the Early Triassic, this section was located on a carbonate platform (the Debao Platform) within the Nanpanjiang Basin (Fig. 4A), a deep-marine embayment on the southwestern (paleo-southeastern) margin of the South China Block that existed from the Late Paleozoic to the Late Triassic (Enos et al., 1997). The Debao Platform was one of many isolated, shallow carbonate platforms within this basin, the largest being the Great Bank of Guizhou (Lehrmann et al., 2007). The Nanpanjiang Basin was adjacent to a subduction-zone volcanic arc along the South China-Indochina plate margin (Cai and Zhang, 2009), where volcanism was more intense than on the northern margin of the South China Block (e.g., Xie et al., 2010). This section ranges from the upper Changhsingian through the lower Spathian, as shown by conodont biostratigraphy (Yang et al., 1986; Tong et al., 2007a). Abundant gastropods and ostracods are found in the upper Griesbachian (Wang et al., 2001) and prolific ammonoids, conodonts, and fishes in the lowermost Smithian (Yang et al., 1986). Estimated depositional water depths in the Zuodeng area were ~30-50 m based on the energy subtidal feature of the Lower Triassic limestones for the Debao isolated platform (next to the Pingguo isolated platform, Lehrmann et al., 2007).

Carbonate content at Zuodeng is much higher than for the other study sections, averaging

~95% in upper Changhsingian to Spathian strata with a small decrease to ~80% in the upper Smithian (Fig. 5, Supplementary Table 4). This section consists mainly of thin- to thick-bedded lime mudstone (cf. Wang et al., 2001). The lack of data around the P-Tr boundary is due to this interval being covered at the time of sample collection.

3.4. Mud, Spiti Valley, India

The Mud section is located in the Spiti Valley, which is part of the district of Lahul and Spiti, a central area of the western Himalaya in northern India. Lower Triassic strata are well exposed in this area. During the Early Triassic, the study area was located at mid-southern latitudes (~30-35°S) on the northern Gondwanan margin (Fig. 4B; Krystyn et al., 2007). Middle Permian rifting (Stampfli et al., 1991; Garzanti et al., 1996) resulted in the formation of the Neo-Tethys Ocean (Stampfli et al., 1991; Garzanti et al., 1996), and the surface uplift of the rift shoulders resulted in widespread non-deposition, erosion and the unconformities in the stratigraphic record (Stampfli et al., 1991; Garzanti et al., 1996). The study section was deposited in a mid-shelf setting having a gentle slope, as implied by the modest water depths of deposition (~50-70 m) despite the distal location of the section (Krystyn et al., 2007).

The base of this section consists of Wuchiapingian to lower Changhsingian strata that are overlain by an unconformity (or highly condensed interval) spanning the upper Changhsingian and lower Griesbachian (Bhargava et al., 2004). The main part of the study section consists of a conformable succession of mid-Griesbachian to lowermost Spathian strata. Ammonoids are common in the upper Griesbachian to lower Smithian interval (Krystyn and Orchard, 1996; Krystyn et al., 2007). Average ammonoid shell size decreases from large in the lower Smithian to small in the middle Smithian (Krystyn et al., 2007), suggesting the development of more hostile environmental conditions at that time. Current bedforms are consistent with a well-oxygenated watermass during the earliest Smithian (Krystyn et al., 2007). The Mud section is a candidate GSSP for the Induan-Olenekian

boundary, which was formerly placed at the Bed 12/13 contact (Krystyn et al., 2007) but has been revised downward to approximately the Bed 9/10 contact (Brühwiler et al., 2010).

The Wuchiapingian to lower Changhsingian strata are composed of siliceous shale, with a ~25% chert fraction (Fig. 5, Supplementary Table 5). A sharp change in lithology occurs at the P-Tr unconformity, with Lower Triassic strata consisting dominantly of carbonates. However, low carbonate content is found in limited intervals of the Dienerian and lower Spathian, which consist mainly of marlstones (cf. Krystyn et al., 2007). For most of Lower Triassic strata, it consists of thin-bedded argillaceous limestone with shale intercalation (e.g., Krystyn et al., 2007) and the average carbonate, shale and chert are ~78%, ~16% and ~6%, respectively (Fig. 5).

4. Results

We report raw values for geochemical proxies for terrestrial chemical weathering, marine productivity, and marine redox conditions in Sections 4.1 to 4.3. We then used an age-thickness model for each study section (see Supplementary Information for details) in order to calculate fluxes for the same proxies (Sections 4.4 to 4.6). All raw chemostratigraphic data and calculated flux values for the four study sections are given in Supplementary Tables 2 to 5.

4.1. Weathering proxies

We used Al and Fe concentrations as well as the chemical index of alteration (CIA) to evaluate terrestrial weathering changes during the Early Triassic. In predominantly carbonate successions such as those of the present study, increases in Al and Fe (which are present mainly in clay minerals) can be due to climatically controlled fluctuations in subaerial weathering rates (cf. Sageman et al., 1997). CIA was calculated as Al_2O_3 / (Al_2O_3 + K_2O + Na_2O) (see Supplementary Information for details). It is a widely used proxy in reconstructing

paleoclimate since it is interpreted as a measure of the extent of conversion of feldspars related to the weathering (Young and Nesbitt, 1998; Price and Velbel, 2003). Note that the CIA results for each study section are described in conjunction with weathering fluxes (Section 4.4).

At Chaohu, Al ranges from <0.1 to 15.0%, with an average value of 4.6% (Fig. 6A). It shows generally high values from the P-Tr boundary to the Smithian, followed by generally lower values in the Spathian. Fe ranges from <0.1 to 14.9%, with an average value of 2.7%. Fe shows a similar pattern to Al throughout the study section.

At Daxiakou, Al ranges from <0.1 to 18.1%, with an average value of 2.3% (Fig. 6B). It shows lower values in the early Griesbachian and the early Smithian and higher values from the late Griesbachian through the Dienerian with a short interlude of relatively low values in the early Dienerian. Fe ranges from <0.1 to 9.0%, with an average value of 1.5%. Fe shows a similar pattern to Al within the Induan stage.

At Zuodeng, Al ranges from <0.1% to 14.3%, with an average value of 0.8% (Fig. 6C). It shows relatively higher values from the late Dienerian to the early Smithian, in the late Smithian, and in the middle Spathian but very low values in other intervals. Fe ranges from <0.1 to 5.0%, with an average value of 0.6%. Fe shows a similar pattern to Al throughout the study section except for the late Griesbachian, where the Al profile shows several peaks that the Fe profile does not.

At Mud, Al ranges from <0.1 to 11.4%, with an average value of 3.5% (Fig. 6D). It shows high values from the end of the Griesbachian to earliest Smithian and at the end of the Smithian but low values during most of the Smithian. Fe ranges from 0.4 to 20.7%, with an average value of 2.8%. Fe shows high values from the late Griesbachian to earliest Dienerian and in the early Smithian but low values during most of the Dienerian and Smithian. The Fe and Al profiles show rather different patterns in this section.

4.2. Productivity proxies

504 We used TOC, phosphorus (P), and excess barium (Ba_{xs}) concentrations to evaluate
505 marine productivity fluxes during the Early Triassic. Ba_{xs} was calculated as the amount of
506 non-detrital barium (see Supplementary Information for details). These are widely used
507 proxies for paleomarine productivity since their accumulation depends on organic matter
508 abundance and preservation (Tribovillard et al., 2006; Calvert and Pedersen, 2007). A method
509 to estimate actual paleomarine productivity values was developed by Schoepfer et al. (2014,
510 this issue), who established regression equations to evaluate primary and export production as
511 a function of TOC and P mass accumulation rates (MARs) using published data from
512 Cenozoic sediment cores.
513 At Chaohu, TOC ranges from 0.02 to 5.17%, with an average value of 0.28% (Fig. 7A).
514 It shows high values at the P-Tr boundary and in the mid Spathian, and moderately high
515 values from the late Griesbachian to early Dienerian, the late Dienerian to earliest Smithian,
516 and the mid to late Smithian. In contrast, it shows low values in the mid-Griesbachian, early
517 Smithian, and most of the Spathian. P ranges from ~0 to 0.52%, with an average value of
518 0.03%. Ba_{xs} ranges from 0.29 to 2992 ppm, with an average value of 176 ppm. Both P and
519 Ba_{xs} show patterns of variation that are similar to that of TOC, although Ba_{xs} exhibits
520 relatively higher values in the late Griesbachian and mid to late Smithian.
521 At Daxiakou, TOC ranges from 0.06 to 4.65%, with an average value of 0.30% (Fig. 7B).
522 It shows high values at the P-Tr boundary but relatively low values from the Griesbachian to
523 early Smithian. P ranges from ~0 to 2.23%, with an average value of 0.03%. It exhibits a
524 different pattern from TOC, showing relatively high values at the P-Tr boundary and in the
525 late Griesbachian to early Smithian and low values in the mid-Griesbachian and early to
526 mid-Smithian. Ba_{xs} ranges from 1.51 to 895 ppm, with an average value of 78 ppm. It shows a
527 slightly different pattern, with high values at the P-Tr boundary and from the
528 end-Griesbachian to the early Smithian and relatively lower values in the mid-Griesbachian
529 and mid-Dienerian.
530 At Zuodeng, TOC ranges from 0.06 to 1.52%, with an average value of 0.15% (Fig. 7C).
531 It shows generally low values for the entire Early Triassic, although with a small increase

during the late Griesbachian-early Dienerian and the early Smithian. P ranges from ~0 to 0.30%, with an average value of 0.01%. It exhibits a different pattern from TOC, with generally high values during the late Smithian and Spathian (punctuated by peaks in the end-Smithian and mid-Spathian) and low values from the Griesbachian to mid-Smithian. Ba_{xs} ranges from 0.39 to 920 ppm, with an average value of 40 ppm. It shows low values (<30 ppm) through most of the Early Triassic but two peaks in the mid-Dienerian and mid-Spathian.

At Mud, TOC ranges from 0.07 to 2.71%, with an average value of 0.49% (Fig. 7D). It shows high values in the Dienerian and low values in the late Griesbachian, Smithian, and early Spathian. P ranges from 0.01 to 0.85%, with an average value of 0.07%. It shows a gradual upsection decrease. Ba_{xs} ranges from 0.1 ppm to 1723 ppm, with an average value of 166 ppm. It shows high values in the Dienerian and late Griesbachian, and low values in the Smithian and early Spathian.

4.3. Redox proxies

We used Mo, U, and V concentrations to evaluate ocean redox changes during the Early Triassic. Redox-sensitive trace elements typically become enriched in marine sediments under reducing conditions (Algeo and Maynard, 2004; Algeo and Lyons, 2006; Tribovillard et al., 2006; Algeo and Tribovillard, 2009). Reducing conditions, characterized by low O_2 and/or high H_2S concentrations in bottomwaters, are produced by some combination of decreased ventilation, commonly due to sluggish watermass circulation, and high respiratory oxygen demand, commonly due to a high sinking flux of organic matter (Pedersen and Calvert, 1990).

At Chaohu, Mo ranges from ~0 to 149 ppm, with an average of 3.4 ppm (Fig. 8A). U ranges from ~0 to 52 ppm, with an average of 3.5 ppm. V ranges from <1 to 2892 ppm, with an average of 110 ppm. For all three proxies, high values are observed at the P-Tr boundary and in the late Griesbachian, Dienerian, and late Smithian. In addition, the V profile exhibits enrichment in the mid-Smithian, and both the Mo and V profiles show a short episode of

somewhat higher values in the early Spathian.

At Daxiakou, Mo ranges from ~0 to 604 ppm, with an average of 7.3 ppm (Fig. 8B). U ranges from ~0 to 39 ppm, with an average of 2.9 ppm. V ranges from <1 to 1326 ppm, with an average of 53 ppm. For all three proxies, high values are observed at the P-Tr boundary and in the Dienerian, and V shows an additional peak in the late Griesbachian that is not seen in the Mo and U profiles.

At Zuodeng, Mo ranges from ~0 to 102 ppm, with an average of 3.8 ppm (Fig. 8C). U ranges from ~0 to 68 ppm, with an average of 6.8 ppm. V ranges from ~0 to 162 ppm, with an average of 14.0 ppm. For all three proxies, high values are observed in the late Dienerian and Smithian, with additional enrichment of V in the early Spathian.

At Mud, Mo ranges from <1 to 24 ppm, with an average of 2.4 ppm (Fig. 8D). U ranges from 0.3 to 7.3 ppm, with an average of 2.0 ppm. V ranges from 10 to 528 ppm, with an average of 132 ppm. For all three proxies, high values are observed in the Dienerian.

4.4. Weathering fluxes

At Chaohu, the Al flux ranges from <0.1 to 36 g m^{-2} y^{-1}, with an average of 6.4 g m^{-2} y^{-1} (Fig. 9A). The Fe flux ranges from <0.1 to 25 g m^{-2} y^{-1}, with an average of 3.9 g m^{-2} y^{-1}. Both fluxes increase sharply at the P-Tr boundary and show peak values during the Griesbachian and Smithian, with a smaller increase in the early Spathian. The CIA ranges from 0.47 to 0.99, with an average of 0.75. High CIA values are found at the P-Tr boundary and in the Griesbachian and Smithian.

At Daxiakou, the Al flux ranges from <0.1 to 33 g m^{-2} y^{-1}, with an average of 3.8 g m^{-2} y^{-1} (Fig. 9B). The Fe flux ranges from <0.1 to 18 g m^{-2} y^{-1}, with an average of 2.7 g m^{-2} y^{-1}. Both fluxes increase sharply at the P-Tr boundary and show peak values during the Griesbachian and Smithian. The CIA ranges from 0.50 to 0.96, with an average of 0.80. High CIA values are found at the P-Tr boundary and in the late Griesbachian and Smithian, with significantly lower values in the mid-Griesbachian and Dienerian.

At Zuodeng, the Al flux ranges from <0.1 to 11.7 g m^{-2} y^{-1}, with an average of 0.46 g m^{-2} y^{-1} (Fig. 9C). The Fe flux ranges from <0.1 to 3.7 g m^{-2} y^{-1}, with an average of 0.37 g m^{-2} y^{-1}. The Fe flux is relatively larger during the late Griesbachian, whereas the Al flux is greater during the late Dienerian; both fluxes exhibit higher values during the Smithian and early Spathian. The CIA ranges from 0.39 to 0.99, with an average of 0.81. Relatively higher CIA values are observed in the Griesbachian and Smithian.

At Mud, the Al flux ranges from <0.1 to 6.2 g m^{-2} y^{-1}, with an average of 1.1 g m^{-2} y^{-1} (Fig. 9D). The Fe flux ranges from <0.1 to 3.7 g m^{-2} y^{-1}, with an average of 0.8 g m^{-2} y^{-1}. Both fluxes are large during the late Griesbachian and late Smithian, and Fe additionally shows a peak around the Dienerian-Smithian boundary. The CIA ranges from 0.40 to 0.98, with an average of 0.72. High CIA values are observed in the late Griesbachian and Smithian.

Summarizing patterns of variation in the weathering proxies, high Al and Fe concentrations are observed mainly at the P-Tr boundary and in the late Griesbachian, Dienerian, and mid to late Smithian (Fig. 6). With regard to fluxes, the main peaks in the Al and Fe profiles are at the P-Tr boundary and in the late Griesbachian and mid to late Smithian (Fig. 9). Thus, these intervals were probably associated with enhanced inputs of terrestrial detrital material to the marine study areas. The similar trends of these geochemical proxies despite differences in lithology among the four study sections suggest that lithologic variation did not exert a strong influence on these proxies. CIA values show essentially the same patterns of secular variation as the Al and Fe fluxes. This is a significant observation because CIA is independent of secular variation in bulk-sediment fluxes and, thus, serves to confirm patterns of secular variation in the other weathering proxies.

4.5. Productivity fluxes

At Chaohu, the TOC flux ranges from 0.01 to 3.9 g m^{-2} y^{-1}, with an average of 0.36 g m^{-2} y^{-1} (Fig. 10A). The P flux ranges from 0.1 to 658 mg m^{-2} y^{-1}, with an average of 48.5 mg m^{-2} y^{-1}. The Ba_{xs} flux ranges from ~0 to 451 mg m^{-2} y^{-1}, with an average of 27 mg m^{-2} y^{-1}. All three

proxies show a similar pattern of secular variation, with peak fluxes in the mid to late Griesbachian and the Smithian, and smaller increases around the P-Tr boundary and in the early Spathian.

At Daxiakou, the TOC flux ranges from <0.01 to 2.1 g $m^{-2} y^{-1}$, with an average of 0.32 g $m^{-2} y^{-1}$ (Fig. 10B). The P flux ranges from 0.5 to 6395 mg $m^{-2} y^{-1}$, with an average of 64.6 mg $m^{-2} y^{-1}$. The Ba_{xs} flux ranges from 0 to 350 mg $m^{-2} y^{-1}$, with an average of 10 mg $m^{-2} y^{-1}$. All three proxies show a similar pattern of secular variation, with peak fluxes in the Griesbachian and Smithian.

At Zuodeng, the TOC flux ranges from 0.03 to 0.93 g $m^{-2} y^{-1}$, with an average of 0.09 g $m^{-2} y^{-1}$ (Fig. 10C). The P flux ranges from 0.1 to 169.5 mg $m^{-2} y^{-1}$, with an average of 5.7 mg $m^{-2} y^{-1}$. The Ba_{xs} flux ranges from ~0 to 61 mg $m^{-2} y^{-1}$, with an average of 2 mg $m^{-2} y^{-1}$. The TOC and Ba_{xs} profiles show similar patterns of secular variation characterized by peak values in the late Griesbachian to early Dienerian, with low values through the remainder of the section. In contrast, the P profile shows peak values in the late Smithian to early Spathian, with low values through the remainder of the section.

At Mud, the TOC flux ranges from 0.01 to 1.5 g $m^{-2} y^{-1}$, with an average of 1.1 g $m^{-2} y^{-1}$ (Fig. 10D). The P flux ranges from 1.9 to 183 mg $m^{-2} y^{-1}$, with an average of 20.3 mg $m^{-2} y^{-1}$. The Ba_{xs} flux ranges from ~0 to 115 mg $m^{-2} y^{-1}$, with an average of 6 mg $m^{-2} y^{-1}$. Patterns of secular variation differ among the three productivity-proxy fluxes. The P flux profile most closely matches secular variation in the South China sections, with high values in the late Griesbachian and Smithian, and low values in the Dienerian. In contrast, the TOC flux profile for Mud peaks in the Dienerian and shows low values in the Griesbachian and Smithian, and the Ba_{xs} flux profile peaks in the mid to late Smithian and shows low values through the remainder of the section.

Summarizing patterns of variation in the productivity proxies, high TOC, P and Ba_{xs} concentrations are found mainly at the P-Tr boundary and in the late Griesbachian, Dienerian, and mid to late Smithian, with a smaller peak in the early Spathian (Fig. 7). With regard to fluxes, the main peaks in the TOC, P and Ba_{xs} profiles are in the late Griesbachian and mid to

644 late Smithian (Fig. 10). Thus, these intervals were probably associated with elevated rates of
645 marine productivity relative to the remainder of the Early Triassic. In contrast to the
646 weathering proxies, the productivity proxies exhibit low values around the P-Tr boundary,
647 suggesting a decline in marine productivity during the end-Permian crisis interval.
648
649 *4.6. Redox fluxes*
650
651 At Chaohu, the Mo flux ranges from 0.01 to 11 mg $m^{-2} y^{-1}$, with an average of 0.29 mg
652 $m^{-2} y^{-1}$ (Fig. 11A). The U flux ranges from 0.01 to 3.0 mg $m^{-2} y^{-1}$, with an average of 0.38 mg
653 $m^{-2} y^{-1}$. The V flux ranges from the 0.1 to 174 mg $m^{-2} y^{-1}$, with an average of 11 mg $m^{-2} y^{-1}$. All
654 three proxies show similar patterns of secular variation, with peak fluxes in the Griesbachian
655 and Smithian. The Mo and U profiles also show a peak around the P-Tr boundary, and the Mo
656 and V profiles show another peak in the early Spathian.
657 At Daxiakou, the Mo flux ranges from 0.01 to 2.1 mg $m^{-2} y^{-1}$, with an average of 0.19 mg
658 $m^{-2} y^{-1}$ (Fig. 11B). The U flux ranges from 0.01 to 2.6 mg $m^{-2} y^{-1}$, with an average of 0.27 mg
659 $m^{-2} y^{-1}$. The V flux ranges from 0.01 to 73 mg $m^{-2} y^{-1}$, with an average of 5.9 mg $m^{-2} y^{-1}$. All
660 three proxies show similar patterns of secular variation, with peak fluxes in the Griesbachian
661 and Smithian. The Mo and U profiles also show a peak around the P-Tr boundary.
662 At Zuodeng, the Mo flux ranges from 0.01 to 7.4 mg $m^{-2} y^{-1}$, with an average of 0.24 mg
663 $m^{-2} y^{-1}$ (Fig. 11C). The U flux ranges from 0.01 to 3.7 mg $m^{-2} y^{-1}$, with an average of 0.41 mg
664 $m^{-2} y^{-1}$. The V flux ranges from 0.01 to 6.4 mg $m^{-2} y^{-1}$, with an average of 0.83 mg $m^{-2} y^{-1}$. The
665 three proxies show similar patterns of secular variation, although with minor differences. Peak
666 values are in the late Dienerian and Smithian for the Mo flux profile, in the mid-Griesbachian,
667 late Dienerian, and Smithian for the U flux profile, and in the Griesbachian, early Dienerian,
668 late Dienerian, and Smithian for the V flux profile.
669 At Mud, the Mo flux ranges from 0.01 to 0.35 mg $m^{-2} y^{-1}$, with an average of 0.06 mg m^{-2}
670 y^{-1} (Fig. 11D). The U flux ranges from 0.01 to 0.41 mg $m^{-2} y^{-1}$, with an average of 0.07 mg m^{-2}
671 y^{-1}. The V flux ranges from 0.49 to 20 mg $m^{-2} y^{-1}$, with an average of 3.5 mg $m^{-2} y^{-1}$. The three

672 proxies show similar patterns of secular variation, with peak values in the late Smithian. The
673 Mo and V profiles exhibit a second, but somewhat smaller, peak in the Dienerian.
674 Summarizing patterns of variation in the redox proxies, high Mo, U and V concentrations
675 are found mainly at the P-Tr boundary and in the late Griesbachian, Dienerian, and mid to late
676 Smithian (Fig. 8). With regard to fluxes, the main peaks are in the Griesbachian and Smithian,
677 although modest increases are found also at the P-Tr boundary and in the early Spathian (Fig.
678 11) and at Mud during the Dienerian. Thus, these intervals were probably associated with
679 more reducing conditions in marine environments than the remainder of the Early Triassic.
680 Secular variation in the redox proxies broadly mirrors that seen for the weathering and
681 productivity proxies, suggesting close connections between all three environmental
682 parameters.
683
684 **5. Discussion**
685
686 *5.1. Relationship of weathering, productivity, and redox variation to Early Triassic global*
687 *events*
688
689 The results above document major secular changes in weathering, productivity, and
690 redox fluxes during the Early Triassic. In the following discussion, we consider relationships
691 of these environmental proxies to coeval global events, in order to explore potential controls
692 on the protracted recovery of Early Triassic marine ecosystems. Our analysis begins with the
693 end-Permian mass extinction and proceeds through the Spathian, thus covering the full Early
694 Triassic recovery interval.
695 The end-Permian crisis is generally regarded as having been triggered by the onset of
696 massive eruptions of the Siberian Traps Large Igneous Province (Renne et al., 1995; Korte et
697 al., 2010). It was marked by a general collapse of marine ecosystems, as reflected in
698 biodiversity, trace fossil, and ecological tiering data (Erwin et al., 2002; Erwin, 2005; Fig. 12).
699 This event was accompanied by an extreme climatic warming of >10°C (Joachimski et al.,

2012; Sun et al., 2012), a major expansion of oceanic anoxia globally (Brennecka et al., 2011), an abrupt incursion of sulfidic waters into the ocean-surface layer (Grice et al., 2005; Algeo et al., 2007, 2008), and large inputs of terrestrial material to shallow-marine areas (Ward et al., 2000; Sephton et al., 2005; Xie et al., 2007; Algeo and Twitchett, 2010), all of which are likely to have contributed to the biocrisis. Strong warming led to intensified stratification of the oceanic water-column, as reflected in a large vertical gradient of $\delta^{13}C_{DIC}$ (Song-HY et al., 2013), and thus to a strongly reduced nutrient supply via upwelling, contributing to a sharp decline in marine productivity. The study sections exhibit only limited evidence for these major environmental changes, however, as the end-Permian and P-Tr boundary are characterized by, at most, a small increase in terrestrial weathering fluxes (Fig. 9) and a transient shift toward more reducing conditions (Fig. 11; cf. Grice et al., 2005; Cao et al., 2009). The muted response of the terrestrial weathering and marine redox proxies in the study sections may be due to their distance from continental sources of siliciclastics and locations in areas with only limited local redox changes. Marine productivity exhibits a more visible change, declining sharply particularly across the South China craton (Fig. 10), a pattern possibly related to a productivity crash (Algeo et al.,2013) or to a shift in dominance from eukaryotic algae to bacterioplankton (Luo et al., 2014).

During the Griesbachian, the development of a hyper-greenhouse climate resulted in tropical sea-surface temperatures that were persistently >35°C (Fig. 12; Sun et al., 2012). This warming contributed to expansion of marine anoxia (Fig. 11) through lowering of the solubility of dissolved oxygen in seawater and increasing the flux of river-borne nutrients to shallow-marine areas via enhanced chemical weathering (Fig. 9; Algeo and Twitchett, 2010). A consistently positive relationship is seen between redox conditions and marine productivity (Fig. 12), suggesting that organic carbon sinking fluxes controlled the expansion of oceanic oxygen-minimum zones (Algeo et al., 2011a). High seawater temperatures and widespread reducing conditions probably operated in tandem to keep benthic biotas under stress and to delay marine ecosystem recovery. As a result, benthic biotas were dominated by opportunistic

727 lineages of eurytopic bivalves, gastropods, and ostracods (Erwin, 1998). Relatively high
728 productivity levels during the Griesbachian (Fig. 10) offered adequate food resources for
729 nekton, resulting in a transient diversification among conodonts and ammonoids (Stanley,
730 2009). High productivity may reflect dominance of bacterioplankton (Xie et al., 2010; Luo et
731 al., 2014), which would have enhanced recycling of nutrients in the ocean-surface layer and
732 reduced the organic carbon sinking flux (D'Hondt et al., 1998) and, thus, account for a
733 decrease in the vertical gradient of $\delta^{13}C_{DIC}$ (Song-HY et al., 2013). However, at the end of
734 Griesbachian, extreme warmth (Sun et al., 2012) and more widespread oceanic anoxia (Fig.
735 11) destroyed this surface-ocean ecosystem, resulting in a second-order mass extinction
736 among conodonts and ammonoids (Brayard et al., 2006; Orchard, 2007; Stanley, 2009) and
737 further depressing the benthic ecosystem. Expansion of the oceanic oxygen-minimum zone at
738 this time would have resulted in a contraction of the ecospace available to planktic and nektic
739 organisms (Fig. 13A).
740 The Dienerian was characterized by a warm climate, although one that was slightly
741 cooler (~32-35°C) than that of the late Griesbachian (Fig. 12; Sun et al., 2012). As a
742 consequence of this relative cooling, terrestrial weathering fluxes were reduced (Fig. 9). In the
743 marine environment, the Dienerian was characterized by lower marine productivity (Fig. 10)
744 and a shift toward more oxidizing (or less reducing) conditions (Fig. 11). This substage was
745 associated with a small negative excursion of $\delta^{13}C_{carb}$ (Tong et al., 2007a) and intermediate
746 and relatively stable vertical $\delta^{13}C_{DIC}$ gradients (Song-HY et al., 2013), which are consistent
747 with reduced marine productivity as well as a modest weakening of oceanic water-column
748 stratification. With regard to marine biotas, the Dienerian exhibits increasing diversity among
749 conodonts and ammonoids (Stanley, 2009) and other marine fauna (Tong et al., 2007a) and an
750 increase in trace-fossil size (Twitchett, 1999; Chen et al., 2011; Fig. 2). Lower levels of
751 oceanic productivity were probably associated with a greater proportion of eukaryotic
752 plankton relative to bacterioplankton, which favored relatively greater export of organic
753 carbon and nutrients from the ocean-surface layer (cf. D'Hondt et al., 1998). Comparatively

754 cooler climatic conditions and contraction of the oceanic oxygen-minimum zone would have
755 resulted in an expansion of the ecospace available to conodonts and ammonoids in the surface
756 ocean (Fig. 13B). Thus, somewhat less severe environmental conditions in the Dienerian
757 (relative to the Griesbachian) triggered a limited marine ecosystem recovery, although the
758 brief interval since the end-Permian mass extinction (~0.5 Myr) may have insufficient for a
759 complete recovery of marine ecosystems (e.g., Kirchner and Weil, 2000).

760 The Dienerian-Smithian boundary was characterized by a transient temperature
761 minimum (~30-32°; Sun et al., 2012) and a large positive excursion (ca. +6‰) of $\delta^{13}C_{carb}$
762 globally (Payne et al., 2004; Tong et al., 2007a; Fig. 12). Positive $\delta^{13}C$ excursions are
763 commonly associated with elevated marine productivity (Kump and Arthur, 1999). All four
764 study sections show a substantial increase in terrestrial weathering fluxes at this time (Fig. 9),
765 with two (Chaohu and Daxiakou) also showing evidence of increased marine productivity
766 (Fig. 10). This pattern suggests that the increase in marine productivity may have been driven
767 by enhanced riverine nutrient fluxes, possibly with an additional stimulus from upwelling of
768 nutrient-rich deep waters owing to more vigorous thermohaline circulation as a consequence
769 of climatic cooling and a steeper latitudinal temperature gradient. A concurrent shift toward
770 somewhat more reducing conditions (Fig. 11) may have been driven by high O_2 demand
771 associated with an enhanced sinking flux of organic matter. With regard to marine biotas, this
772 interval witnessed the maximum diversification of conodonts and ammonoids during the
773 Early Triassic (Stanley, 2009; Fig. 12), and a limited increase in the diversity of echinoderms,
774 brachiopods, and forams (Chen et al., 2005; Chen and McNamara, 2006; Song et al., 2011),
775 suggesting improvements in both the ocean-surface and benthic ecosystems. Cooler
776 temperatures and a contraction of oceanic oxygen-minimum zones resulted in an expansion of
777 the ecospace available to marine faunas, and high productivity offered rich food resources for
778 this ecosystem (Brayard et al., 2006; Orchard, 2007; Stanley, 2009). Enhanced oceanic
779 overturning circulation generally results in improved ventilation of the global ocean (resulting
780 in more ecospace availability), while simultaneously intensifying anoxia in limited areas of
781 active upwelling (owing to greater nutrient fluxes to the ocean surface layer). The

782 Dienerian-Smithian boundary thus represents an episode of significantly ameliorated marine
783 environmental conditions prior to the onset of the Smithian crisis, and it may have laid a
784 foundation for more rapid ecosystem recovery at the beginning of the Spathian, ~0.5 Myr
785 later (e.g., Erwin, 2008; Chen and Benton, 2012).

786 The Smithian coincided with a major environmental and biotic crisis within the Early
787 Triassic. It was characterized by development of a second hyper-greenhouse, with peak
788 temperatures >38°C (Sun et al., 2012; Romano et al., 2013), a large negative excursion of
789 $\delta^{13}C_{carb}$ (Payne et al., 2004; Tong et al., 2007), and a maximum vertical gradient in the $\delta^{13}C$ of
790 DIC (Song-HY et al., 2013; Fig. 12). The negative shift in $\delta^{13}C_{carb}$ is likely to reflect a strong
791 decline in marine productivity, and the large vertical $\delta^{13}C$ gradient an intensification of
792 oceanic water-column stratification, both in response to extreme warming of the
793 ocean-surface layer. In the study sections, the Smithian exhibits a large increase in terrestrial
794 weathering fluxes (Fig. 9), reflecting stronger chemical weathering due to warming, and
795 intensified marine anoxia (Fig. 11), due to a combination of riverine nutrient inputs and
796 stronger water-column stratification. Productivity levels appear to have increased at this time
797 in two of the study sections (Chaohu and Daxiakou; Fig. 10), although it is possible that these
798 deep-water sections are recording enhanced organic matter preservation as a consequence of
799 OMZ expansion rather than actual increases in surface-water productivity. Warming and other
800 environmental stresses resulted in a major extinction event among conodonts and ammonoids
801 at the end of the Smithian (Brayard et al., 2006; Orchard, 2007; Stanley, 2009; Fig. 12).
802 Expansion of the oceanic oxygen-minimum zone at this time would have resulted in a
803 contraction of the ecospace available to planktic and nektic organisms (Fig. 13C).

804 The Spathian marks the onset of a sustained recovery of marine ecosystems that was
805 completed in the Middle Triassic (Bottjer et al., 2008; Chen and Benton, 2012). It was
806 characterized by a pronounced climatic cooling from the hyper-greenhouse conditions of the
807 preceding ~2 Myr, with tropical sea-surface temperatures falling to ~30-32°C (Sun et al.,
808 2012; Romano et al., 2013; Fig. 12). In the study sections, it is marked by large declines in

terrestrial weathering fluxes, marine productivity, and the intensity of marine anoxia (Figs. 9-11). The decline in productivity can be attributed to a reduced supply of nutrients from riverine sources following climatic cooling and stabilization of terrestrial landscapes (Looy et al., 1999, 2001; Hermann et al., 2011) and from upwelling sources following a flushing out of the deep-ocean nutrient inventory as a result of re-invigorated thermohaline circulation at the Smithian-Spathian boundary (Zhang et al., 2014). Improved ocean ventilation and reduced organic carbon sinking fluxes were responsible for a shift toward less reducing conditions globally (Fig. 12). These environmental changes coincided with a gradual rediversification of pelagic organisms, rapid rediversification among benthic organisms and trace-makers, and higher-level integration of marine trophic systems (Chen et al., 2005; Orchard, 2007; Stanley, 2009; Song et al., 2011; Chen et al., 2011; Chen and Benton, 2012). The more sustained ecosystem recovery of the Spathian relative to the Dienerian can be attributed to several factors, including a longer time interval, a cooler climate, less widespread marine anoxia, and generally more stable environmental conditions (Fig. 13D).

5.2. Spatial variation in Early Triassic marine environmental conditions

Although the four study sections generally show similar patterns of secular variation in weathering, productivity, and redox proxies, some differences exist among the sections that are probably controlled by paleogeographic location, water depth, and local bathymetry. First, the deep-ramp sections (Chaohu and Daxiakou) show peak weathering fluxes that are ~3X greater than for the mid-shelf section (Mud) and ~10X greater than for the shallow-platform section (Zuodeng; Fig. 9). These differences reflect relative proximity to sources of detrital siliciclastics and local bathymetry (e.g., the relative isolation of the shallow-platform section from detrital influx). Second, average CIA values are somewhat higher in the peri-equatorial South China sections (~0.75-0.80) relative to the mid-latitude Mud section (0.72), a difference that is attributable to variations in weathering intensity as a function of climate. Third, productivity proxy fluxes show some variation among the study sections (Fig. 10). Fluxes are

similar for Chaohu, Daxiakou, and Mud but lower for Zuodeng, suggesting diminished marine productivity on shallow-platform tops relative to open-marine ramp and shelf settings. Fourth, redox proxy fluxes differ significantly among the study sections, with Chaohu exhibiting comparatively large fluxes, Daxiakou and Zuodeng intermediate fluxes, and Mud small fluxes (Fig. 11). These differences appear to be related to both water depth and paleogeographic location. Chaohu was the deepest section, with water depths of ~300-500 m putting it within the ocean thermocline and, thus, subject to influence by an expanding oxygen-minimum zone. However, the higher redox proxy fluxes for all South China sections relative to Mud suggest that the eastern Paleo-Tethys Ocean was subject to generally more strongly reducing conditions than the southern Neo-Tethys Ocean during the Early Triassic (Fig. 4B). Finally, all types of proxies exhibit a better-defined pattern of secular variation in the deep-ramp sections (Chaohu and Daxiakou) than elsewhere (Figs. 9-11). We attribute this relationship to differences in depositional water depth, which was >200 m for the deep-ramp sections but <100 m for the mid-shelf and shallow-platform sections (Section 3). With increasing water depths, sections were under greater influence by the oceanic oxygen-minimum zone, expansion of which occurred over discrete time intervals (Feng and Algeo, 2014). In contrast, the study sections located within the ocean-surface layer (<100 m) may have experienced more irregular secular variation in environmental conditions.

5.3. Influences on weathering, productivity, and redox fluxes

Modeling of geochemical proxy fluxes suggests a close relationship of changes in terrestrial weathering intensity, marine productivity rates, and ocean redox conditions throughout the Early Triassic (Figs. 9-11). Our interpretation, as presented above, is that this covariation reflects real relationships among these environmental parameters. Specifically, higher weathering intensities tend to result in increased riverine nutrient fluxes, leading to enhanced marine productivity (at least in coastal areas), and thus to intensified marine anoxia (again, possibly focused in coastal areas) (cf. Algeo et al., 1995, 2011a). These relationships

865 are natural consequences of strong climate warming, as occurred repeatedly during the Early
866 Triassic (Fig. 12; Joachimski et al., 2012; Sun et al., 2012; Romano et al., 2013). We
867 recognize, however, that the relationships among these environmental parameters may vary in
868 detail and can have alternative linkages. For example, expansion of marine anoxia can
869 potentially lead to enhanced organic carbon burial fluxes in the absence of any change in
870 marine productivity. We also recognize that the patterns exhibited by the four study sections
871 inherently represent local marine environmental conditions (Fig. 13) that may or may not
872 mirror contemporaneous global oceanographic changes. However, the strong similarities
873 among some of the study sections, particularly those deposited at deeper water depths (i.e.,
874 Chaohu and Daxiakou), suggest that our results have probably captured some aspect of global
875 marine environmental changes during the Early Triassic.
876 An additional important influence on the proxy fluxes is sediment bulk accumulation rate
877 (BAR). These fluxes represent the multiplicative product of raw proxy concentrations and
878 BAR (Supplementary Information), so an increase in either input variable can lead to higher
879 calculated fluxes. The observation that, for each study section, the concentration profiles (Figs.
880 6-8) and flux profiles (Figs. 9-11) tend to exhibit similar features reflects the influence of raw
881 concentrations on calculated fluxes. However, a degree of auto-correlation among the various
882 proxy fluxes results from the use of a common age-thickness model for each study section
883 and is unavoidable in studies of this type. The analysis of four widely separated sections (note
884 that the three Chinese sections cover >1500 km of the South China craton) helps to
885 compensate for this situation and serves as a test of the validity of results because each study
886 section makes use of an independent, site-specific age-thickness model (e.g., Section 5.2).
887 Moreover, our use of CIA also provides a check on the degree of procedural auto-correlation
888 of results because CIA is a proxy that is completely independent of BAR. CIA shows
889 unambiguous positive covariation with BAR-based weathering proxies (i.e., Al and Fe) in the
890 Chaohu, Daxiakou, and Mud sections (Fig. 9), in which CIA exhibits maxima at the PTB or
891 early Griesbachian, the late Griesbachian, the Dienerian-Smithian boundary or early Smithian,
892 and the Smithian-Spathian boundary. The weathering proxies in general do not show a

893 coherent pattern of secular variation in the third study section (Zuodeng), possibly because its
894 paleodepositional setting (i.e., a shallow-marine carbonate platform) was not conducive to
895 recording weathering fluxes.
896
897 *5.4. Recovery patterns following other Phanerozoic mass extinctions*
898
899 The marine ecosystem recovery following the end-Permian mass extinction is regarded
900 as having been longer than those following other major Phanerozoic biocrises (Bottjer et al.,
901 2008; Chen and Benton, 2012), although a detailed comparison with other recovery events
902 has been lacking to date. In the following analysis, we examine patterns of marine ecosystem
903 recovery following the other four "Big Five" Phanerozoic mass extinctions and consider their
904 relationship to contemporaneous environmental conditions. This analysis reveals both
905 commonalities and dissimilarities in the ecosystem recoveries following different mass
906 extinction events.
907 The Cretaceous-Paleogene (K-Pg; formerly the Cretaceous-Tertiary, or K-T) boundary
908 mass extinction at 66.0 Ma (Renne et al., 2013) is the most thoroughly investigated to date. It
909 killed off ~50% of marine genera and ~70% of species (Jablonski and Chaloner, 1994;
910 Sepkoski, 1998; Alroy et al., 2008), with high extinction rates among marine reptiles,
911 ammonoids, rudist bivalves, planktonic foraminifera, and calcareous nanofossils (Pospichal,
912 1994; Marshall and Ward, 1996; Arenillas et al., 2000; Bown, 2005; Fastovsky and Sheehan,
913 2005; Fig. 14A). The coincidence in timing between the Chicxulub bolide impact and the
914 K-Pg boundary extinction suggests that the impactor was the major cause of this mass
915 extinction (Jolley et al., 2010; Renne et al., 2013), although the lethality of the impact may
916 have been enhanced by long-term environmental stresses associated with the Deccan Traps
917 eruptions (Courtillot et al., 1986; Courtillot et al., 1988; White and Saunders, 2005; Chenet et
918 al., 2007).
919 Algal primary productivity may have recovered very rapidly, in less than a century
920 following the K-Pg boundary impact (Fig. 14A, Sepúlveda et al., 2009). However,

redevelopment of an integrated marine ecosystem with extended trophic chains took longer and proceeded in two stages: a rapid initial phase and a delayed second phase (Coxall et al., 2006). The initial phase took about 1 Myr (Sepúlveda et al., 2009; Hull et al., 2011; Alegret, 2012) and involved recovery of planktonic organisms such as dinoflagellates (Brinkhuis et al., 1998; Hildebrand-Habel and Streng, 2003), planktic foraminifera (Coccioni and Luciani, 2006; Hull et al., 2011), and radiolarians (Hollis et al., 2003), as well as coralline red algae (Aguirre et al., 2007). The delayed second phase of recovery lasted for ~4 Myr following the boundary crisis (Coxall et al., 2006) and culminated in a new diversity peak among planktic foraminifera (Olsson et al., 1999) and re-establishment of reef communities (Baceta et al., 2005).

The nutrient status of the early Danian ocean remains controversial, with some studies inferring high nutrient levels (Alegret and Thomas, 2009; Alegret et al., 2012) and others low nutrient levels (Coxall et al., 2006; Fuqua et al., 2008). Warmer conditions (as documented by a $\delta^{18}O$ shift; Fig. 14A) caused the oceanic oxygen-minimum zone to expand, decreasing the ecospace available to pelagic organisms. These adverse conditions abated 3-4 Myr after the K-Pg boundary crisis, stimulating an increase in pelagic biodiversity and full redevelopment of the marine food web (Coxall et al., 2006; Yamamoto et al., 2010). The post-K-Pg-boundary recovery can be traced through carbon cycle changes in the early Paleocene (Fig. 14A). The vertical (shallow-to-deep) $\delta^{13}C$ gradient in seawater DIC increased in two steps, corresponding to the two stages of ecosystem recovery (Coxall et al., 2006, Fig. 14A). The first step is marked by an increase in $\Delta^{13}C_{vert}$ from 0 to ~1‰ within 1 Myr of the crisis, and the second step by an increase to ~2‰ within 3 million years of the crisis. The latter value is similar to the $\Delta^{13}C_{vert}$ observed in modern marine systems and, thus, marks the re-establishment of an efficient biological pump by the late Danian, that is, less intense recycling of organic matter in the ocean-surface layer resulted in more export to the chemocline and deep ocean (D'Hondt et al., 1998; Coxall et al., 2006).

The Triassic-Jurassic (Tr-J) boundary mass extinction resulted in the demise of ~53% of

948 marine genera (Sepkoski, 1996) and ~80% of species (Sepkoski, 1994). It eliminated
949 conodonts and severely affected brachiopods and gastropods (McRoberts et al., 1997;
950 Tomašových and Siblík, 2007), as well as ammonoids, bivalves, corals and ostracods
951 (McRoberts and Newton, 1995; Kiessling, 2001, 2005; van de Schootbrugge et al., 2007;
952 Mander and Twitchett, 2008; Fig. 14B). Eruption of the Central Atlantic magmatic province
953 (CAMP) and the resulting global warming were the major causes of this mass extinction
954 (Marzoli et al., 1999; McElwain et al., 1999; Hesselbo et al., 2002; van de Schootbrugge et al.,
955 2009; Schoene et al., 2010; Ruhl et al., 2011).
956 Marine ecosystem recovery began rapidly in the Early Jurassic, within 120 k.y. (Ruhl et
957 al., 2010) to 290 k.y. of the extinction event (Bartolini et al., 2012). Recovery was marked by
958 increases in diversity during the earliest Hettangian among pelagic carbonate producers
959 (radiolarians, calcareous nanofossils) (Clémence et al., 2010), molluscs (McRoberts et al.,
960 1997), ammonoids (Hesselbo et al., 2002; Guex et al., 2012), and brachiopods (Tomašových
961 and Siblík, 2007). This initial recovery (Fig. 14B) was followed by a second extinction event
962 among ammonoids during the early Hettangian (Guex et al., 2004, 2012). A second, longer
963 (~2-3-Myr) recovery phase (Fig. 14B) is evidenced by more diverse radiolarian assemblages
964 in the mid to late Hettangian (Longridge et al., 2007), rediversification of ammonoids in the
965 late Hettangian (Guex et al., 2012), and increases in the diverse of gastropod and coral faunas
966 in the early Sinemurian (Seuß et al., 2005).
967 A large (~5‰), rapid negative carbon isotope excursion occurred at the end of Triassic
968 (Korte et al., 2009; Schoene et al., 2010; Bartolini et al., 2012), and was followed a positive
969 excursion (~3%) in the lower Hettangian (Williford et al., 2007; Korte et al., 2009; Schoene et
970 al., 2010; Bartolini et al., 2012; Fig. 14B), suggesting an extreme carbon cycle disturbance at
971 the T-J boundary. Paleobotanical data provide evidence of a rapid global warming at the T-J
972 boundary (McElwain et al., 1999; Ruhl et al., 2011), and a subsequent cooling resulted from
973 high marine productivity and enhanced organic matter burial (Korte et al., 2009). A long-term
974 negative carbon isotope excursion during the early and middle Hettangian coincided with a
975 greenhouse climate and widespread oceanic anoxia (Ruhl and Kürschner, 2011; Richoz et al.,

976 2012; Bartolini et al., 2012), hindering the recovery of marine ecosystems until the
977 Hettangian-Sinemurian boundary (Bartolini et al., 2012; van de Schootbrugge et al., 2013),
978 when the carbon cycle stabilized (Bartolini et al., 2012; Guex et al., 2012). The initial
979 recovery of pelagic and benthic organisms during the early Hettangian was impeded first by
980 large climate fluctuations and then by a long-term global warming that resulted in marine
981 environmental stresses including warming, seawater acidification, and anoxia (Richoz et al.,
982 2012; van de Schootbrugge et al., 2013). These factors contributed to an extinction event
983 among ammonoids in the mid-Hettangian and a protracted recovery among many elements of
984 the marine nekton and benthon during the Hettangian (Guex et al., 2004, 2012). Falling
985 atmospheric pCO_2 by the late Hettangian resulted in a cooler climate and ameliorated marine
986 environmental conditions, leading to a second stage of recovery among plankton (Bartolini et
987 al., 2012) and benthon (Seuß et al., 2005) during the Sinemurian stage. Thus, the Early
988 Jurassic marine ecosystem recovery tracks contemporaneous environmental changes very
989 well.

990 The Late Devonian mass extinction comprised a series of crises during an interval of ~20
991 Myr, of which the largest were at the Givetian-Frasnian (G-F), Frasnian-Famennian (F-F), and
992 Devonian-Carboniferous (D-C) boundaries (Walliser, 1996, House, 2002; Morrow et al., 2011;
993 Fig. 14C). Collectively, these crises killed ~50-60% of marine genera and ~82% of species
994 (Jablonski, 1991; McGhee, 1996). Many clades of marine invertebrates suffered multiple
995 declines, including brachiopods, trilobites, corals, and stromatoporoids (Copper, 1986; Stearn,
996 1987), and most colonial rugose corals went extinct at the F-F boundary (Fig. 14C, Copper,
997 2002; Shen and Webb, 2004). The F-F mass extinction evidenced a collapse of the metazoan
998 reef ecosystem after the mid-late Devonian acme of metazoan reefs and a replacement by
999 microbial reefs (Copper, 2002).

1000 The immediate cause of the Late Devonian crisis appears to have been rapid changes in
1001 seawater temperatures and redox conditions (Joachimski et al., 2004; Chen et al., 2005). For
1002 example, the F-F cooling event severely affected the tropical-marine ecosystem, especially
1003 reef metazoans and, thus, is the probable cause of this mass extinction (Copper, 1986, 2002).

1004 However, the ultimate cause of the Late Devonian crisis is likely to have been the spread of
1005 higher land plants and consequent changes in nutrient cycling (Algeo et al., 1995, 2001;
1006 Algeo and Scheckler, 1998). A progressive expansion of terrestrial floras during the Devonian
1007 resulted in intensified chemical weathering of land areas, releasing more nutrients that
1008 stimulated algal blooms and a consequent expansion of anoxia in epicontinental seas. These
1009 paleobotanical developments resulted in a long-term decline in atmospheric pCO_2 owing to an
1010 increase in both organic carbon burial and silicate weathering, resulting in strong global
1011 climatic cooling (Algeo et al., 1995). The Late Devonian was a time of transition from the
1012 Middle Paleozoic greenhouse to the Late Paleozoic icehouse (Fig. 14C; Isaacson et al., 2008).
1013 Each of the Late Devonian crises coincided with a major global cooling event, the episodes at
1014 the F-F and D-C boundaries being particularly pronounced (Joachimski et al., 2004; Buggisch
1015 and Joachimski, 2006; Kaiser et al., 2006, 2008). It is not certain whether the spread of higher
1016 land plants was gradual and merely created background conditions for the development of
1017 episodic marine biocrises, or whether it actively triggered each crisis through pulses of
1018 expansion (Algeo and Scheckler, 2010).

1019 Because of the multi-episode nature of the crisis, there was at least a partial recovery of
1020 marine ecosystems following each extinction event. For example, brachiopods and ostracods
1021 underwent a modest recovery during early Famennian, following the F-F boundary event,
1022 although they remained low in diversity (Casier and Lethiers, 1998; Baliński, 2002; Sokiran,
1023 2002, Fig. 14C), and stromatoporoids began to recover during the early and middle
1024 Famennian but went extinct at the D-C boundary (Metherell and Workman, 1969; Stearn,
1025 1987; Webb, 1998). A permanent recovery did not begin until after the D-C boundary crisis.
1026 Bryozoans recovered to their pre-extinction level of diversity during the Early Carboniferous
1027 (Bigey, 1989). Some corals (e.g., *Pseudouralinia*, *Siphonophyllia*) and brachiopods (e.g.,
1028 *Eochoristites*, *Martiniella*) recovered in the middle Tournaisian of the Early Carboniferous
1029 (Liao, 2002). The extinction of colonial rugose corals at the F-F boundary resulted in
1030 replacement of metazoan reefs by small microbial patch reefs (Pickett and Wu, 1990; Webb,
1031 1998; Morrow et al., 2011), with regrowth of large barrier reefs delayed until the Visean (Dix

and James, 1987; Webb, 1998, 1999; Wahlmann, 2002; Fig. 14C). Loss of large metazoans during this crisis permitted the establishment of novel ecologies dominated by microbial communities (Wood, 2004). However, the final marine ecosystem recovery required the high-trophic-level ecosystem community establishment (e.g., Chen and Benthos, 2012).

The Late Ordovician (Hirnantian) mass extinction (Fig. 14D) eliminated ~24% of families and 85% of species of marine invertebrates (Jablonski, 1991; Sepkoski, 1996; Brenchley et al., 2001; Sheehan, 2001). It was particularly severe among trilobites, brachiopods, molluscs (Sepkoski, 1984; Adrain et al., 2000; Harper and Rong, 2008), and graptolites and conodonts (Brenchley et al., 2001; Sheehan, 2001; Fan and Chen, 2007; Rasmussen and Harper, 2011a,b). The immediate cause of this extinction was the Hirnantian glaciation (Brenchley et al., 1995; Gibbs et al., 1997; Sheehan, 2001; Sutcliffe et al., 2006). A second extinction, ~1 Myr later, decimated the cool-adapted 'Hirnantian fauna' and was caused by a rapid termination of glaciation (Sheehan and Coorough, 1990). The Early Silurian (Llandovery epoch) was a transitional interval from the Late Ordovician icehouse to a middle Paleozoic greenhouse (Kaljo and Martma, 2000; Brand et al., 2006). Warming conditions, the killing factor in the second extinction, prevailed during the Llandovery, although interrupted by two brief glaciations during the Aeronian stage (Caputo, 1998; Azmy et al., 1998, 1999; Delabroye et al., 2011; Finnegan et al., 2011; Fig. 14D).

Marine ecosystems began to recover following the end-Ordovician extinctions, although climate fluctuations during the Aeronian stage complicated the recovery pattern. Microbialite resurgence in the immediate aftermath of the Late Ordovician extinction coincided with an interval of low-diversity megafaunal communities (Sheehan and Harris, 2004). Diversification of brachiopods and trilobites proceeded during the Rhuddanian, the first stage of the Early Silurian (Krug and Patzkowsky, 2004; Owen et al., 2008; Huang et al., 2012), representing the initial recovery of marine faunas (Fig. 14D). Crinoids and coral began to diversify from the Rhuddanian in the Early Silurian (Kaljo, 1996; Ausich and Deline, 2012). Climate fluctuations during the Llandovery resulted in a delay in the recovery of marine ecosystems (Copper, 2001; Gouldey et al., 2010). Full recovery of reef ecosystems took place

by the mid-Aeronian stage, ~4 Myr after the end-Ordovician crisis (Copper, 2001).

5.5. Evaluation of hypotheses regarding controls on marine ecosystem recovery

Three hypotheses have been advanced for the apparent delay in recovery of marine ecosystems following the end-Permian mass extinction, linking the duration of the recovery interval to: (1) the intensity of the mass extinction (Sepkoski, 1984; Solé et al., 2002), (2) the persistence of harsh environmental conditions (Hallam, 1991; Isozaki, 1997; Payne et al., 2004; Erwin, 2007), and (3) episodic occurrence of strong environmental disturbances during the recovery interval (Algeo et al., 2007, 2008; Orchard, 2007; Retallack et al., 2011; Fig. 1). Our analysis above of four Lower Triassic sections (Chaohu, Daxiakou, Zuodeng, and Mud) demonstrates unambiguously that there were large fluctuations in marine environmental conditions during the Early Triassic, and these disturbances were linked to transient biodiversity crises among coeval marine faunas and relapses in marine ecosystem complexity and integration. We conclude that episodic environmental disturbances were integral to the pattern and pace of marine ecosystem recovery during the Early Triassic.

Is it possible to draw general inferences about controls on marine ecosystem recovery following mass extinctions? With regard to duration, there is considerable variation among the recovery intervals following the "Big Five" Phanerozoic mass extinctions. If defined on the basis of (1) re-attainment of biodiversity equal to or exceeding pre-crisis levels, and (2) re-development of stable, well-integrated trophic systems, then the duration of the recovery interval was ~4 Myr for the end-Ordovician crisis, ~10 Myr for the F-F crisis, ~5 Myr for the end-Permian crisis, ~2.5 Myr for the end-Triassic crisis, and ~3 Myr for the end-Cretaceous crisis (Fig. 14). These durations are closely linked to the interval of disturbed environmental conditions that followed each extinction event. The shortest recovery interval, ~2.5 Myr after the end-Triassic crisis, was associated with rapid cooling with minimal climate fluctuations during the earliest Jurassic (Korte et al., 2009), suggesting that amelioration of marine environmental conditions proceeded quickly following the CAMP eruptions (Marzoli et al.,

1088 1999; McElwain et al., 1999; Hesselbo et al., 2002; Schoene et al., 2010; Ruhl et al., 2011).
1089 The ~3-Myr-long interval of recovery following the end-Cretaceous crisis was also associated
1090 with comparatively stable environmental conditions during the early Paleogene (Coxall et al.,
1091 2006). In contrast, the longest recovery interval, ~10 Myr after the F-F crisis, was interrupted
1092 by two glaciation episodes (Joachimski et al., 2004; Kaiser et al., 2006, 2008; Isaacson et al.,
1093 2008) during which environmental conditions deteriorated and marine ecosystem recovery
1094 was halted or reversed (Chen et al., 2005). The second-longest recovery interval, ~5 Myr after
1095 the end-Permian crisis, was also associated with repeated environmental disturbances (Algeo
1096 et al., 2007, 2008; Retallack et al., 2011). Thus, unsettled environmental conditions following
1097 the main extinction crisis appear to be a strong control on the pattern and pace of marine
1098 ecosystem recovery.

1099 Various types of environmental perturbations can contribute to destabilization of
1100 recovering marine ecosystems. First, temperature is clearly important, as most marine
1101 creatures are adapted to live within a relatively narrow temperature range (Brenchley and
1102 Harper, 1998). Extreme temperatures were a major factor in delayed ecosystem recovery
1103 during the Early Triassic (Sun et al., 2012; Romano et al., 2013), and strong climate
1104 fluctuations were important during other recovery intervals, e.g., the Late Devonian
1105 (Joachimski et al., 2004; Buggisch and Joachimski, 2006; Isaacson et al., 2008) and the Early
1106 Silurian (Finney et al., 1999; Gouldey et al., 2010; Finnegan et al., 2011). Second, nutrient
1107 inventories and patterns of nutrient cycling can be important. Changes related to shifts from
1108 eukaryotic to microbial primary production following the end-Cretaceous (D'Hondt et al.,
1109 1998) and end-Permian mass extinctions (Grice et al., 2005; Xie et al., 2010) probably
1110 influenced rebuilding of marine trophic systems (e.g., Chen and Benton, 2012). Third, ocean
1111 redox conditions, which are linked to temperature and nutrient cycling, influence the
1112 availability of ecospace for metazoans (e.g., Fig. 13). Development of reducing conditions
1113 leads to hypercapnia and hypoxemia, which are lethal to most marine invertebrates (Pörtner,
1114 2001). Fourth, ocean acidification, which is commonly linked to elevated atmospheric pCO_2,
1115 impedes the growth of calcifying organisms. A possible transient increase in seawater acidity

during the Early Triassic (Payne et al., 2010; Hinojosa et al., 2012) and early Paleocene (Alegret et al., 2012) are thought to have influenced the rate of recovery of some faunal components of marine ecosystems.

Other potential influences on rates of marine ecosystem recovery, i.e., persistently harsh environmental conditions (Hallam, 1991; Isozaki, 1997; Payne et al., 2004; Erwin, 2007) or magnitude of the extinction event (Sepkoski, 1984; Solé et al., 2002), may play a role as well. Although environmental conditions exhibit a tendency to fluctuate strongly following a biocrisis rather than remaining persistently harsh, at least some crises were followed by protracted intervals of generally inhospitable conditions. The best-documented example is the Early Triassic, during which tropical sea-surface temperatures remained persistently high (>32°C) for at least 2 Myr following the end-Permian crisis (Sun et al., 2012; Romano et al., 2013). The Late Devonian may provide another example, owing to the persistence of strongly oxygen-depleted conditions in shallow-marine seas for intervals of millions of years following the G-F and F-F crises (Algeo et al., 1995). In both cases, conditions fluctuated during these extended intervals of environmental deterioration, yielding no distinct dividing line between persistently harsh conditions and recurrent environmental disturbances. With regard to the influence of magnitude of the extinction event, there appears to be no strong correlation with the duration of the recovery interval (e.g., Kirchner and Weil, 2000; Erwin, 2001). There are intrinsic limits to how quickly ecosystems are capable of recovery that depend on rates of biotic evolution and, thus, re-occupation of vacated ecological niches (Sepkoski, 1998; Kirchner and Weil, 2000). However, it appears that such rates are at least an order-of-magnitude faster than the durations of even the shorter marine ecosystem recoveries (Hairston et al., 2008).

6. **Conclusions**

The overriding control on the pattern and pace of marine ecosystem recovery following a mass extinction event is environmental stability or lack thereof. An analysis of environmental variation following the end-Permian mass extinction demonstrates that the protracted (~5-Myr)

interval of recovery of Early Triassic marine ecosystems was due to recurrent environmental perturbations. These perturbations were associated with high terrestrial weathering fluxes, elevated marine productivity, and more intensely reducing oceanic redox conditions, and they appear to have been triggered by episodes of strong climatic warming, possibly linked to stages of increased magmatism in the Siberian Traps Large Igneous Province. The main perturbations following the end-Permian extinction occurred during the early Griesbachian, late Griesbachian, mid-Smithian, and (more weakly) the mid-Spathian. These episodes were stronger and more temporally discrete in deepwater sections (Chaohu and Daxiakou) relative to shallow and intermediate sections (Zuodeng and Mud), probably because warming and attendant effects were felt most strongly in the oceanic thermocline region. The observed relationships between weathering and productivity fluxes imply that nutrient and energy flows were key influences on the pattern and pace of marine ecosystem recovery. Comparison with recovery patterns following the other four "Big Five" Phanerozoic mass extinctions suggests that marine ecosystem recovery in general depends on the stability of the post-crisis marine environment. Persistent environmental stresses may also play a role in the pace of ecosystem recovery, but there is no clear correlation to the magnitude of mass extinction event.

Acknowledgments

Research by TJA is supported by the Sedimentary Geology and Paleobiology program of the U.S. National Science Foundation, the NASA Exobiology program, and the State Key Laboratory of Geological Processes and Mineral Resources, China University of Geosciences, Wuhan (Program: GPMR201301). This paper is a contribution to IGCP Project 572.

References

Adrain, J.M., Westrop, S.R., Chatterton, B.D.E., Ramsköld, L., 2000. Silurian trilobite alpha diversity and the end-Ordovician mass extinction. Paleobiology 26, 625-646.

1172 Aguirre, J., Baceta, J.I., Braga, J.C., 2007. Recovery of marine primary producers after the
1173 Cretaceous-Tertiary mass extinction: Paleocene calcareous red algae from the Iberian
1174 Peninsula. Palaeogeography, Palaeoclimatology, Palaeoecology 249, 393-411.
1175 Alegret, L., Thomas, E., 2009. Food supply to the seafloor in the Pacific Ocean after the
1176 Cretaceous/Paleogene boundary event. Marine Micropaleontology 73, 105-116.
1177 Alegret, L., Thomas, E., Lohmann, K.C., 2012. End-Cretaceous marine mass extinction not
1178 caused by productivity collapse. Proceedings of National Academy of Sciences (U.S.A.)
1179 109, 728-732.
1180 Algeo, T.J., Lyons, T.W., 2006. Mo-total organic carbon covariation in modern anoxic marine
1181 environments: Implications for analysis of paleoredox and paleohydrographic conditions.
1182 Paleoceanography 21, PA1016.
1183 Algeo, T.J., Maynard, J.B., 2004. Trace-element behavior and redox facies in core shales of
1184 Upper Pennsylvanian Kansas-type cyclothems. Chemical Geology 206, 289-318.
1185 Algeo, T.J., Scheckler, S.E., 1998. Terrestrial-marine teleconnections in the Devonian: links
1186 between the evolution of land plants, weathering processes, and marine anoxic events.
1187 Philosophical Transactions of the Royal Society B—Biological Sciences 353, 113-130.
1188 Algeo, T.J., Scheckler, S.E., 2010. Land plant evolution and weathering rates changes in the
1189 Devonian. Journal of Earth Science 21, 75-78.
1190 Algeo, T.J., Tribovillard, N., 2009. Environmental analysis of paleoceanographic systems
1191 based on molybdenum-uranium covariation. Chemical Geology 268, 211-225.
1192 Algeo, T.J., Twitchett, R.J., 2010. Anomalous Early Triassic sediment fluxes due to elevated
1193 weathering rates and their biological consequences. Geology 38, 1023-1026.
1194 Algeo, T.J., Berner, R.A., Maynard, J.B., Scheckler, S.E., 1995. Late Devonian oceanic
1195 anoxic events and biotic crises: ‘rooted’ in the evolution of vascular land plants? GSA
1196 Today 5, 64-66.
1197 Algeo, T.J., Scheckler, S.E., Maynard, J.B., 2001. Effects of the Middle to Late Devonian
1198 spread of vascular land plants on weathering regimes, marine biotas, and global climate,
1199 in: Gensel, P., Edwards, D. (Eds.), Plants Invade the Land: Evolutionary and

Environmental Perspectives. Columbia University Press, New York, pp. 213-216.

Algeo, T.J., Ellwood, B.B., Nguyen, T.K.T., Rowe, H., Maynard, J.B., 2007. The Permian-Triassic boundary at Nhi Tao, Vietnam: evidence for recurrent influx of sulfidic watermasses to a shallow-marine carbonate platform. Palaeogeography, Palaeoclimatology, Palaeoecology 252, 304-327.

Algeo, T.J., Shen, Y., Zhang, T., Lyons, T.W., Bates, S.M., Rowe, H., Nguyen, T.K.T., 2008. Association of ^{34}S-depleted pyrite layers with negative carbonate $\delta^{13}C$ excursions at the Permian/Triassic boundary: evidence for upwelling of sulfidic deep-ocean watermasses. Geochemistry, Geophysics, Geosystems 9, 1-10.

Algeo, T.J., Chen, Z.Q., Fraiser, M.L., Twitchett, R.J., 2011a. Terrestrial-marine teleconnections in the collapse and rebuilding of Early Triassic marine ecosystems. Palaeogeography, Palaeoclimatology, Palaeoecology 308, 1-11.

Algeo, T.J., Kuwahara, K., Sano, H., Bates, S., Lyons, T., Elswick, E., Hinnov, L., Ellwood, B., Moser, J., Maynard, J.B., 2011b. Spatial variation in sediment fluxes, redox conditions, and productivity in the Permian-Triassic Panthalassic Ocean. Palaeogeography, Palaeoclimatology, Palaeoecology 308, 65-83.

Algeo, T.J., Henderson, C., Ellwood, B., Rowe, H., Elswick, E., Bates, S., Lyons, T., Hower, J.C., Smith, C., Maynard, J.B., Hays, L., Summons, R., Fulton, J., Freeman, K., 2012. Evidence for a diachronous Late Permian marine crisis from the Canadian Arctic region. Geological Society of American Bulletin 124, 1424-1448.

Algeo, T.J., Henderson, C.M., Tong, J., Feng, Q., Yin, H., Tyson, R., 2013. Plankton and productivity during the Permian-Triassic boundary crisis: An analysis of organic carbon fluxes. Global and Planetary Change 105, 52-67.

Alroy, J., Aberhan, M., Bottjer, D.J., Foote, M., Fürsich, F.T., Harries, P.J., Hendy, A.J.W., Holland, S.M., Ivany, L.C., Kiessling, W., Kosnik, M.A., Marshall, C.R., McGowan, A.J., Miller, A.I., Olszewski, T.D., Patzkowsky, M.E., Peters, S.E., Villier, L., Wagner, P.J., Bonuso, N., Borkow, P.S., Brenneis, B., Clapham, M.E., Fall, L.M., Ferguson, C.A., Hanson, V.L., Krug, A.Z., Layou, K.M., Leckey, E.H., Nürnberg, S., Powers, C.M.,

1228 Sessa, J.A., Simpson, C., Tomašových, A., Visaggi, C.C., 2008. Phanerozoic trends in the
1229 global diversity of marine invertebrates. Science 321, 97-100.
1230 Arenillas, I., Arz, J.A., Molina, E., Dupuis, C., 2000. The Cretaceous/Paleogene (K/P)
1231 boundary at Aïn Settara, Tunisia: sudden catastrophic mass extinction in planktic
1232 foraminifera. Journal of Foraminiferal Research 30, 202-218.
1233 Ausich, W.I., Deline, B., 2012. Macroevolutionary transition in crinoids following the Late
1234 Ordovician extinction event (Ordovician to Early Silurian). Palaeogeography,
1235 Palaeoclimatology, Palaeoecology 361-362, 38-48.
1236 Azmy, K., Veizer, J., Bassett, M.G., Copper, P., 1998. Oxygen and carbon isotopic
1237 composition of Silurian brachiopods: implications for coeval seawater and glaciations.
1238 Geological Society of America Bulletin 110, 1499-1512.
1239 Azmy, K., Veizer, J., Wenzel, B., Bassett, M.G., Copper, P., 1999. Silurian strontium isotope
1240 stratigraphy. Geological Society of American Bulletin 111, 475-483.
1241 Baceta, J.I., Pujalte, V., Bernaola, G., 2005. Paleocene coralgal reefs of the western Pyrenean
1242 basin, northern Spain: new evidence supporting an earliest Paleogene recovery of reefal
1243 ecosystems. Palaeogeography, Palaeoclimatology, Palaeoecology 224, 117-143.
1244 Baliński, A., 2002. Frasnian-Famennian brachiopod extinction and recovery in southern
1245 Poland. Acta Palaeontologica Polonica 47, 289-305.
1246 Bambach, R.K., 1977. Species richness in marine benthic habitats through the Phanerozoic.
1247 Paleobiology 3, 152-167.
1248 Bartolini, A., Guex, J., Spangenberg, J.E., Schoene, B., Taylor, D.G., Schaltegger, U.,
1249 Atudorei, V., 2012. Disentangling the Hettangian carbon isotope record: implications for
1250 the aftermath of the end-Triassic mass extinction. Geochemistry, Geophysics,
1251 Geosystems 13, Q01007, doi:10.1029/2011GC003807.
1252 Baud, A., Richoz, S., Pruss, S., 2007. The lower Triassic anachronistic carbonate facies in
1253 space and time. Global and Planetary Change 55, 81-89.
1254 Baud, A., Nakrem, H.A., Beauchamp, B., Beatty, T., Embry, A.F., Henderson, C.M.B., 2008.
1255 Lower Triassic bryozoan beds from Ellesmere Island, High Arctic, Canada. Polar

Research 27, 428-440.

Beauchamp, B., Baud, A., 2002. Growth and demise of Permian biogenic chert along northwest Pangea: evidence for end-Permian collapse of thermohaline circulation. Palaeogeography, Palaeoclimatology, Palaeoecology 184, 37-63.

Benton, M.J., Twitchett, R.J., 2003. How to kill (almost) all life: the end-Permian extinction event. Trends in Ecology & Evolution 18, 358-365.

Benton, M.J., Zhang, Q., Hu, S., Chen, Z.Q., Wen, W., Liu, J., Huang, J., Zhou, C., Xie, T., Tong, J., Choo, B., 2013. Exceptional vertebrate biotas from the Triassic of China, and the expansion of marine ecosystems after the Permo-Triassic mass extinction. Earth-Science Reviews 125, 199-243.

Berner, R.A., 1994. Geocarb II: a revised model of atmospheric CO_2 over Phanerozoic time. American Journal of Science 294, 56-91.

Bhargava, O.N., Krystyn, L., Balini, M., Lein, R., Nicora, A., 2004. Revised litho- and sequence stratigraphy of the Spiti Triassic. Albertiana 30, 21-39.

Bigey, F.P., 1989. Devonian Bryozoan and global events: the Frasnian/Famennian extinction, in: McMillan, N.J., Embry, A.F., Glass, D.J. (Eds.), Devonian of the World, v. III, Paleontology, Paleoecology, and Biostratigraphy. Canadian Society of Petroleum Geologists Memoir 14, pp. 53-62.

Black, B.A., Elkins-Tanton, L.T., Rowe, M.C., Peate, I.U., 2012. Magnitude and consequences of volatile release from the Siberian Traps. Earth and Planetary Science Letters 317-318, 363-373.

Blätter, C.L., Jenkyns, H.C., Reynard, L.M., Henderson, G.M., 2011. Significant increases in global weathering during Oceanic Anoxic Events 1a amd 2 indicated by calcium isotopes. Earth and Planetary Science Letters 309, 77-88.

Bond, D.P.G., Wignall, P.B., 2010. Pyrite framboid study of marine Permo-Triassic boundary sections: a complex anoxic event and its relationship to contemporaneous mass extinction. Geological Society of America Bulletin 122, 1265-1279.

Bottjer, D.J., Clapham, M.E., Fraiser, M.L., Powers, C.M., 2008. Understanding mechanisms

for the end-Permian mass extinction and the protracted Early Triassic aftermath and recovery. GSA Today 18, 4-10.

Bown, P., 2005. Selective calcareous nannoplankton survivorship at the Cretaceous-Tertiary boundary. Geology 33, 653-656.

Brand, U., Azmy, K., Veizer, J., 2006. Evaluation of the Salinic I tectonic, Cancaniri glacial and Ireviken biotic events: biochemostratigraphy of the Lower Silurian succession in the Niagara Gorge area, Canada and U.S.A. Palaeogeography, Palaeoclimatology, Palaeoecology 241, 192-213.

Brayard, A., Bucher, H., Escarguel, G., Fluteau, F., Bourquin, S., Galfetti, T., 2006. The Early Triassic ammonoid recovery: Paleoclimatic significance of diversity gradients. Palaeogeography, Palaeoclimatology, Palaeoecology 239, 374-395.

Brayard, A., Escarguel, G., Bucher, H., Monnet, C., Brühwiler, T., Goudemand, N., Galfetti, T., Guex, J., 2009. Good genes and good luck: ammonoid diversity and the end-Permian mass extinction. Science 325, 1118-1121.

Brayard, A., Vennin, E., Olivier, N., Bylund, K.G., Jenks, J., Stephen, D.A., Bucher, H., Hofman, R., Goudemand, N., Escarguel, G., 2011. Transient metazoan reefs in the aftermath of the end-Permian mass extinction. Nature Geoscience 4, 693-697.

Brenchley, P.J., Harper, D.A.T., 1998. Palaeoecology: Ecosystems, Environments and Evolution. Thomson Science, Weinheim, Germany, 402 pp.

Brenchley, P.J., Carden, G.A.F., Marshall, J.D., 1995. Environmental changes associated with the “first strike” of the Late Ordovician mass extinction. Modern Geology 20, 69-82.

Brenchley, P.J., Marshall, J., Underwood, C.J., 2001. Do all mass extinctions represent an ecological crisis? Evidence from the Late Ordovician. Geological Journal 36, 329–340.

Brennecka, G.A., Herrmann, A.D., Algeo, T.J., Anbar, A.D., 2011. Rapid expansion of oceanic anoxia immediately before the end-Permian mass extinction. Proceedings of the National Academy of Sciences (U.S.A.) 108, 17631-17634.

Brinkhuis, H., Bujak, J.P., Smit, J., Versteegh, G.J.M., Visscher, H., 1998. Dinoflagellate-based sea surface temperature reconstructions across the

Cretaceous-Tertiary boundary. Palaeogeography, Palaeoclimatology, Palaeoecology 141, 67-83.

Bruckschen, P., Oesmann, S., Veizer, J., 1999. Isotope stratigraphy of the European Carboniferous: proxy signals for ocean chemistry, climate and tectonics. Chemical Geology 161, 127-163.

Brühwiler, T., Ware, D., Bucher, H., Krystyn, L., Goudemand, N., 2010. New Early Triassic ammonoid faunas from the Dienerian/Smithian boundary beds at the Induan/Olenekian GSSP candidate at Mud (Spiti, northern India). Journal of Asian Earth Sciences 39, 724-739.

Buggisch, W., Joachimski, M.M., 2006. Carbon isotope stratigraphy of the Devonian of Central and Southern Europe. Palaeogeography, Palaeoclimatology, Palaeoecology 240, 68-88.

Burgess, S.D., Bowring, S., Shen, S.Z., 2014. High-precision timeline for Earth's most severe extinction. doi/10.1073/pnas.1317692111, 6 pp.

Cai, J.X., Zhang, K.J., 2009. A new model for the Indochina and South China collision during the Late Permian to the Middle Triassic. Tectonophysics 467, 35-43.

Callaway, J.M., Brinkman, D.B., 1989. Ichthyosaurs (Reptilia, Ichthyosauria) from the Lower and Middle Triassic Sulphur Mountain Formation, Wapiti Lake area, British Columbia, Canada. Canadian Journal of Earth Sciences 26, 1491-1500.

Calvert, S.E., Pedersen, T.F., 2007. Elemental proxies for palaeoclimatic and palaeoceanographic variability in marine sediments: Interpretation and application, in: Hillaire-Marcel, C., De Vernal, A. (Eds.), Proxies in Late Cenozoic Paleoceanography. Developments in Marine Geology 1. Elsevier, Amsterdam, pp. 567-644.

Campbell, I.H., Czamanske, G.K., Fedorenko, V.A., Hill, R.I., Stepanov, V., 1992. Synchronism of the Siberian Traps and the Permian-Triassic boundary. Science 258, 1760-1763.

Cao, C., Love, G.D., Hays, L.E., Wang, W., Shen, S., Summons, R.E., 2009. Biogeochemical evidence for euxinic oceans and ecological disturbance presaging the end-Permian mass

1340 extinction event. Earth and Planetary Science Letters 281, 188-201.
1341 Caputo, M.V., 1998. Ordovician-Silurian glaciations and global sea-level changes, in:
1342 Landing, E., Johnson, M.E. (Eds.), Silurian cycles: linkages of dynamic stratigraphy with
1343 atmospheric, oceanic and tectonic changes. New York State Museum Bulletin 491,
1344 15-25.
1345 Casier, J.-G., Lethiers, F., 1998. The recovery of the ostracod fauna after the Late Devonian
1346 mass extinction: the Devils Gate Pass section example (Nevada, USA). Palaeontology
1347 327, 501-507.
1348 Chen, D., Qing, H., Li, R., 2005. The Late Devonian Frasnian-Famennian (F/F) biotic crisis:
1349 insights from $\delta^{13}C_{carb}$, $\delta^{13}C_{org}$ and $^{87}Sr/^{86}Sr$ isotopic systematics. Earth and Planetary
1350 Science Letters 235, 151-166.
1351 Chen, Y., Twitchett, R.J., Jiang, H., Richoz, S., Lai, X., Yan, C., Sun, Y., Liu, X., Wang, L.,
1352 2013. Size variation of conodonts during the Smithian-Spathian (Early Triassic) global
1353 warming event. Geology 41, 823-826.
1354 Chen, Z.Q., Benton, M.J., 2012. The timing and pattern of biotic recovery following the
1355 end-Permian mass extinction. Nature Geoscience 5, 375-383.
1356 Chen, Z.Q., Kaiho, K., George, A.D., 2005. Early Triassic recovery of the brachiopod faunas
1357 from the end-Permian mass extinction: a global review. Palaeogeography,
1358 Palaeoclimatology, Palaeoecology 224, 270-290.
1359 Chen, Z.Q., Tong, J., Fraiser, M.L., 2011. Trace fossils evidence for restoration of marine
1360 ecosystems following the end-Permian mass extinction in the Lower Yangtze region,
1361 South China. Palaeogeography, Palaeoclimatology, Palaeoecology 299, 449-474.
1362 Chenet, A.-L., Quidelleur, X., Fluteau, F., Courtillot, V., Bajpai, S., 2007. ^{40}K-^{40}Ar dating of
1363 the Main Deccan large igneous province: Further evidence of KTB age and short
1364 duration. Earth and Planetary Science Letters 263, 1-15.
1365 Clapham, M.E., Payne, J.L., 2011. Acidification, anoxia, and extinction: a multiple logistic
1366 regression analysis of extinction selectivity during the Middle and Late Permian.
1367 Geology 39, 1059-1062.

1368 Clapham, M.E., Bottjer, D.J., Powers, C.M., Bonuso, N., Fraiser, M.L., Marenco, P.J.,
1369 Dornbos, S.Q., Pruss, S.B., 2006. Assessing the ecological dominance of Phanerozoic
1370 marine invertebrates. Palaios 21, 431-441
1371 Clarkson, M.O., Richoz, S., Wood, R.A., Maurer, F., Krystyn, L., McGurty, D.J., Astratti, D.,
1372 2013. A new high-resolution $\delta^{13}C$ record for the Early Triassic: Insights from the Arabian
1373 platform. Gondwana Research 24, 233-242.
1374 Clémence, M.E., Bartolini, A., Gardin, S., Paris, G., Beaumont, V., Page, K.N., 2010. Early
1375 Hettangian benthic-planktonic coupling at Doniford (SW England) palaeoenvironmental
1376 implications for the aftermath of the end-Triassic crisis. Palaeogeography,
1377 Palaeoclimatology, Palaeoecology 295, 102-115.
1378 Coccioni, R., Luciani, V., 2006. *Guembelitria irregularies* bloom at the K-T boundary:
1379 Morphological abnormalities induced by impact-related extreme environmental stress? in:
1380 Cockell, C., Koeberl, C., Gilmour, I. (Eds.), Biological processes associated with impact
1381 events. Springer, Berlin, pp. 179-196.
1382 Copper, P., 1986. Frasnian-Famennian mass extinction and cold-water oceans. Geology 14,
1383 835-839.
1384 Copper, P., 2001. Reefs during the multiple crises towards the Ordovician-Silurian boundary:
1385 Anticostic Island, eastern Canada, and worldwide. Canadian Journal of Earth Sciences
1386 38, 153-171.
1387 Copper, P., 2002. Reef development at the Frasnian/Famennian mass extinction boundary.
1388 Palaeogeography, Palaeoclimatology, Palaeoecology 181, 27-65.
1389 Courtillot, V., Besse, J., Vandamme, D., Montigny, R., 1986. Deccan flood basalts at the
1390 Cretaceous/Tertiary boundary? Earth and Planetary Science Letters 80, 361-374.
1391 Courtillot, V., Féraud, G., Maluski, H., Vandamme, D., Moreau, M.G., Besse, J., 1988. Deccan
1392 flood basalts and the Cretaceous/Tertiary boundary. Nature 333, 844-846.
1393 Cox, C.B., Smith, D.G., 1973. A review of the Triassic vertebrate faunas of Svalbard.
1394 Geological Magazine 110, 405-418.
1395 Coxall, H.K., D'Hondt, S., Zachos, J.C., 2006. Pelagic evolution and environmental recovery

1396 after the Cretaceous-Paleogene mass extinction. Geology 34, 297-300.
1397 Cramer, B.D., Brett, C.E., Melchin, M.A., Männik, P., Kleffner, M.A., McLaughlin, P.I.,
1398 Loydell, D.K., Munnecke, A., Jeppson, L., Corradini, C., Brunton, F.R., Saltzman, M.R.,
1399 2011. Revised chronostratigraphic correlation of the Silurian System of North America
1400 with global and regional chronostratigraphic units and $\delta^{13}C_{carb}$ chemostratigraphy.
1401 Lethaia 44, 185-202.
1402 Crasquin-Soleau, S.T., Galfetti, H., Bucher, H., Kershaw, S., Feng, Q., 2007. Ostracod
1403 recovery in the aftermath of the Permian-Triassic crisis: Palaeozoic-Mesozoic turnover.
1404 Hydrobiologia 585, 13-27.
1405 Delabroye, A., Munnecke, A., Vecoli, M., Copper, P., Tribovillard, N., Joachimski, M.M.,
1406 Desrochers, A., Servais, T., 2011. Phytoplankton dynamics across the
1407 Ordovician/Silurian boundary at low palaeolatitudes: Correlations with carbon isotopic
1408 and glacial events. Palaeogeography, Palaeoclimatology, Palaeoecology 312, 79-97.
1409 De La Rocha, C.L., DePaolo, D.J., 2000. Isotopic evidence for variations in the marine
1410 calcium cycle over the Cenozoic. Science 289, 1176-1178.
1411 Devine, J.D., Sigurdsson, H., Havis, A.N., Self, S., 1984. Estimates of sulfur and chlorine
1412 yield to the atmosphere from volcanic eruptions and potential climatic effects. Journal of
1413 Geophysical Research 89, 6309-6325.
1414 D'Hondt, S., Donaghay, P., Zachos, J.C., Luttenberg, D., Lindinger, M., 1998. Organic carbon
1415 fluxes and ecological recovery from the Cretaceous-Tertiary mass extinction. Science
1416 282, 276-279.
1417 Dix, G.R., James, J.P., 1987. Late Mississippian bryozoan/microbial build-ups on a drowned
1418 karst terrain, Port Au Port Peninsula, western Newfoundland. Sedimentology 34,
1419 779-793.
1420 Enos, P., Wei, J., Yan, Y., 1997. Facies distribution and retreat of Middle Triassic platform
1421 margin, Guizhou Province, south China. Sedimentology 44, 563-584.
1422 Erwin, D.H., 1998. The end and the beginning: recoveries from mass extinctions. Trends in
1423 Ecology & Evolution 13, 344-349.

1424 Erwin, D.H., 2001. Lessons from the past: biotic recoveries from mass extinctions.
1425 Proceedings of the National Academy of Sciences (U.S.A.) 98, 5399-5403.
1426 Erwin, D.H., 2005. Extinction: How Life on Earth Nearly Died 250 Millions Years Ago.
1427 Princeton University Press, Princeton, New Jersey, pp. 306.
1428 Erwin, D.H., 2007. Increasing returns, ecological feedback and the Early Triassic recovery.
1429 Palaeoworld 16, 9-15.
1430 Erwin, D.H., 2008. Macroevolution of ecosystem engineering, niche construction and
1431 diversity. Trends in Ecology & Evolution 23, 304-310.
1432 Erwin, D.H., Pan, H., 1996. Recoveries and radiations: gastropods after the Permo-Triassic
1433 mass extinction, in: Hart, M.B. (Ed.), Biotic Recovery from Mass Extinction Events.
1434 Geological Society of London Special Publication 102, 223-229.
1435 Erwin, D.H., Bowring, S.A., Jin, Y.G., 2002. End-Permian mass-extinctions: a review, in:
1436 Koeberl, C., MacLeod, K.G. (Eds.), Catastrophic Events and Mass Extinctions: Impacts
1437 and Beyond. Geological Society of America Special Paper 356, pp. 353-383.
1438 Fan, J., Chen, X., 2007. Preliminary report on the Late Ordovician graptolite extinction in the
1439 Yangtze region. Palaeogeography, Palaeoclimatology, Palaeoecology 245, 82-94.
1440 Fantle, M.S., DePaolo, D.J., 2005. Variations in the marine Ca cycle over the past 20 million
1441 years. Earth and Planetary Science Letters 237, 102-117.
1442 Fastovsky, D.E., Sheehan, P.M., 2005. The extinction of the dinosaurs in North America. GSA
1443 Today 15, 4-10.
1444 Feng, Q., Algeo, T.J., 2014. Evolution of oceanic redox conditions during the Permo-Triassic:
1445 Evidence from radiolarian deepwater facies. Earth-Science Reviews, in press.
1446 Finnegan, S., Heim, N.A., Peters, S.E., Fischer, W.W., 2012. Climate change and the selective
1447 signature of the Late Ordovician mass extinction. Proceedings of the National Academy of
1448 Sciences (U.S.A.) 109, 6829-6834.
1449 Finney, S.C., Berry, W.B.N., Cooper, J.D., Ripperdan, R.L., Sweet, W.C., Jacobson, S.R.,
1450 Soufiane, A., Achab, A., Noble, P.J., 1999. Late Ordovician mass extinction: a new
1451 perspective from stratigraphic sections in central Nevada. Geology 27, 215-218.

1452 Fischer, A.G., Bottjer, D.J., 1995. Oxygen-depleted waters: A lost biotope and its role in
1453 ammonite and bivalve evolution. Neues Jahrbuch für Geologie und Paläontologie
1454 Abhandlungen 195, 133-146.
1455 Fontugne, M.R., Calvert, S.E., 1992. Late Pleistocene variability of the carbon isotopic
1456 composition of organic matter in the Eastern Mediterranean: Monitor of changes in
1457 carbon sources and atmospheric CO_2. Paleoceanography 7, 1-20.
1458 Fraiser, M.L., 2011. Paleoecology of secondary tierers from Western Pangean tropical marine
1459 environments during the aftermath of the end-Permian mass extinction. Palaeogeography,
1460 Palaeoclimatology, Palaeoecology 308, 181-189.
1461 Fraiser, M.L., Bottjer, D.J., 2004. The non-actualistic Early Triassic gastropod fauna: a case
1462 study of the Lower Triassic Sinbad Limestone member. Palaios 19, 259-275.
1463 Fraiser, M.L., Twitchett, R.J., Bottjer, D.J., 2005. Unique microgastropod biofacies in the
1464 Early Triassic: Indicator of long-term biotic stress and the pattern of biotic recovery after
1465 the end-Permian mass extinction. Comptes Rendus Palevol 4, 543-552.
1466 Fuqua, L.M., Bralower, T.J., Arthur, M.A., Patzkowsky, M.E., 2008. Evolution of calcareous
1467 nannoplankton and the recovery of marine food webs after the Cretaceous-Paleocene
1468 mass extinction. Palaios 23, 185-194.
1469 Galfetti, T., Hochuli, P.A., Brayard, A., Bucher, H., Weissert, H., Vigran, J.O., 2007a.
1470 Smithian-Spathian boundary event: Evidence for global climatic change in the wake of
1471 the end-Permian biotic crisis. Geology 35, 291-294.
1472 Galfetti, T., Bucher, H., Brayard, A., Hochuli, P.A., Weissert, H., Kuang, G., Atudorei, V.,
1473 Guex, J., 2007b. Late Early Triassic climate change: Insights from carbonate carbon
1474 isotopes, sedimentary evolution and ammonoid paleobiogeography. Palaeogeography,
1475 Palaeoclimatology, Palaeoecology 243, 394-411.
1476 Ganino, C., Arndt, N.T., 2009. Climate changes caused by degassing of sediments during the
1477 emplacement of large igneous provinces. Geology 37, 323-326.
1478 Garzanti, E., Angiolini, L., Sciunnach, D., 1996. The Mid-Carboniferous to lowermost
1479 Permian succession of Spiti (Po Group and Ganmachidam Formation, Tethys Himalaya,

Northern India): Gondwana glaciation and rifting of Neo-Tethys. Geodinamica Acta 9, 78-100.

Gee, D.G., 1975. A tectonic model for the central part of the Scandinavian Caledonides. American Journal of Science 275a, 532-568.

Gibbs, M.T., Barron, E.J., Kump, L.R., 1997. An atmospheric pCO_2 threshold for glaciation in the Late Ordovician. Geology 25, 447-450.

Goto, M., 1994. Palaeozoic and early Mesozoic fish faunas of the Japanese islands. Island Arc 3, 247-254.

Gouldey, J.C., Saltzman, M.R., Young, S.A., Kaljo, D., 2010. Strontium and carbon isotope stratigraphy of the Llandovery (Early Silurian): implications for tectonics and weathering. Palaeogeography, Palaeoclimatology, Palaeoecology 296, 264-275.

Grasby, S.E., Beauchamp, B., Embry, A., Sanei, H., 2013. Recurrent Early Triassic ocean anoxia. Geology 41, 175-178.

Grice, K., Cao, C., Love, G.D., Bottcher, M.E., Twitchett, R.J., Grosjean, E., Summons, R.E., Turgeon, S.C., Dunning, W., Jin, Y., 2005. Photic zone euxinia during the Permian-Triassic superanoxic event. Science 307, 706-709.

Guex, J., Bartolini, A., Atudorei, V., Taylor, D., 2004. High-resolution ammonite and carbon isotope stratigraphy across the Triassic-Jurassic boundary at New York Canyon (Nevada). Earth and Planetary Science Letters 225, 29-41.

Guex, J., Schoene, B., Bartolini, A., Spangenberg, J., Schaltegger, U., O'Dogherty, L., Taylor, D., Bucher, H., Atudorei, V., 2012. Geochronological constraints on post-extinction recovery of the ammonoids and carbon cycle perturbations during the Early Jurassic. Palaeogeography, Palaeoclimatology, Palaeoecology 346-347, 1-11.

Guo, G., Tong, J., Zhang, S., Zhang, J., Bai, L., 2008. Cyclostratigraphy of the Induan (Early Triassic) in West Pingdingshan Section, Chaohu, Anhui Province. Science in China Series D—Earth Sciences 51, 22-29.

Hairstone, N.G., Ellner, S.P., Geber, M.A., Yoshida, T., Fox, J.A., 2008. Rapid evolution and the convergence of ecological and evolutionary time. Ecology Letters 8, 1114-1127.

1508 Hallam, A., 1991. Why was there a delayed radiation after the end-Palaeozoic extinctions?
1509 Historical Biology 5, 257-262.
1510 Hallam, A., Wignall, P.B., 1999. Mass extinctions and sea-level changes. Earth-Science
1511 Reviews 48, 217-250.
1512 Haq, B.U., Hardenbol, J., Vail, P.R., 1987. Chronology of fluctuating sea level since the
1513 Triassic. Science 235, 1156-1167.
1514 Haq, B.U., Schutter, S.R., 2008. A chronology of Paleozoic sea-level changes. Science 322,
1515 64-68.
1516 Harper, D.A.T., Rong, J., 2008. Completeness of the Hirnantian brachiopod record: spatial
1517 heterogeneity through the end Ordovician extinction event. Lethaia 41, 195-197.
1518 Harries, P.J., Kauffman, E.J., 1990. Patterns of survival and recovery following
1519 Cenomanian-Turonian (Late Cretaceous) mass extinction in the western Interior Basin,
1520 United States, in: Kauffman, E.G., Walliser, O.H. (Eds.), Extinction Events in Earth
1521 History, Springer, Berlin, pp. 277-298.
1522 Hautmann, M., Bucher, H., Brühwiler, T., Goudemand, N., Kaim, A., Nützel, A., 2011. An
1523 usually diverse mollusc fauna from the earliest Triassic of South China and its
1524 implications for benthic recovery after the end-Permian biotic crisis. Geobios 44, 71-85.
1525 Hermann, E., Hochuli, P.A., Méhay, S., Bucher, H., Brühwiler, T., Ware, D., Hautmann, M.,
1526 Roohi, G., ur-Rehman K., Yaseen, A., 2011. Organic matter and palaeoenvironmental
1527 signals during the Early Triassic biotic recovery: The Salt Range and Surghar Range
1528 records. Sedimentary Geology 234, 19-41.
1529 Hesselbo, S.P., Robinson, S.A., Surlyk, F., Piasecki, S., 2002. Terrestial and marine extinction
1530 at the Triassic-Jurassic boundary synchronized with major carbon-cycle perturbation: a
1531 link to initiation of massive volcanism? Geology 30, 251-254.
1532 Hildebrand-Habel, T., Streng, M., 2003. Calcareous dinoflagellate associations and
1533 Maastrichtian-Tertiary climatic changes in a high latitude core (ODP Hole 689B, Maud
1534 Rise, Weddell Sea). Palaeogeography, Palaeoclimatology, Palaeoecology 197, 293-321.
1535 Hilting, A.K., Kump, L.R., Bralower, T.J., 2008. Variations in the oceanic vertical carbon

isotope gradient and their implications for the Paleocene-Eocene biological pump. Paleoceanography 23, PA3222, doi:10.1029/2007PA001458.

Hinojosa, J.L., Brown, S.T., Chen, J., DePaolo, D.J., Paytan, A., Shen, S.Z., Payne, J.L., 2012. Evidence for end-Permian ocean acidification from calcium isotopes in biogenic apatite. Geology 40, 743-746.

Hofmann, R., Hautmann, M., Bucher, H., 2013. A new paleoecological look at the Dinwoody Formation (Lower Triassic, western US): intrinsic versus extrinsic controls on ecosystem recovery after the end-Permian mass extinction. Journal of Paleontology 87, 854-880.

Hofmann, R., Hautmann, M., Brayard, A., Nützel, Bylund, K.G., Jenks, J.F., Vennin, E., Oliver, N., Bucher, H., 2014. Recovery of benthic marine communities from the end-Permian mass extinction at the low latitudes of eastern Panthalassa. Palaeontology 57, 547-589.

Hollis, C.J., Strong, C.P., Rodgers, K.A., Rogers, K.M., 2003. Paleoenvironmental changes across the Cretaceous/Tertiary boundary at Flaxbourne River and Woodside Creek, eastern Marlborough, New Zealand. New Zealand Journal of Geology and Geophysics 46, 177-197.

Horacek, M., Richoz, S., Brandner, R., Krystyn, L., Spötl, C., 2007. Evidence for recurrent changes in Lower Triassic oceanic circulation of the Tethys: The $\delta^{13}C$ record from marine sections in Iran. Palaeogeography, Palaeoclimatology, Palaeoecology 252, 355-369.

House, M.R., 2002. Strength, timing, setting and cause of mid-Paleozoic extinctions. Palaeogeography, Palaeoclimatology, Palaeoecology 181, 5-25.

Hu, S., Zhang, Q., Chen, Z., Zhou, C., Lü, T., Xie, T., Wen, W., Huang, J., Benton, M.J., 2011. The Luoping biota: exceptional preservation, and new evidence on the Triassic recovery from end-Permian mass extinction. Proceedings of the Royal Society—Biological Sciences 278, 2274-2282.

Huang, B., Rong, J., Cocks, L.R.M., 2012. Global palaeobiogeographical patterns in brachiopods from survival to recovery after the end-Ordovician mass extinction.

1564 Palaeogeography, Palaeoclimatology, Palaeoecology 317-318, 196-205.
1565 Hull, P.M., Norris, R.D., Bralower, T.J., Schueth, J.D., 2011. A role for chance in marine
1566 recovery from end-Cretaceous extinction. Nature Geoscience 4, 856-860.
1567 Ingall, E.D., van Cappellen, P., 1990. Relation between sedimentation rate and burial of
1568 organic phosphorus and organic carbon in marine sediments. Geochimica et
1569 Cosmochimica Acta 54, 373-386.
1570 Irmis, R.B., Whiteside, J.H., 2011. Delayed recovery of non-marine tetrapods after the
1571 end-Permian mass extinction tracks global carbon cycle. Proceedings of the Royal
1572 Society B—Biological Sciences, 9 pp. doi:10/1098/rspb.2011.1895.
1573 Isaacson, P.E., Díza-Martínez, E., Grader, G.W., Kalvoda, J., Babek, O., Devuyst, F.X., 2008.
1574 Late Devonian-earliest Mississippian glaciation in Gondwanaland and its biogeographic
1575 consequences. Palaeogeography, Palaeoclimatology, Palaeoecology 268, 126-142.
1576 Isozaki, Y., 1997. Permo-Triassic boundary superanoxia and stratified superocean: Records
1577 from lost deep sea. Science 276, 235-238.
1578 Jablonski, D., 1991. Extinctions: a paleontological perspective. Science 253, 754-757.
1579 Jablonski, D., Chaloner, W.G., 1994. Extinctions in the fossil record. Philosophical
1580 Transactions of the Royal Society of London B—Biological Sciences 344, 11-16.
1581 Jacobsen, N.D., Twitchett, R.J., Krystyn, L., 2011. Palaeoecological methods for assessing
1582 marine ecosystem recovery following the Late Permian mass extinction event.
1583 Palaeogeography, Palaeoclimatology, Palaeoecology 308, 200-212.
1584 Jin, F., 2006. An overview of Triassic fishes from China. Vertebrata Palasiatica 44, 28-42.
1585 Jin, Y.G., Wang, Y., Wang, W., Shang, Q.H., Cao, C.Q., Erwin, D.H., 2000. Pattern of marine
1586 mass extinction near the Permian-Triassic boundary in South China. Science 289,
1587 432-436.
1588 Joachimski, M.M., van Geldern, R., Breisig, S., Buggisch, W., Day, J., 2004. Oxygen isotope
1589 evolution of biogenic calcite and apatite during the Middle and Late Devonian.
1590 International Journal of Earth Science 93, 542-553.
1591 Joachimski, M.M., Lai, X., Shen, S., Jiang, H., Luo, G., Chen, B., Chen, J., Sun, Y., 2012.

1592 Climate warming in the latest Permian and the Permian-Triassic mass extinction.
1593 Geology 40, 195-198.
1594 Johnston, D.A., 1980. Volcanic contribution of chlorine to the stratosphere – more significant
1595 to ozone than previously estimated. Science 209, 491-493.
1596 Jolley, D., Gilmour, I., Gurov, E., Kelley, S., Watson, J., 2010. Two large meteorite impacts at
1597 the Cretaceous-Paleogene boundary. Geology 38, 835-838.
1598 Kaiser, S.I., Steuber, T., Becker, R.T., Joachimski, M.M., 2006. Geochemical evidence for
1599 major environmental change at the Devonian-Carboniferous boundary in the Carnic Alps
1600 and the Rhenish Massif. Palaeogeography, Palaeoclimatology, Palaeoecology 240,
1601 146-160.
1602 Kaiser, S.I., Steuber, T., Becker, R.T., 2008. Environmental change during the Late
1603 Famennian and Early Tournaisian (Late Devonian-Early Carboniferous): implications
1604 from stable isotopes and conodont biofacies in southern Europe. Geological Journal 43,
1605 241-260.
1606 Kakuwa, Y., 1996. Permian-Triassic mass extinction event recorded in bedded chert sequence
1607 in southwest Japan. Palaeogeography, Palaeoclimatology, Palaeoecology 121, 35-51.
1608 Kaljo, D., 1996. Diachronous recovery patterns in Early Silurian corals, graptolites and
1609 acritarchs, in: Hart, M.B. (Ed.), Biotic Recovery from Mass Extinction Events.
1610 Geological Society of London Special Publication 102, 127-133.
1611 Kaljo, D., Martma, T., 2000. Carbon isotopic composition of Llandovery rocks (east Baltic
1612 Silurian) with environmental interpretation. Proceedings of the Estonian Academy of
1613 Sciences 49, 267-283.
1614 Kamo, S.L., Czamanske, G.K., Amelin, Y., Fedorenko, V.A., Davis, D.W., Trofimov, V.R.,
1615 2003. Rapid eruption of Siberian flood-volcanic rocks and evidence for coincidence with
1616 the Permian-Triassic boundary and mass extinction at 251 Ma. Earth and Planetary
1617 Science Letters 214, 75-91.
1618 Keller, G., 2003. Biotic effects of impacts and volcanism. Earth and Planetary Science Letters
1619 215, 249-264.

1620 Kershaw, S., Crasquin, S., Li, Y., Collin, P.Y., Forel, M.B., Mu, X., Baud, A., Wang, Y., Xie,
1621 S., Maurer, F., Guo, L., 2011. Microbialites and global environmental change across the
1622 Permian-Triassic boundary: a synthesis. Geobiology 10, 25-47.
1623 Kershaw, S., Crasquin, S., Li, Y., Collin, P-Y., Forel, M-B., 2012. Ocean acidification and the
1624 end-Permian mass extinction: to what extent does evidence support hypothesis?
1625 Geosciences 2, 221-234. doi:10.3390/geosciences2040221.
1626 Kiessling, W., 2001. Paleoclimatic significance of Phanerozoic reefs. Geology 29, 751-754.
1627 Kiessling, W., 2005. Long-term relationships between ecological stability and biodiversity in
1628 Phanerozoic reefs. Nature 433, 410-413.
1629 Kiessling, W., Simpson, C., 2011. On the potential for ocean acidification to be a general
1630 cause of ancient reef crises. Global Change Biology 17, 56-67.
1631 Kirchner, J.W., Weil, A., 2000. Delayed biological recovery from extinctions throughout the
1632 fossil record. Nature 404, 177-180.
1633 Knaust, D., 2007. Invertebrate trace fossils and ichnodiversity in shallow-marine carbonates
1634 of the German Middle Triassic (Muschelkalk), in: Bromley, R., Buatois, L.A., Mángano,
1635 M.G., Genise, J., Melchor, R. (Eds.), Sediment-Organism Interactions: A Multifaceted
1636 Ichnology, SEPM Special Publication 88, 223-240.
1637 Knoll, A.H., Bambach, R.K., Payne, J.L., Pruss, S., Fischer, W.W., 2007. Paleophysiology and
1638 end-Permian mass extinction. Earth and Planetary Science Letters 256, 295-313.
1639 Korte, C., Hesselbo, S.P., Jenkyns, H.C., Rickaby, R.M., Spötl, C., 2009. Palaeoenvironmental
1640 significance of carbon- and oxygen-isotope stratigraphy of marine Triassic-Jurassic
1641 boundary sections in SW Britain. Journal of the Geological Society of London 166,
1642 431-445.
1643 Kozur, H.W., Weems, R.E., 2011. Detailed correlation and age of continental late
1644 Changhsingian and earliest Triassic beds: Implications for the role of the Siberian Trap in
1645 the Permian-Triassic biotic crisis. Palaeogeography, Palaeoclimatology, Palaeoecology
1646 308, 22-40.
1647 Krishnamurthy, R.V., Meyers, P.A., Lovan, N.A., 2000. Isotopic evidence of sea-surface

freshening, enhanced productivity, and improved organic matter preservation during sapropel deposition in the Tyrrhenian Sea. Geology 28, 263-266.

Krug, A.Z., Patzkowsky, M.E., 2004. Rapid recovery from the Late Ordovician mass extinction. Proceedings of the National Academy of Sciences (U.S.A.) 101, 17605-17610.

Krystyn, L., Orchard, M., 1996. Lowermost Triassic ammonoids and conodont biostratigraphy of Spiti, India. Albertiana 17, 10-21.

Krystyn, L., Richoz, S., Baud, A., Twitchett, R.J., 2003. A unique Permian-Triassic boundary section from Oman. Palaeogeography, Palaeoclimatology, Palaeoecology 191, 329-344.

Krystyn, L., Bhargava, O.N., Richoz, S., 2007. A candidate GSSP for the base of the Olenekian Stage: Mud at Pin Valley, district Lahul & Spiti, Himachal Pradesh (Western Himalaya), India. Albertiana 35, 5-29.

Kump, L.R., Arthur, M.A., 1999. Interpreting carbon-isotope excursions: carbonates and organic matter. Chemical Geology 161, 181-198.

Kump, L.R., Arthur, M.A., Patzkowsky, M.E., Gibbs, M.T., Pinkus, D.S., Sheehan, P.M., 1999. A weathering hypothesis for glaciation at high atmospheric pCO_2 during the Late Ordovician. Palaeogeography, Palaeoclimatology, Palaeoecology 152, 173-187.

Kump, L.R., Pavlov, A., Arthur, M.A., 2005. Massive release of hydrogen sulfide to the surface ocean and atmosphere during intervals of oceanic anoxia. Geology 33, 397-400.

Kuzmichev, A.B., Pease, V.L., 2007. Siberian trap magmatism on the New Siberian Islands: constraints for Arctic Mesozoic plate tectonic reconstructions. Journal of the Geological Society of London 164, 959-968.

Lehrmann, D.J., 1999. Early Triassic calcimicrobial mounds and biostromes of the Nanpanjiang basin, south China. Geology 27, 359-362.

Lehrmann, D.J., Ramezani, J., Bowring, S.A., Martin, M.W., Montgomery, P., Enos, P., Payne, J.L., Orchard, M.J., Wang, H., Wei, J., 2006. Timing of recovery from the end-Permian extinction: geochronologic and biostratigraphic constraints from south China. Geology 34, 1053-1056.

1676 Lehrmann, D.J., Pei, D., Enos, P., Minzoni, M., Ellwood, B.B., Orchard, M.J., Zhang, J., Wei,
1677 J., Dillett, P., Koenig, J., Steffen, K., Druke, D., Druke, J., Kessel, B., Newkirk, T., 2007.
1678 Impact of differential tectonic subsidence on isolated carbonate-platform evolution:
1679 Triassic of the Nanpanjiang Basin, south China. American Association of Petroleum
1680 Geologists Bulletin 91, 287-320.
1681 Li, H., Tong, J., Ren, J., Zhang, J., 2009. Early Triassic bivalve biostratigraphy and
1682 paleocommunities at Xiakou section in Xingshan, Hubei Province. Earth
1683 Science—Journal of China University of Geosciences 34, 733-742 (in Chinese with
1684 English abstract).
1685 Li, J., 2001. Pattern and time of collision between the Sino-Korean and Yangtze Blocks:
1686 evolution of the Sinian-Jurassic sedimentary settings in the middle-lower reaches of the
1687 Yangtze River. Acta Geologica Sinica 75, 25-34 (in Chinese with English abstract).
1688 Li, J., Liu, J., Li, C., Huang, Z., 2002. The horizon and age of the marine reptiles from Hubei
1689 Province, China. Vertebrata Palasiatica 40, 241-244.
1690 Li, S., Tong, J., Liu, K., Wang, F., Huo, Y., 2007. The Lower Triassic cyclic deposition in
1691 Chaohu, Anhui Province, China. Palaeogeography, Palaeoclimatology, Palaeoecology
1692 252, 188-199.
1693 Liao, W.H., 2002. Biotic recovery from the Late Devonian F-F mass extinction event in China.
1694 Science in China Series D—Earth Sciences 45, 380-384.
1695 Longridge, L.M., Carter, E.S., Smith, P.L., Tipper, H.W., 2007. Early Hettangian ammonites
1696 and radiolarians from the Queen Charlotte Islands, British Columbia and their bearing on
1697 the definition of the Triassic-Jurassic boundary. Palaeogeography, Palaeoclimatology,
1698 Palaeoecology 244, 142-169.
1699 Looy, C.V., Brugman, W.A., Dilcher, D.L., Visscher, H., 1999. The delayed resurgence of
1700 equatorial forests after the Permian-Triassic ecological crisis. Proceedings of the
1701 National Academy of Sciences (U.S.A.) 96, 13857-13862.
1702 Looy, C.V., Twitchett, R.J., Dilcher, D.L., van Konijnenburg-van Citter, J.H.A., Visscher, H.,

2001. Life in the end-Permian dead zone. Proceedings of the National Academy of Sciences (U.S.A.) 98, 7879-7883.

Luo, G., Wang, Y., Algeo, T.J., Kump, L.R., Bai, X., Yang, H., Yao, L., Xie, S., 2011. Enhanced nitrogen fixation in the immediate aftermath of the latest Permian marine mass extinction. Geology 39, 647-650.

Luo, G.M., Algeo, T.J., Zhou, W.F., Wang, Y.B., Yang, H., Huang, J.H., Richoz, S., Xie, S.C., 2014. Vertical $\delta^{13}C_{org}$ gradients record changes in planktonic microbial community composition during the end-Permian mass extinction. Palaeogeography, Palaeoclimatology, Palaeoecology 396, 119-131.

Mander, L., Twitchett, R.J., 2008. Quality of the Triassic-Jurassic bivalve fossil record in northwest Europe. Palaeontology 51, 1213-1223.

Marshall, C.R., Ward, P.D., 1996. Sudden and gradual molluscan extinction in the latest Cretaceous of Western European Tethys. Science 274, 1360-1363.

Martinez-Ruiz, F., Kastner, M., Paytan, A., Ortega-Huertas, M., Bernasconi, S.M., 2000. Geochemical evidence for enhanced productivity during S1 sapropel deposition in the eastern Mediterranean. Paleoceanography 15, 200-209.

Marzoli, A., Renne, P.R., Piccirillo, E.M., Ernesto, M., Bellieni, G., De Min, A., 1999. Extensive 200-million-year-old continental flood basalts of the central Atlantic magmatic province. Science 284, 616-618.

McElwain, J.C., Beerling, D.J., Woodward, F.I., 1999. Fossil plants and global warming at the Triassic-Jurassic boundary. Science 285, 1386-1390.

McGhee, G.R., Jr., 1996. The Late Devonian Mass Extinction: The Frasnian/Famennian Crisis. Columbia University Press, New York, 303 pp.

McKinney, M., 1995. Extinction selectivity among lower taxa–gradational patterns and rarefaction error in extinction estimates. Paleobiology 21, 300-313.

McRoberts, C.A., Newton, C.R., 1995. Selective extinction among end-Triassic European bivalves. Geology 23, 102-104.

McRoberts, C.A., Furrer, H., Jones, D.S., 1997. Palaeoenvironmental interpretation of a

1731 Triassic-Jurassic boundary section from Western Austria based on palaeoecological and
1732 geochemical data. Palaeogeography, Palaeoclimatology, Palaeoecology 136, 79-95.
1733 Melchin, M.J., Holmden, C., 2006. Carbon isotope chemostratigraphy of the Llandovery in
1734 Arctic Canada: implications for global correlation and sea-level change. GFF 128,
1735 173-180.
1736 Metherell, R.G., Workman, L.E., 1969. Sedimentary features of the Crossfield Member.
1737 Bulletin of Canadian Petroleum Geology 17, 444-459.
1738 Meyer, K.M., Yu, M., Jost, A.B., Kelley, B.M., Payne, J.L., 2011. $\delta^{13}C$ evidence that high
1739 primary productivity delayed recovery from end-Permian mass extinction. Earth and
1740 Planetary Science Letters 302, 378-384.
1741 Morrow, J., Harries, P.J., Krivanek, J.G., 2011. Reef recovery following the
1742 Frasnian-Famennian (Late Devonian) mass extinction: evidence from the Dugway Range,
1743 west-central Utah. Palaios 26, 607-622.
1744 Mundil, R., Ludwig, K.R., Metcalfe, I., Renne, P.R., 2004. Age and timing of the Permian
1745 mass extinctions: U/Pb dating of closed-system zircons. Science 305, 1760-1763.
1746 Mutter, R.J., Neuman, A.G., 2006. An enigmatic chondrichthyan with Paleozoic affinities
1747 from the Lower Triassic of western Canada. Acta Palaeontologica Polonica 51, 271-282.
1748 Olsen, P.E., Kent, D.V., Sues, H.D., Koeberl, C., Huber, H., Montanari, A., Rainforth, E.C.,
1749 Fowell, S.J., Szajna, M.J., Hartline, B.W., 2002. Ascent of dinosaurs linked to an iridium
1750 anomaly at the Triassic-Jurassic boundary. Science 296, 1305-1307.
1751 Olsson, R.K., Hemleben, C., Berggren, W.A., Huber, B.T., 1999. Atlas of Paleocene
1752 Planktonic Foraminifera. Smithsonian Contributions to Paleobiology, v. 85. Smithsonian
1753 Institution, Washington, D.C., 252 pp.
1754 Orchard, M.J., 2007. Conodont diversity and evolution through the latest Permian and Early
1755 Triassic upheavals. Palaeogeography, Palaeoclimatology, Palaeoecology 252, 93-117.
1756 Ovtcharova, M., Bucher, H., Schaltegger, U., Galfetti, T., Brayard, A., Guex, J., 2006. New
1757 Early to Middle Triassic U–Pb ages from South China: Calibration with ammonoid
1758 biochronozones and implications for the timing of the Triassic biotic recovery. Earth and

1759 Planetary Science Letters 243, 463-475.
1760 Owen, A.W., Harper, D.A.T., Heath, R.A., 2008. A route to recovery: the early Silurian
1761 shallow-water shelly fauna in the northern Oslo basin. Lethaia 41, 173-184.
1762 Payne, J.L., 2005. Evolutionary dynamics of gastropod size across the end-Permian extinction
1763 and through the Triassic recovery interval. Paleobiology 31, 269-290.
1764 Payne, J.L., Lehrmann, D.J., Wei, J., Orchard, M.J., Schrag, D.P., Knoll, A.H., 2004. Large
1765 perturbations of the carbon cycle during recovery from the end-Permian extinction.
1766 Science 305, 506-509.
1767 Payne, J.L., Lehrmann, D.J., Christensen, S., Wei, J., Knoll, A., 2006. Environmental and
1768 biological controls on the initiation and growth of a Middle Triassic (Anisian) reef
1769 complex on the Great Bank of Guizhou, Guizhou Province, China. Palaios 21, 325-343.
1770 Payne, J.L., Turchyn, A.V., Paytan, A., DePaolo, D.J., Lehrmann, D.J., Yu, M., Wei, J., 2010.
1771 Calcium isotope constraints on the end-Permian mass extinction. Proceedings of the
1772 National Academy of Sciences (U.S.A.) 107, 8543-8548.
1773 Payne, J.L., Summers, M., Rego, B.L., Altiner, D., Wei, J., Yu, M., Lehrmann, D.J., 2011.
1774 Early and Middle Triassic trends in diversity, evenness, and size of foraminifers on a
1775 carbonate platform in south China: implications for tempo and mode of biotic recovery
1776 from the end-Permian mass extinction. Paleobiology 37, 409-425.
1777 Pedersen, T.F., Calvert, S.E., 1990. Anoxia vs. productivity: what controls the formation of
1778 organic-rich sediments and sedimentary rocks? American Association of Petroleum
1779 Geologists Bulletin 74, 454-466.
1780 Pickett, J.W., Wu, W.S., 1990. The succession of Early Carboniferous coral faunas in eastern
1781 Australia and China. Alcheringa 14, 89-108.
1782 Pörtner, H.O., 2001. Climate change and temperature-dependent biogeography: oxygen
1783 limitation of thermal tolerance in animals. Naturwissenschaften 88, 137-146.
1784 Pospichal, J.J., 1994. Calcareous nannofossils at the K-T boundary, El Kef: no evidence for
1785 stepwise, gradual or sequential extinctions. Geology 22, 99-102.
1786 Price, J.R., Velbel, M.A., 2003. Chemical weathering indices applied to weathering profiles

developed on heterogeneous felsic metamorphic parent rocks. Chemical Geology 202, 397-416.

Pruss, S.B., Bottjer, D.J., 2004. Early Triassic trace fossils of the Western United States and their implications for prolonged environmental stress from the end-Permian mass extinction. Palaios 19, 551-564.

Rampino, M.R., Adler, A.C., 1998. Evidence for abrupt latest Permian mass extinction of foraminifera: Results of tests for the Signor-Lipps effect. Geology 26, 415-418.

Rasmussen, C.M.Ø., Harper, D.A.T., 2011a. Interrogation of distributional data for the end-Ordovician crisis interval: where did disaster strike? Geological Journal 46, 478-500.

Rasmussen, C.M.Ø., Harper, D.A.T., 2011b. Did the amalgamation of continents drive the end Ordovician mass extinction? Palaeogeography, Palaeoclimatology, Palaeoecology 311, 48-62.

Raup, D.M., 1991. A kill curve for Phanerozoic marine species. Paleobiology 17, 37-48.

Reichow, M.K., Pringle, M.S., Al'Mukhamedov, A.I., Allen, M.B., Andreichev, V.L., Buslov, M.M., Davies, C.E., Fedoseev, G.S., Fitton, J.G., Inger, S., Medvedev, A.Ya., Mitchell, C., Puchkov, V.N., Safonova, I.Yu., Scott, R.A., Saunders, A.D., 2009. The timing and extent of the eruption of the Siberian Traps large igneous province: implications for the end-Permian environmental crisis. Earth and Planetary Science Letters 277, 9-20.

Renne, P.R., Zhang, Z., Richards, M.A., Black, M.T., Basu, A.R., 1995. Synchrony and causal relations between Permian-Triassic boundary crises and Siberian flood volcanism. Science 269, 1413-1416.

Renne, P.R., Deino, A.L., Hilgen, F.J., Kuiper, K.F., Mark, D.F., Mitchell III, W.S., Morgan, L.E., Mundil, R., Smit, J., 2013. Time scales of critical events around the Cretaceous-Paleogene boundary. Science 339, 684-687.

Retallack, G.J., 1999. Postpocalyptic greenhouse paleoclimate revealed by earliest Triassic paleosols in the Sydney Basin, Australia. Geological Society of American Bulletin 111, 52-70.

1815 Retallack, G.J., Jahren, A.H., 2008. Methane release from igneous intrusion of coal during
1816 Late Permian extinction events. Journal of Geology 116, 1-20.
1817 Retallack, G.J., Sheldon, N.D., Carr, P.F., Fanning, M., Thompson, C.A., Williams, M.L.,
1818 Jones, B.G., Hutton, A., 2011. Multiple Early Triassic greenhouse crises impeded
1819 recovery from Late Permian mass extinction. Palaeogeography, Palaoclimatology,
1820 Palaeoecology 308, 233-251.
1821 Richoz, S., Krystyn, L., Baud, A., Brandner, R., Horacek, M., Mohtat-Aghai, P., 2010.
1822 Permian-Triassic boundary interval in Middle East (Iran and N. Oman): Progressive
1823 environmental change from detailed carbonate carbon isotope marine curve and
1824 sedimentary evolution. Journal of Asian Earth Sciences 39, 236-253.
1825 Richoz, S., van de Schootbrugge, B., Pross, J., Püttmann, W., Quan, T.M., Lindström, S.,
1826 Heunisch, C., Fiebig, J., Maquil, R., Schouten, S., Hauzenberger, C.A., Wignall, P.B.,
1827 2012. Hydrogen sulphide poisoning of shallow seas following the end-Triassic extinction.
1828 Nature Geoscience 5, 662-667.
1829 Romano, C., Brinkmann, W., 2010. A new specimen of the hybodont shark *Palaeobates*
1830 *polaris* with three-dimensionally preserved Meckel's cartilage from the Smithian (Early
1831 Triassic) of Spitsbergen. Journal of Vertebrate Paleontology 30, 1673-1683.
1832 Romano, C., Goudeman, N., Vennemann, T.W., Ware, D., Schneebeli-Hermann, E., Hochuli,
1833 P.A., Brühwiler, T., Brinkmann, W., Bucher, H., 2013. Climatic and biotic upheavals
1834 following the end-Permian mass extinction. Nature Geoscience 6, 57-60.
1835 Ruhl, M., Kürschner, W.M., 2011. Multiple phases of carbon cycle disburbance from large
1836 igneous province formation at the Triassic-Jurassic transition. Geology 39, 431-434.
1837 Ruhl, M., Deenen, M.H.L., Abels, H.A., Bonis, N.R., Krijgsman, W., Kürschner, W.M., 2010.
1838 Astronomical constraints on the duration of the early Jurassic Hettangian stage and
1839 recovery rates following the end-Triassic mass extinction (St Audrie's Bay/East
1840 Quantoxhead, UK). Earth and Planetary Science Letters 295, 262-276.
1841 Ruhl, M., Bonis, N.R., Reichart, G.-J., Sinninghe Damsté, J.S., Kürschner, W.M., 2011.
1842 Atmospheric carbon injection linked to end-Triassic mass extinction. Science 333,

430-434.

Sageman, B.B., Rich, J., Arthur, M.A., Birchfield, G.E., Dean, W.E., 1997. Evidence for Milankovitch periodicities in Cenomanian-Turonian lithologic and geochemical cycles: Western Interior, U.S. Journal of Sedimentary Research 67, 286-301.

Sano, H., Kuwahara, K., Yao, A., Agematsu, S., 2010. Panthalassan seamount-associated Permian-Triassic boundary siliceous rocks, Mino Terrane, Central Japan. Paleontological Research 14, 293-314.

Scheaffer, B., Mangus, M., Laudon, L.R., 1976. An early Triassic fish assemblage from British Columbia. Bulletin of the American Museum of Natural History 156, 517-563.

Schoene, B., Guex, J., Bartolini, A., Schaltegger, U., Blackburn, T.J., 2010. Correlating the end-Triassic mass extinction and flood basalt volcanism at the 100 ka level. Geology 38, 387-390.

Schoepfer, S.D., Shen, J., Wei, H., Tyson, R.V., Ingall, E., Algeo, T.J., 2014. TOC, organic P, and biogenic Ba accumulation rates as proxies for marine primary productivity and export flux. Earth-Science Reviews, in press.

Schrader, H., Matherne, A., 1981. Sapropel formation in the eastern Mediterranean Sea: Evidence from preserved opal assemblage. Micropaleontology 27, 191-203.

Sephton, M.A., Looy, C.V., Brinkhuis, H., Wignall, P.B., de Leeuw, J.W., Visscher, H., 2005. Catastrophic soil erosion during the end-Permian biotic crisis. Geology 33, 941-944.

Sepkoski, J.J., Jr., 1984. A kinetic model of Phanerozoic taxonomic diversity. III. Post Paleozoic families and mass extinctions. Paleobiology 10, 246-267.

Sepkoski, J.J., Jr., 1986. Phanerozoic overview of mass extinction, in: Raup, D.M., Jablonski, D. (Eds.), Patterns and Processes in the History of Life, Springer-Verlag, Berlin, pp. 277-295.

Sepkoski, J.J., Jr., 1994. Extinction and the fossil record. Geotimes 39, 15-17.

Sepkoski, J.J., Jr., 1996. Patterns of Phanerozoic extinction: a perspective from global data bases, in: Walliser, O.H. (Ed.), Global Events and Event Stratigraphy in the Phanerozoic, Springer-Verlag, Berlin, pp. 35-51.

1871 Sepkoski, J.J., Jr., 1998. Rates of speciation in the fossil record. Philosophical Transactions of
1872 the Royal Society of London B—Biological Sciences 353, 315-326.
1873 Sepúlveda, J., Wendler, J.E., Summons, R.E., Hinrichs, K., 2009. Rapid resurgence of marine
1874 productivity after the Cretaceous-Paleogene mass extinction. Science 326, 129-132.
1875 Seuß, B., Höfling, R., Nützel, A., 2005. Triassic/Jurassic carbonates from the Hochfelln
1876 Mountain (northern calcareous Alps)—its facies, silicified fauna and implications for the
1877 end-Triassic biotic crisis. Facies 51, 405-418.
1878 Sheehan, P.M., 2001. The Late Ordovician mass extinction. Annual Review of Earth and
1879 Planetary Sciences 29, 331-364.
1880 Sheehan, P.M., Coorough, P.J., 1990. Brachiopod zoogeography across the
1881 Ordovician-Silurian extinction event, in: McKerrow, W.S., Scotese, C.R. (Eds.),
1882 Palaeozoic Palaeogeography and Biogeography, Geological Society of London Memoir
1883 12, pp. 181-187.
1884 Sheehan, P.M., Harris, M.T., 2004. Microbialite resurgence after the Late Ordovician
1885 extinction. Nature 430, 75-78.
1886 Sheldon, N.D., 2006. Abrupt chemical weathering increase across the Permian-Triassic
1887 boundary. Palaeogeography, Palaeoclimatology, Palaeoecology 231, 315-321.
1888 Shen, J.W., Webb, G.E., 2004. Famennian (Upper Devonian) calcimicrobial (*Renalcis*) reef at
1889 Miaomen, Guilin, Guangxi, South China. Palaeogeography, Palaeoclimatology,
1890 Palaeoecology 204, 373-394.
1891 Shen, J., Algeo, T.J., Hu, Q., Xu, G., Zhou, L., Feng, Q., 2013. Volcanism in South China
1892 during the Late Permian and its relationship to marine ecosystem and environmental
1893 changes. Global and Planetary Change 105, 121-134.
1894 Shen, S.Z., Crowley, J.L., Wang, Y., Bowring, S.A., Erwin, D.H., Sadler, P.M., Cao, C.,
1895 Rothman, D.H., Henderson, C.M., Ramezani, J., Zhang, H., Shen, Y., Wang, X., Wang,
1896 W., Mu, L., Li, W., Tang, Y., Liu, X., Liu, L., Zeng, Y., Jiang, Y., Jin, Y., 2011.
1897 Calibrating the end-Permian mass extinction. Science 334, 1367-1372.
1898 Shen, Y., Farquhar, J., Zhang, H., Masterson, A., Zhang, T., Wing, B., 2011. Multiple

1899 S-isotopic evidence for episodic shoaling of anoxic water during Late Permian mass
1900 extinction. Nature Communications 2, no. 210. doi:10.1038/ncomms1217.
1901 Sigurdsson, H., D'Hondt, S., Carey, S., 1992. The impact of the Cretaceous/Tertiary bolide on
1902 evaporite terrane and generation of major sulfuric acid aerosol. Earth and Planetary
1903 Science Letters 109, 543-559.
1904 Skulan, J., DePaolo, D.J., Owens, T.L., 1997. Biological control of calcium isotopic
1905 abundances in the global calcium cycle. Geochimica et Cosmochimica Acta 61,
1906 2505-2510.
1907 Sobolev, S.V., Sobolev, A.V., Kuzmin, D.V., Krivolutskaya, N.A., Petrunin, A.G., Arndt, N.T.,
1908 Radko, V.A., Vasiliev, Y.R., 2011. Linking mantle plumes, large igneous provinces and
1909 environmental catastrophes. Nature 477, 312-319.
1910 Sokiran, E.V., 2002. Frasnian-Famennian extinction and recovery of rhychonellid brachiopods
1911 from the East European Platform. Acta Palaeontologica Polonica 47, 339-354.
1912 Solé, R.V., Montoya, J.M., Erwin, D.H., 2002. Recovery from mass extinction: evolutionary
1913 assembly in large-scale biosphere dynamics. Philosophical Transactions of the Royal
1914 Society B—Biological Sciences 357, 697-707.
1915 Song, H.J., Wignall, P.B., Chen, Z.-Q., Tong, J., Bond, D.P.G., Lai, X., Zhao, X., Jiang, H.,
1916 Yan, C., Niu, Z., Chen, J., Yang, H., Wang, Y., 2011. Recovery tempo and pattern of
1917 marine ecosystems after the end-Permian mass extinction. Geology 39, 739-742.
1918 Song, H.J., Wignall, P.B., Tong, J., Bond, D.P.G., Song, H., Lai, X., Zhang, K., Wang, H.,
1919 Chen, Y., 2012. Geochemical evidence from bio-apatite for multiple oceanic anoxic
1920 events during Permian-Triassic transition and the link end-Permian extinction and
1921 recovery. Earth and Planetary Science Letters 353-354, 12-21.
1922 Song, H.J., Wignall, P.B., Tong, J.N., Yin, H.F., 2013. Two pulses of extinction during the
1923 Permian-Triassic crisis. Nature Geoscience 6, 52-56.
1924 Song, H.Y., Tong, J., Algeo, T.J., Horacek, M., Qiu, H., Song, H.J., Tian, L., Chen, Z., 2013.
1925 Large vertical $\delta^{13}C_{DIC}$ gradients in Early Triassic seas of the South China craton:
1926 Implications for oceanographic changes related to Siberian Traps volcanism. Global and

1927 Planetary Change 105, 7-20.
1928 Song, H.Y., Tong, J., Algeo, T.J., Song, H.J., Qiu, H., Zhu, Y., Tian, L., Bates, S., Lyons, T.W.,
1929 Luo, G., Kump, L.R., 2014. Early Triassic seawater sulfate drawdown. Geochimica et
1930 Cosmochimica Acta 128, 95-113.
1931 Stampfli, G., Marcoux, J., Baud, A., 1991. Tethyan margins in space and time.
1932 Palaeogeography, Palaeoclimatology, Palaeoecology 87, 373-409.
1933 Stanley, S.M., 2009. Evidence from ammonoids and conodonts for multiple Triassic mass
1934 extinctions. Proceedings of the National Academy of Sciences (U.S.A.) 106,
1935 15264-15267.
1936 Stearn, C.W., 1987. Effect of the Frasnian-Famennian extinction event on the stromatoporoids.
1937 Geology 15, 677-679.
1938 Stemmerik, L., Bendix-Almgreen, S.E., Piasecki, S., 2001. The Permian-Triassic boundary in
1939 central East Greenland: Past and present views. Bulletin of the Geological Society of
1940 Denmark 48, 159-167.
1941 Sun, Y.D., Joachimski, M.M., Wignall, P.B., Yan, C.B., Chen, Y.L., Jiang, H.S., Wang, L.N.,
1942 Lai, X.L., 2012. Lethally hot temperatures during the early Triassic greenhouse. Science
1943 388, 366-370.
1944 Sutcliffe, O.E., Dowdeswell, J.A., Whitington, R.J., Theron, J.N., Craig, J., 2006. Calibrating
1945 the Late Ordovician glaciation and mass extinction by the eccentricity cycles of Earth's
1946 orbit. Geology 28, 967-970.
1947 Svensen, H., Planke, S., Malthe-Sørenssen, A., Jamtveit, B., Myklebust, R., Eidem, T.R., Rey,
1948 S.S., 2004. Release of methane from a volcanic basin as a methanism for initial Eocene
1949 global warming. Nature 429, 542-545.
1950 Takemura, A., Sakai, M., Sakamoto, S., Aono, R., Takemura, S., Yamakita, S., 2007. Earliest
1951 Triassic radiolarians from the ARH and ARF sections on Arrow Rocks, Waipapa Terrane,
1952 Northland, New Zealand, in: Sporli, K.B., Takemura, A., Hori, R.S. (Eds.), The Oceanic
1953 Permian/Triassic Boundary Sequence at Arrow Rocks (Oruatemanu) Northland, New

Zealand. GNS Science Monograph 24, Lower Hutt, New Zealand, pp. 97-107.

Tang, J., Kohler, S.J., Dietzel, M., 2008. Sr^{2+}/Ca^{2+} and $^{44}Ca/^{40}Ca$ fractionation during inorganic calcite formation: II. Ca isotopes. Geochimica et Cosmochimica Acta 72, 3733-3745.

Timmreck, C., Graf, H.F., Lorenz, S.J., Niemeier, U., Zanchettin, D., Matei, D., Jungdaus, J.H., Crowley, T.J., 2010. Aerosol size confines climate response to volcanic super-eruptions. Geophysical Research Letters 37, L24705, doi:10.1029/2010GL045464.

Tomašových, A., Siblík, M., 2007. Evaluating compositional turnover of brachiopod communities during the end-Triassic mass extinction (Northern Calcareous Alps): removal of dominant groups, recovery and community reassembly. Palaeogeography, Palaeoclimatology, Palaeoecology 244, 170-200.

Tong, J., 1997. The ecosystem recovery after the end-Paleozoic mass extinction in South China. Earth Science—Journal of China University of Geoscience 22, 373-376 (in Chinese with English abstract).

Tong, J., Yin, H., 2002. The Lower Triassic of South China. Journal of Asian Earth Sciences 20, 803-815.

Tong, J., Yin, H., Zhang, J., Zhao, L., 2001. Proposed new Lower Triassic stages in South China. Science in China Series D—Earth Sciences 44, 961-967.

Tong, J., Zakharov, Y.D., Orchard, M.J., Yin, H., Hansen, H.J., 2003. A candidate of the Induan-Olenekian boundary stratotype in the Tethyan region. Science in China Series D—Earth Sciences 46, 1182-1200.

Tong, J., Zhao, X., Erwin, D.H., Zuo, J., Zhao, L., 2006. Fossil fishes from the Lower Triassic of Majiashan, Chaohu, Anhui Province, China. Journal of Paleontology 80, 146-161.

Tong, J., Zuo, J., Chen, Z.Q., 2007a. Early Triassic carbon isotope excursions from South China: Proxies for devastation and restoration of marine ecosystems following the end-Permian mass extinction. Geological Journal 42, 371-389.

Tong, J., Zhang, S., Zuo, J., Xiong, X., 2007b. Events during Early Triassic recovery from the

1981 end-Permian extinction. Global and Planetary Change 55, 66-80.
1982 Tribovillard, N., Algeo, T.J., Lyons, T., Riboulleau, A., 2006. Trace metals as paleoredox and
1983 paleoproductivity proxies: an update. Chemical Geology 232, 12-32.
1984 Twitchett, R.J., 1999. Palaeoenvironments and faunal recovery after the end-Permian mass
1985 extinction. Palaeogeography Palaeoclimatology, Palaeoecology 154, 27-37.
1986 Twitchett, R.J., 2007. The Lilliput effect in the aftermath of the end-Permian extinction event.
1987 Palaeogeography, Palaeoclimatology, Palaeoecology 252, 132-144.
1988 Twitchett, R.J., Barras, C.G., 2004. Trace fossils in the aftermath of mass extinction events, in:
1989 McIlroy, D. (Ed.), Application of Ichnology to Palaeoenvironmental and Stratigraphic
1990 Analysis. Geological Society of London Special Publication 228, 395-415.
1991 Twitchett, R.J., Wignall, P.B., 1996. Trace fossils and the aftermath of the Permo-Triassic
1992 mass extinction: evidence from northern Italy. Palaeogeography, Palaeoclimatology,
1993 Palaeoecology 124, 137-151.
1994 Twitchett, R.J., Krystyn, L., Baud, A., Wheeley, J.R., Richoz, S., 2004. Rapid marine recovery
1995 after the end-Permian extinction event. Geology 32, 805-808.
1996 van de Schootbrugge, B., Tremolada, F., Bailey, T.R., Rosenthal, Y., Feist-Burkhardt, S.,
1997 Brinkhuis, H., Pross, J., Kent, D.V., Falkowski, P.G., 2007. End-Triassic calcification
1998 crisis and blooms of organic-walled disaster species. Palaeogeography,
1999 Palaeoclimatology, Palaeoecology 244, 126-141.
2000 van de Schootbrugge, B., Quan, T.M., Lindström, S., Püttmann, W., Heunisch, C., Pross, J.,
2001 Fiebig, J., Petschick, R., Röhling, H.-G., Richoz, S., Rosenthal, Y., Falkowski, P.G., 2009.
2002 Floral changes across the Triassic/Jurassic boundary linked to flood basalt volcanism.
2003 Nature Geoscience 2, 589-594.
2004 van de Schootbrugge, B., Bachan, A., Suan, G., Richoz, S., Payne, J.L., 2013. Microbes, mud
2005 and methane: cause and consequence of recurrent Early Jurassic anoxia following the
2006 end-Triassic mass extinction. Palaeontology 54, 685-709.
2007 Wahlmann, G.P., 2002. Upper Carboniferous-Lower Permian (Bashkirian-Kungurian) mounds
2008 and reefs, in: Kiessling, W., Flügel, E., Golonka, J. (Eds.), Phanerozoic Reef Patterns,

SEPM (Society of Sedimentary Geology) Special Publication 72, pp. 271-338.

Walliser, O.H., 1996. Global events in the Devonian and Carboniferous, in: Walliser, O.H., (Ed.), Global Events and Event Stratigraphy in the Phanerozoic, Springer-Verlag, Berlin, pp. 225-250.

Wang, N., Yang, S., Jin, F., Wang, W., 2001. Early Triassic Hybodontoidea from Tiandong of Guangxi, China—First report on the fish sequence study near the Permian-Triassic boundary in South China. Vertebrata Palasiatica 39, 237-250.

Wang, Y.B., Tong, J.N., Wang, J.S., Zhou, X., 2005. Calcimicrobialite after end-Permian mass extinction in South China and its paleoenvironmental significance. Chinese Science Bulletin 50, 665-671.

Ward, P.D., Montgomery, D.R., Smith, R., 2000. Altered river morphology in South Africa related to the Permian-Triassic extinction. Science 289, 1740-1743.

Webb, G.E., 1998. Earliest known Carboniferous shallow-water reefs, Gudman Formation (Tn1b), Queensland, Australia: implications for Late Devonian reef collapse and recovery. Geology 26, 951-954.

Webb, G.E., 1999. Youngest Early Carboniferous (Late Visean) shallow-water patch reefs in eastern Australia (Rockhampton Group, Queensland): combining quantitative micro- and macro-scale data. Facies 41, 111-140.

White, R.V., Saunders, A.D., 2005. Volcanism, impact and mass extinctions: incredible or credible coincidences? Lithos 79, 299-316.

Wignall, P.B., 2001. Large igneous provinces and mass extinctions. Earth-Science Reviews 53, 1-33.

Wignall, P.B., Twitchett, R.J., 1996. Oceanic anoxia and the end Permian mass extinction. Science 272, 1155-1158.

Williford, K.H., Ward, P.D., Garrison, G.H., Buick, R., 2007. An extended organic carbon-isotope record across the Triassic-Jurassic boundary in the Queen Charlotte Islands, British Columbia, Canada. Palaeogeography, Palaeoclimatology, Palaeoecology

244, 290-296.

Wood, R., 2004. Palaeoecology of a post-extinction reef: Famennian (Late Devonian) of the Canning Basin, north-western Australia. Palaeontology 47, 415-445.

Wu, H., Zhang, S., Feng, Q., Jiang, G., Li, H., Yang, T., 2012. Milankovitch and sub-Milankovitch cycles of the early Triassic Daye Formation, South China and their geochronological and paleoclimatic implications. Gondwana Research 22, 748-759.

Xie, S., Pancost, R.D., Yin, H., Wang, H., Evershed, R., 2005. Two episodes of microbial change coupled with Permo/Triassic faunal mass extinction. Nature 434, 494-497.

Xie, S., Pancost, R.D., Huang, J., Wignall, P.B., Yu, J., Tang, X., Chen, L., Huang, X., Lai, X., 2007. Changes in the global carbon cycle occurred as two episodes during the Permian-Triassic crisis. Geology 35, 1083-1086.

Xie, S., Pancost, R.D., Wang, Y., Yang, H., Wignall, P.B., Luo, G., Jia, C., Chen, L., 2010. Cyanobacterial blooms tied to volcanism during the 5 m.y. Permo-Triassic biotic crisis. Geology 38, 447-450.

Yamamoto, S., Hasegawa, T., Tada, R., Goto, K., Rojas-Consuegra, R., Díaz-Otero, C., García-Delgado, D.E., Yamamoto, S., Sakuma, H., Matsui, T., 2010. Environmental and vegetational changes recorded in sedimentary leaf wax *n*-alkanes across the Cretaceous-Paleogene boundary at Loma Capiro, Central Cuba. Palaeogeography, Palaeoclimatology, Palaeoecology 295, 31-41.

Yang, S., Wang, X., Hao, W., 1986. New knowledge on the Lower Triassic of Zuodeng, Tiandong County, Guangxi. Acta Scientiarum Naturalium Univerisitatis Pekinensis 4, 105-117.

Yin, H.F., Xie, S.C., Luo, G.M., Algeo, T.J., Zhang, K.X., 2012. Two episodes of environmental change at the Permian-Triassic boundary of the GSSP section Meishan. Earth-Science Reviews 115, 163-172.

Young, G.M., Nesbitt, H.W., 1998. Processes controlling the distribution of Ti and Al in weathering profiles, siliciclastic sediments and sedimentary rocks. Journal of Sedimentary Research 68, 448-455.

Zhang, L., Zhao, L., Chen, Z.Q., Algeo, T.J., Chen, J., Wang, R., Chen, L., Hou, J., Yang, L., Qiu, H., Feng, X., Wang, X., 2014. Amelioration of marine environments at the Smithian-Spathian boundary, as recorded in the Shitouzhai section, Guizhou Province, South China. Biogeosciences Discussions, in press.

Zhang, Q., Zhou, C., Lu, T., Lou, X., Liu, W., Sun, Y., Huang, J., Zhao, L., 2009. A conodont-based Middle Triassic age assignment for the Luoping Biota of Yunnan, China. Science in China Series D—Earth Sciences 52, 1673-1678.

Zhang, Q., Zhou, C., Lü, T., Bai, J., 2010. Discovery of Middle Triassic Saurichthys in the Luoping area, Yunnan, China. Geological Bulletin of China 29, 26-30.

Zhao, L., Lu, L., 2007. A new genus of Early Triassic perleidid fish from Changxing, Zhejiang, China. Acta Palaeontologica Sinica 46, 238-243.

Zhao, L., Xiong, X., Yang, F., Wang, Z., He, W., 2005. Conodonts from the Lower Triassic in the Nantuowan Section of Daxiakou, Xingshan County, Hubei Province. Albertiana 33, 113-114.

Zhao, L., Orchard, M.J., Tong, J., Sun, Z., Zuo, J., Zhang, S., Yun, A., 2007. Lower Triassic conodont sequence in Chaohu, Anhui Province, China and its global correlation. Palaeogeography, Paleoclimatology, Palaeoecology 252, 24-38.

Zhao, L., Wang, L., Li, C., 2008. Studies of the Triassic marine reptiles of China: a review. Acta Palaeontologica Sinica 47, 232-239.

Zonneveld, J., Gingras, M.K., Beatty, T.W., 2010. Diverse ichnofossil assemblages following the P-Tr mass extinction, Lower Triassic, Alberta and British Columbia, Canada: evidence for shallow marine refugia on the northwestern coastal of Pangaea. Palaios 25, 368-392.

FIGURE CAPTIONS

Figure 1. Three hypotheses to account for the protracted recovery of Early Triassic marine ecosystems, linking it to (A) the intensity of the mass extinction (Solé et al., 2002); (B) the persistence of harsh environmental conditions (Hallam, 1991; Isozaki, 1997; Payne et al., 2004); and (C) the episodic recurrence of major environmental perturbations (Orchard, 2007; Stanley, 2009; Algeo et al., 2011a; Retallack et al., 2011). The heavy solid line represents a general biodiversity trend (cf. Tong et al., 2007b), and the shaded lines represent extinction intensity (A) or environmental stresses (B and C). PTB: Permian-Triassic boundary. ET: Early Triassic. MT: Middle Triassic.

Figure 2. General patterns of biodiversity and ecological change during the Permian-Triassic transition and Early Triassic. Gr. = Griesbachian; Dien. = Dienerian; Sm. = Smithian; SWI = sediment-water interface. For the tiering column, positive and negative values are elevations in centimeters relative to the sediment-water interface (SWI). Biodiversity data: conodont (Orchard, 2007; Stanley, 2009), ammonoid (Stanley, 2009; Yuri and Abnavi, 2013), radiolarian (Racki and Cordey, 2000), foraminifera (Song et al., 2011; Payne et al., 2011a), brachiopod (Chen et al., 2005; Yuri and Abnavi, 2013), and echinoderm (Chen and McNamara, 2006). Trace fossils: diameter (Twitchett, 1999; Chen et al., 2011) and ichnodiversity (Chen et al., 2011). Lilliput effect: maximum gastropod size (Payne, 2005) and mean foraminifer size (Payne et al., 2011b; Rego et al., 2012). Tiering data (Twitchett, 1999) and alpha diversity data (Hofmann et al., 2013, 2014). Recovery stages 1 and 2 are defined in this study. The timescale is a modified version of that of Algeo et al. (2013) (see Supplementary Table 1).

Figure 3. Volcanic and oceanic environmental changes during the Permian-Triassic transition and Early Triassic. Abbreviations as in Figure 2. Timing of Siberian Traps eruptions

is interpretative. Data sources: $\delta^{13}C_{carb}$ (Payne et al., 2004), sea-level elevations (Haq et al., 1987; Haq and Schutter, 2008), vertical $\Delta^{13}C$ of DIC (Song-HY et al., 2013), bioapatite $\delta^{18}O$ (Sun et al., 2012; Romano et al., 2013), $\delta^{34}S_{sulf}$ (Song et al., 2014), $\delta^{44/40}Ca$ (Payne et al., 2010; Hinojosa et al., 2012), and ocean redox (Kakuwa, 2008; Wignall et al., 2010; Song et al., 2012; Grasby et al., 2013).

Figure 4. Permian-Triassic paleogeography of (A) South China (modified from Tong et al., 2007a), and (B) the world (modified from Algeo et al., 2013). Am = Amuria; Kz = Kazakhstan; NC = North China; SC = South China; Tm = Tarim.

Figure 5. Stratigraphic variation in lithology of the four study sections. Lithologies calculated per Eqs. 1-3 in Supplementary Information. The timescale at left is plotted relative to thickness in the Chaohu section and is non-linear; note the different thickness scales for the four sections.

Figure 6. Chemostratigraphic profiles of weathering proxies (Al and Fe) for the four study sections. Vertical scales are identical to those in Figure 5.

Figure 7. Chemostratigraphic profiles of productivity proxies (TOC, P, and Ba_{xs}) for the four study sections. Vertical scales are identical to those in Figure 5.

Figure 8. Chemostratigraphic profiles of redox proxies (Mo, U, and V) for the four study sections. Vertical scales are identical to those in Figure 5.

Figure 9. Profiles of weathering fluxes and CIA (chemical index of alteration) for the four study sections.

Figure 10. Profiles of productivity proxy fluxes for the four study sections.

Figure 11. Profiles of redox proxy fluxes for the four study sections.

Figure 12. Generalized patterns of marine environmental, biodiversity, and ecosystem change in the four study sections during the Early Triassic. The weathering, productivity, and redox profiles are based on Figures 9-11. Data sources: sea-surface temperatures (SST) (Sun et al., 2012); $\delta^{13}C_{carb}$ and generic diversity (Tong et al., 2007a); fossil abundance (Yang et al., 1986; Wang et al., 2001; Tong et al., 2003; Zhao et al., 2007; Krystyn et al., 2007; Li et al., 2009; Song et al., 2011); trace fossil burrow size, ichnodiversity, and tiering (Chen et al., 2011); and alpha diversity (Hofmann et al., 2013, 2014).

Figure 13. Integrated model showing relationships between environmental change, shallow-marine ecospace, and marine ecosystem recovery during the Early Triassic. The Griesbachian (A) and Smithian (C) are generally characterized by stronger volcanism, enhanced weathering and riverine nutrient fluxes, an expanded OMZ, more intense water-column stratification, weaker upwelling, and limited ecospace. In contrast, the Dienerian (B) and Spathian (D) are generally characterized by weaker volcanism, decreased weathering and riverine nutrient fluxes, a contracted OMZ, less intense water-column stratification, stronger upwelling, and expanded ecospace.

Figure 14. Patterns of environmental change and marine ecosystem recoveries following other major mass extinctions: (A) Cretaceous-Paleogene (K-Pg) boundary, (B) Triassic-Jurassic (Tr-J) boundary, (C) Late Devonian, and (D) Ordovician-Silurian (O-S) boundary. Data sources: (A) volcanism (Renne et al., 2013; Keller, 2003), impacts (Keller, 2003), $\delta^{13}C_{carb}$ (D'Hondt et al., 1998; Coxall et al., 2006), $\delta^{18}O$ (D'Hondt and Zachos, 1993; Norris, 1996; Birch et al., 2012), planktic foraminifera diversity (Keller, 2003; Coxall et al., 2006; Gallala et al., 2009), nanoplankton diversity (Hull et al., 2011), algal productivity

(Sepúlveda et al., 2009; n.b., S/(S+H) = sterane/(sterane+hopane) ratio), nektonic carnivore alpha diversity (Sessa et al., 2012), ecological tiering at the sediment-water interface (Sessa et al., 2012); (B) CAMP volcanism (Olsen et al., 2002; Deenen et al., 2010; Blackburn et al., 2013; Guex et al., 2012; Deenen et al., 2010; Ruhl et al., 2010), $\delta^{13}C_{org}$ (Ruhl et al., 2011; Bartolini et al., 2012; Williford et al., 2007), $\delta^{18}O$ (Korte et al., 2009), warm and cool intervals (Schoene et al., 2010), sea-level elevations (Haq et al., 1987), diversity of bivalves, ammonites, brachiopods, and reefs (Hallam, 1996); (C) sea-level elevations (Johnson et al., 1985; Algeo et al., 2007; Isaacson et al., 2008), $\delta^{13}C_{carb}$ (Buggisch and Joachimski, 2006), climatic oscillations (Isaacson et al., 2008), tropical sea surface temperatures (SSTs) (Joachimski et al., 2004), R-$CO_{2(atm)}$ (Berner, 1994; n.b., RCO_2 = ratio of atmospheric CO_2 in past to "modern" value of ~300 ppmv), stromatoporoid diversity (Stearn, 1987; Webb, 1998; Morrow et al., 2011), reef-building coral diversity (Webb, 1998); and (D) sea-level elevations (Johnson et al., 1991; Couto et al., 2013); $\delta^{13}C_{carb}$ (Finney et al., 1999; Cramer et al., 2011; Kaljo and Martma, 2000; Gouldey et al., 2010; Delabroye et al., 2011), $^{87}Sr/^{86}Sr$ (Azmy et al., 1999; Gouldey et al., 2010), tropical SSTs (Finnegan et al., 2011), glaciations (Caputo, 1998; Azmy et al., 1998; Delabroye et al., 2011), crinoid diversity (Ausich and Deline, 2012), graptolite diversity (Fan and Chen, 2007), coral diversity (Kaljo, 1996), brachiopod recovery stage (Rong and Harper, 1999).

Figure

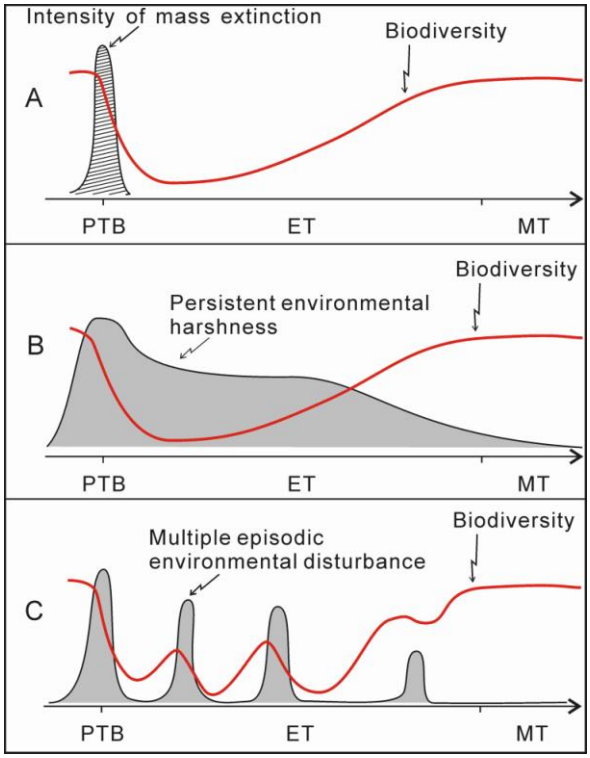

Figure 1.

Figure

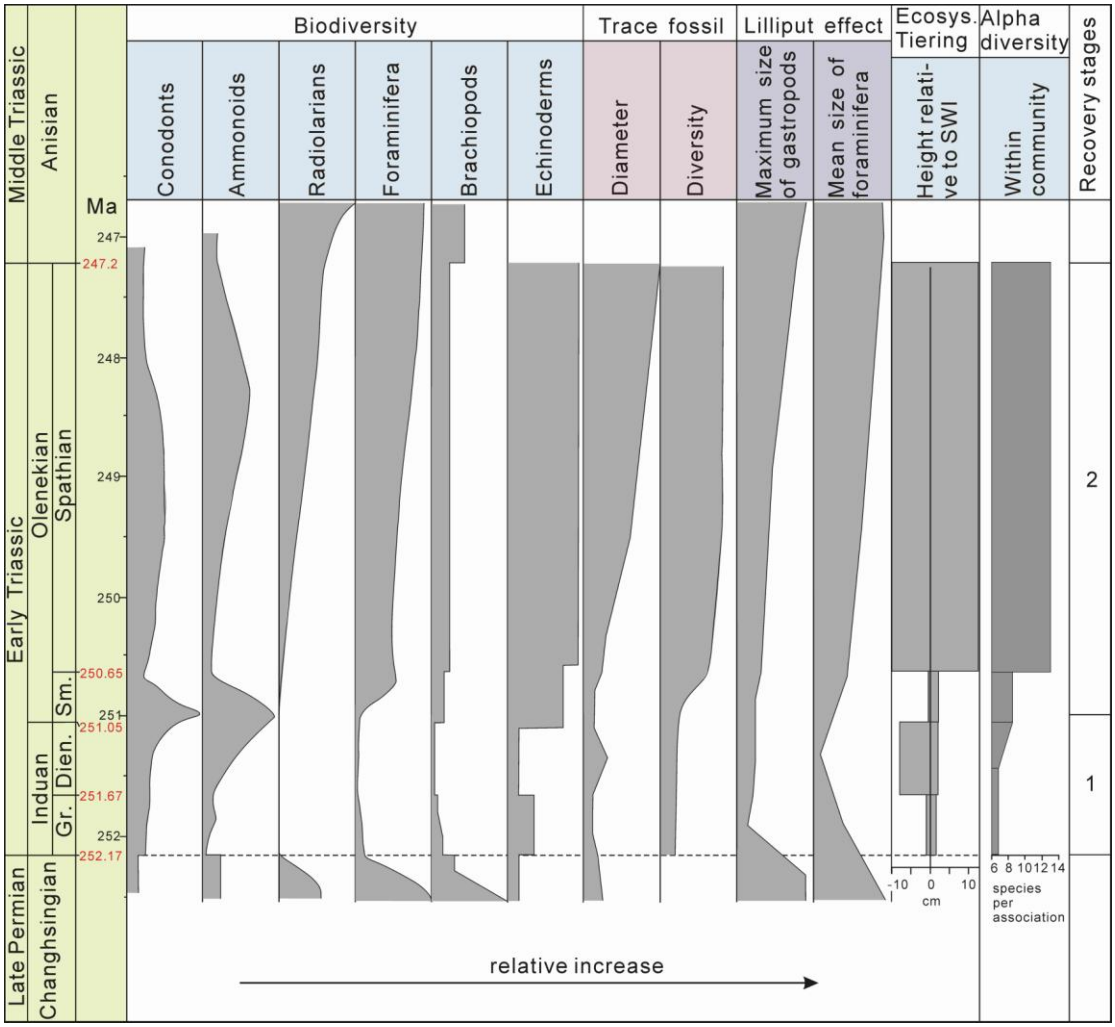

Figure 2.

Figure

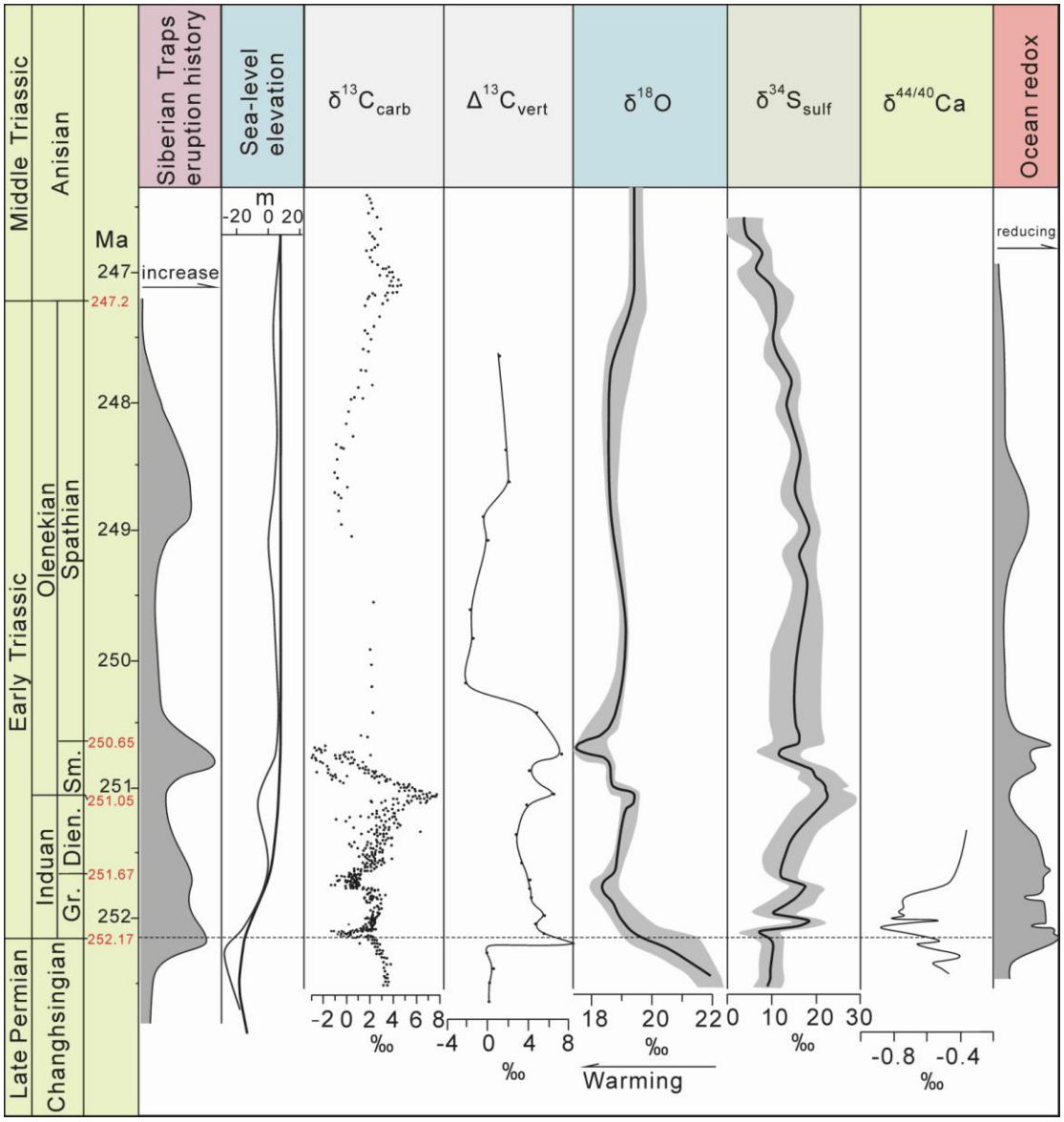

Figure 3.

Figure

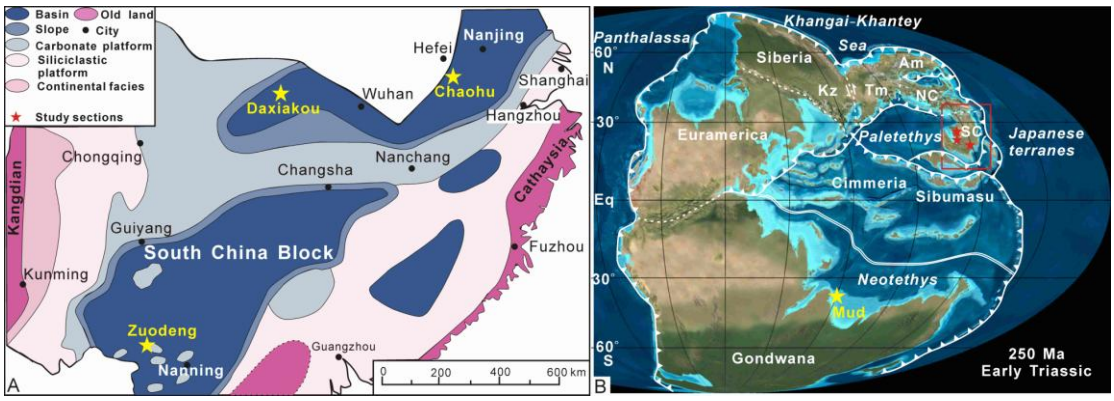

Figure 4.

Figure

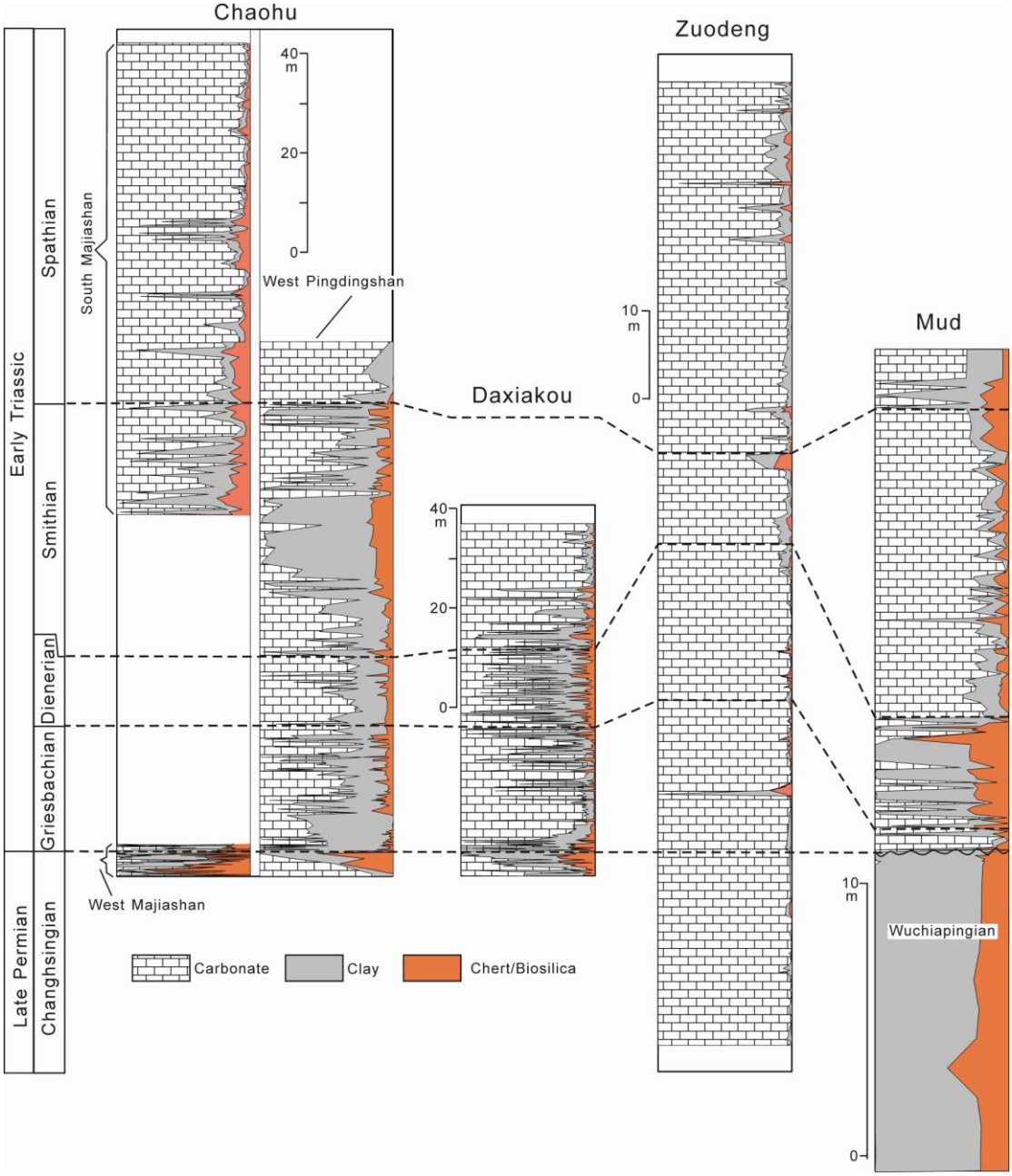

Figure 5.

Figure

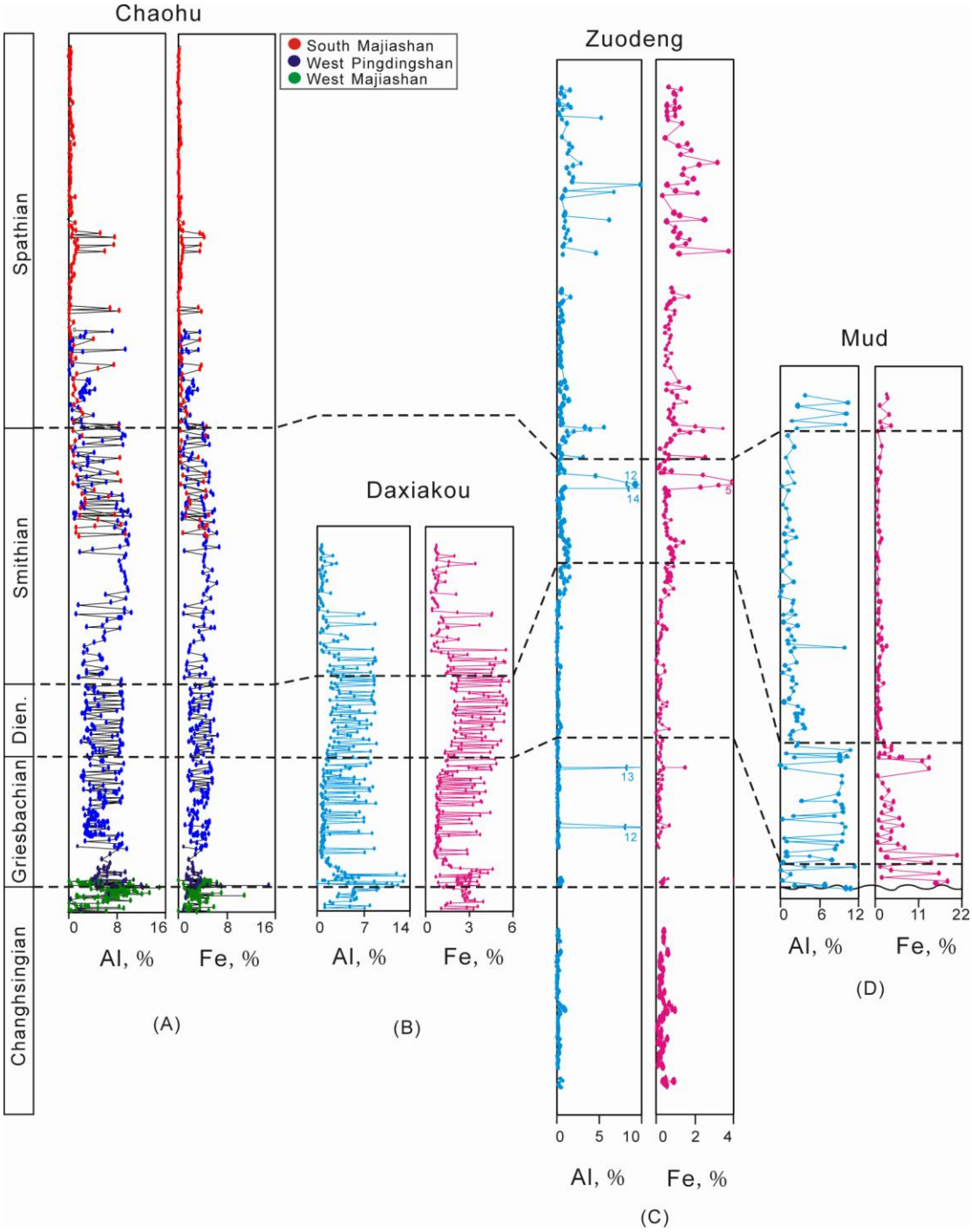

Figure 6.

Figure

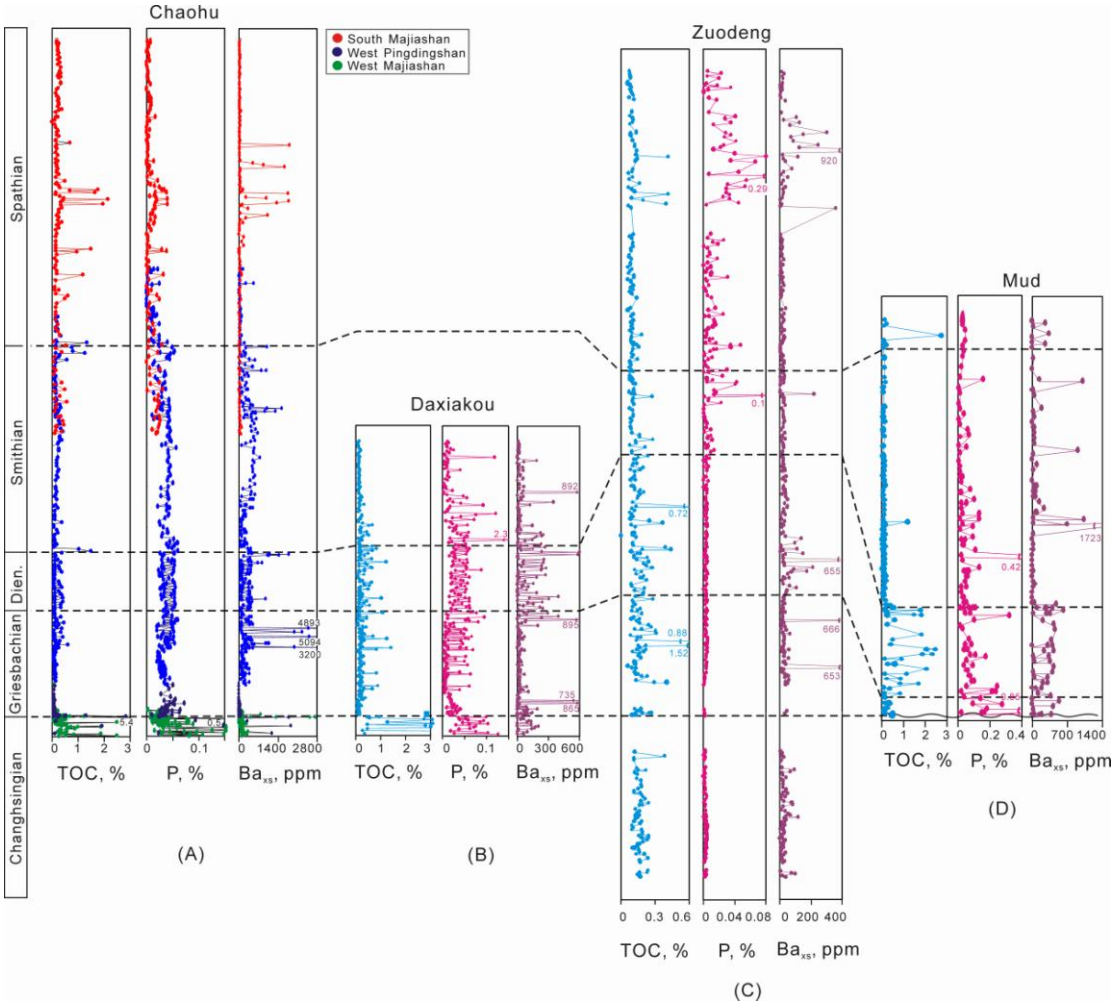

Figure 7.

Figure

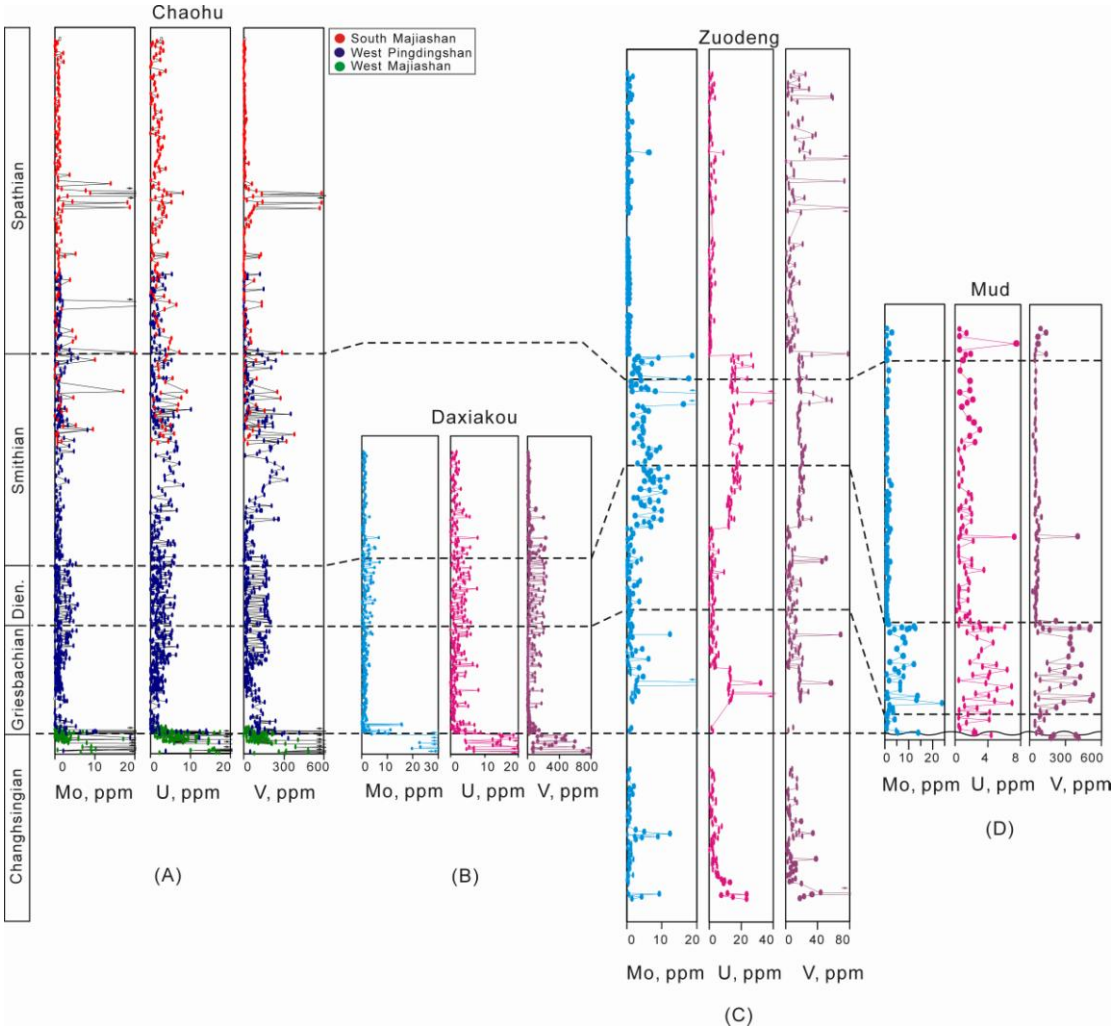

Figure 8.

Figure

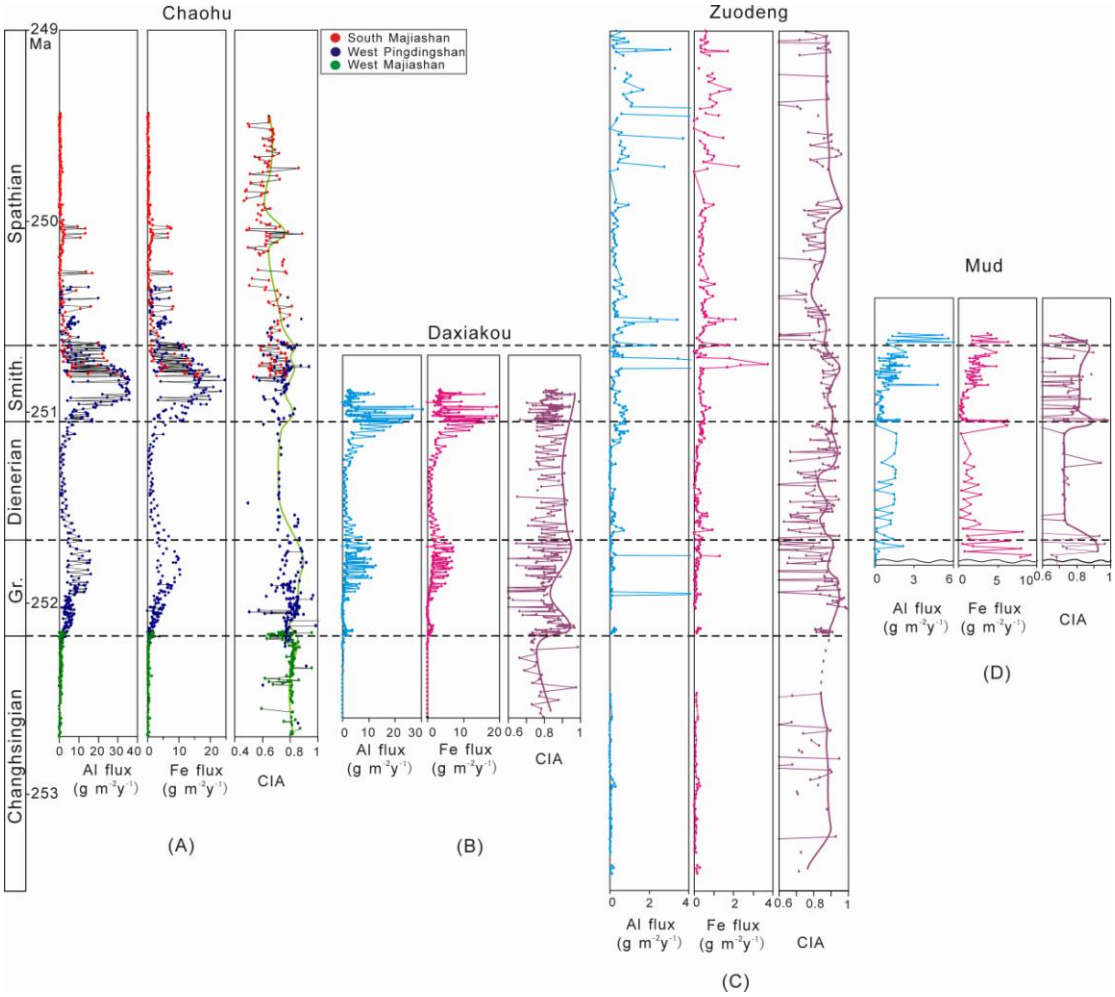

Figure 9.

Figure

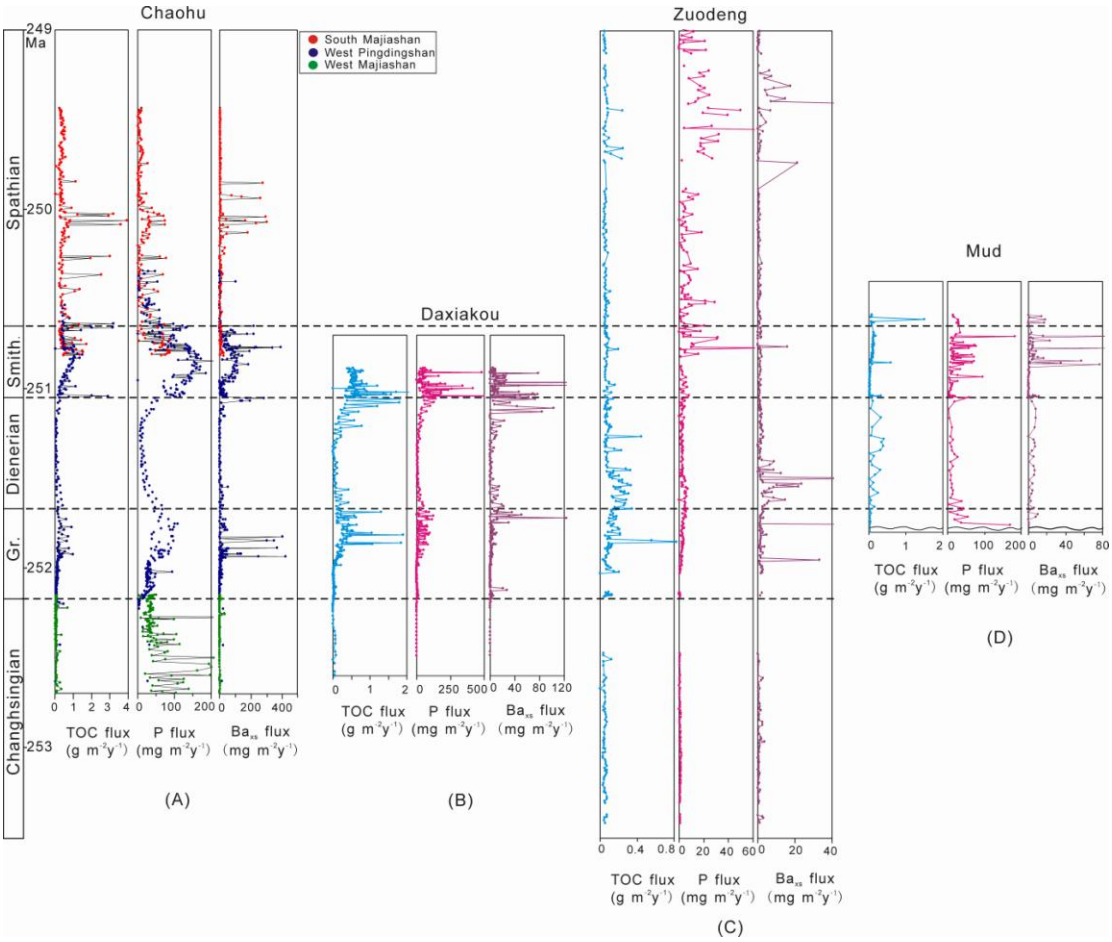

Figure 10.

Figure

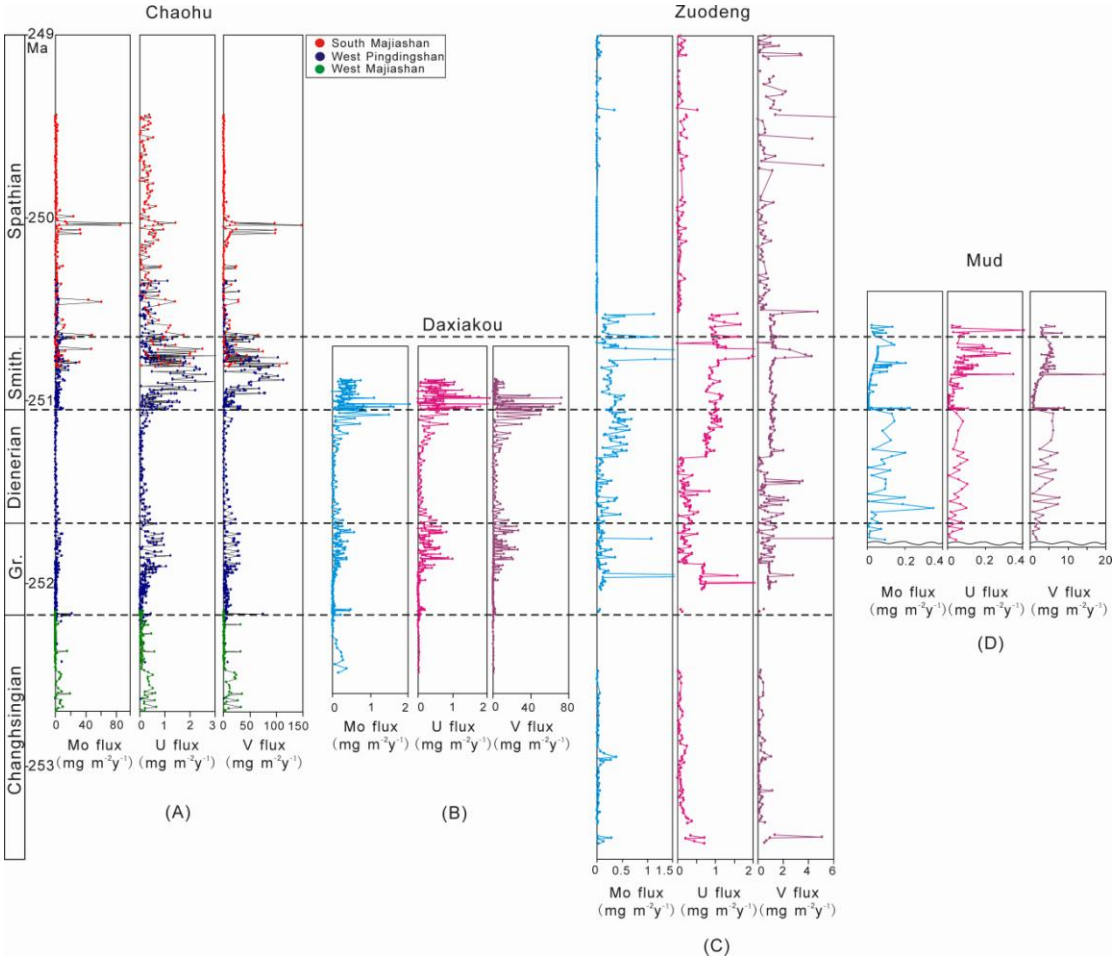

Figure 11.

Figure

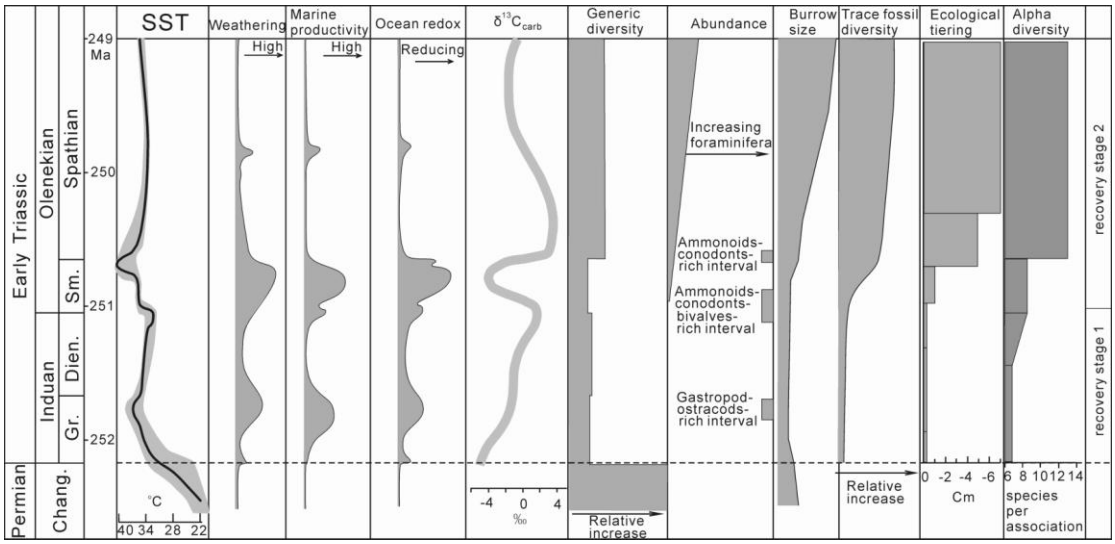

Figure 12.

Figure

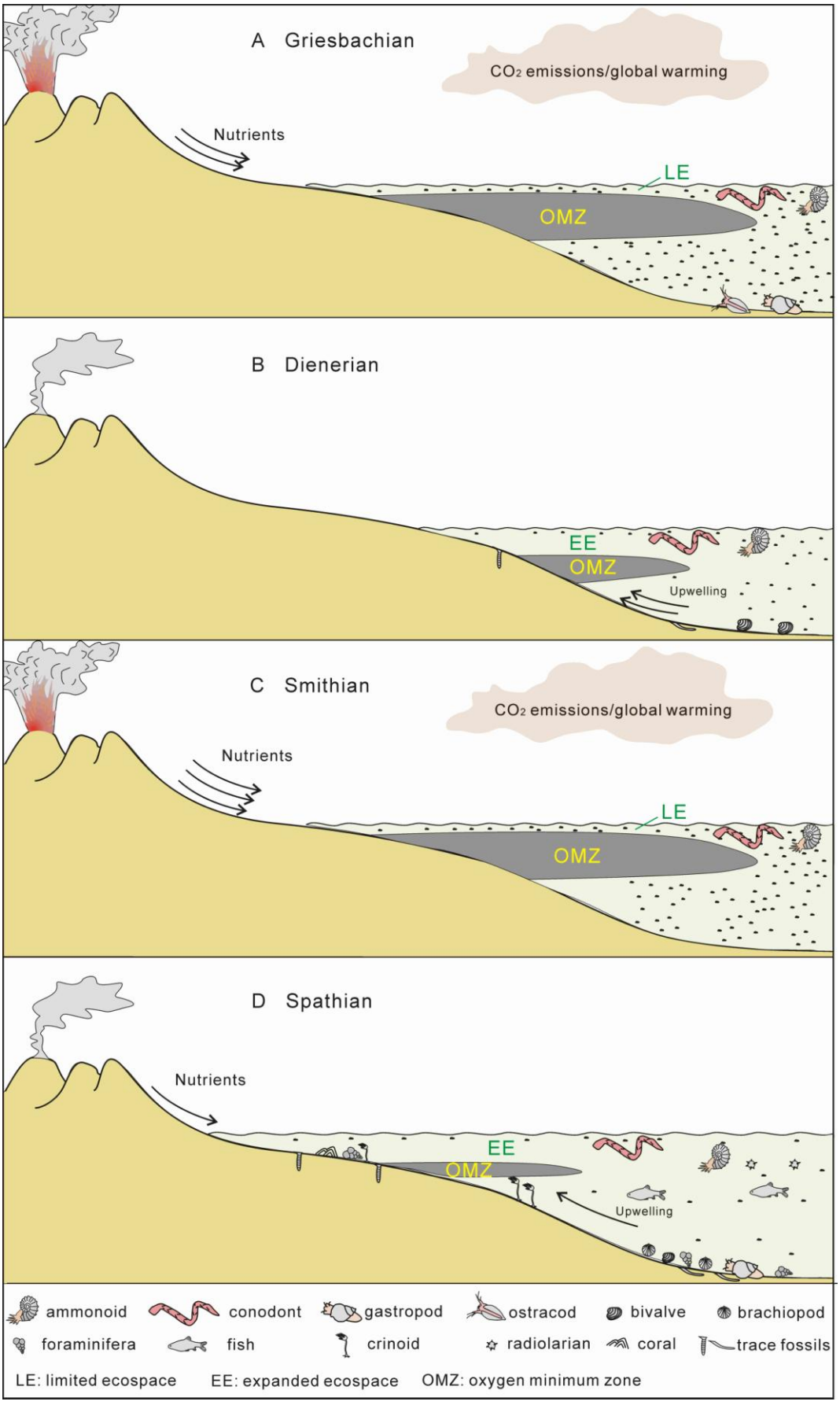

Figure 13.

Figure

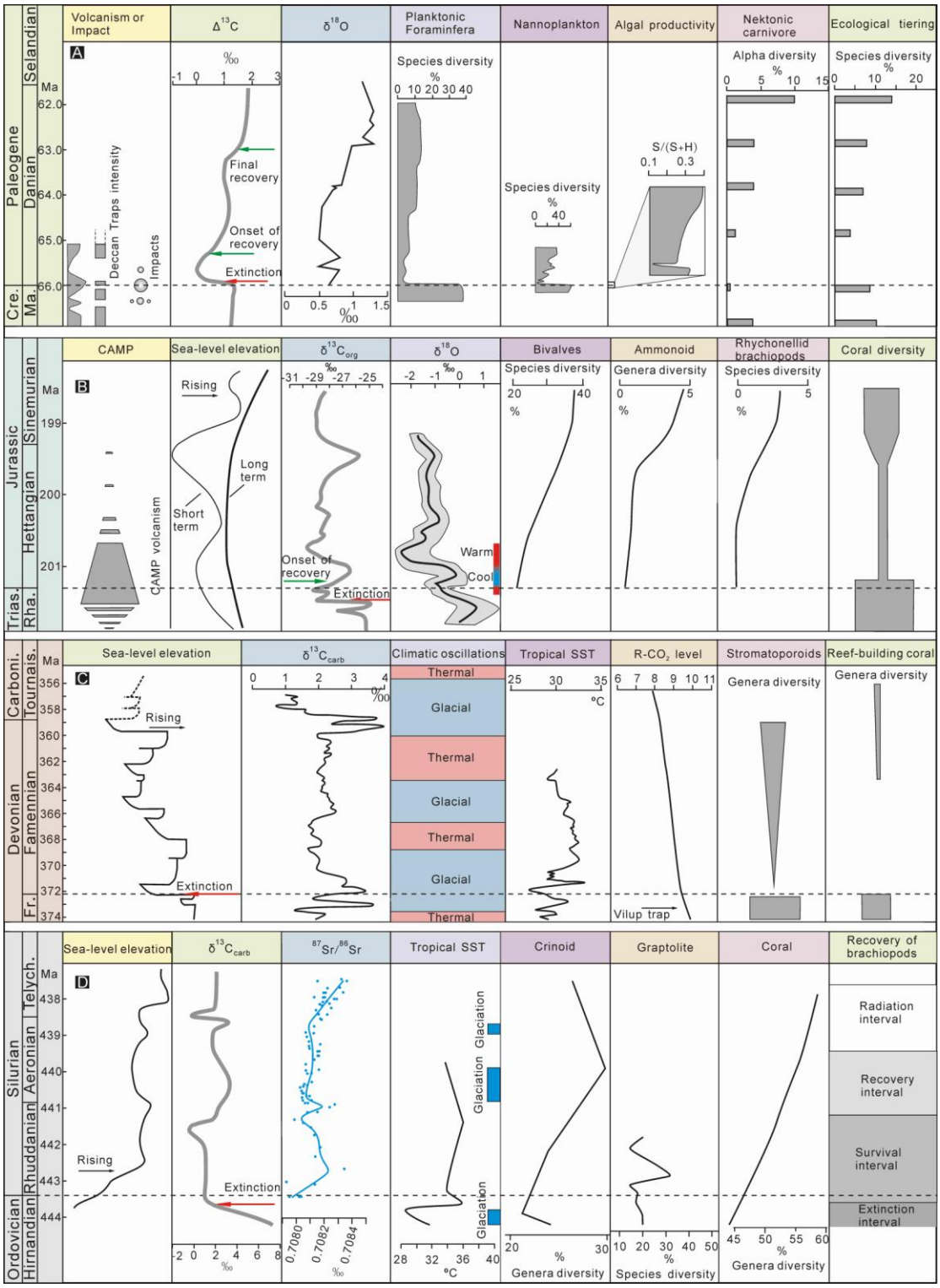

Figure 14.